CREATION OF AN IN VITRO GENERATED COLONIC STEM-CELL NICHE USING GRADIENT-GENERATING MICRODEVICES

Asad Ali Ahmad

A dissertation submitted to the faculty at the University of North Carolina at Chapel Hill in partial fulfillment of the requirements for the degree of Doctor of Philosophy in the School of Medicine (Biomedical Engineering).

Chapel Hill
2015

Approved by:

Nancy L. Allbritton

Scott T. Magness

J. Michael Ramsey

Elizabeth G. Loboa

Scott J. Bultman

ABSTRACT

Asad Ali Ahmad: Creation of an *In Vitro* Generated
Colonic Stem-Cell Niche Using Gradient-generating Microdevices
(Under the direction of Nancy L. Allbritton)

The limitations of existing cell culture and animal studies have provided an impetus for the development of alternative cell based *in vitro* models that better mimic the complex structures and functions of living organs. This thesis lays the groundwork for the development of an *in vitro* model of the colonic epithelium by focusing on the development of microdevices to recreating the colonic stem-cell niche.

New advances enable long-term organotypic culture of colonic epithelial stem cells that develop into structures known as colonoids. Colonoids represent a primary tissue source acting as a potential starting material for development of an *in vitro* model of the colon. However for that to be possible, there needs to an improved crypt isolation and 3-D colonoid protocols. In the first chapter, an incubation buffer and time are outlined, along with the finding that 50% Matrigel resulted in the highest colonoid formation efficiency.

In the second chapter, threshold concentrations of the key Wnt-signaling factors are discovered. While critically important to homeostatic renewal, the threshold concentrations of factors such as Wnt-3a and R-spondin1 that promote stem cell renewal are unknown. A simple, linear gradient-generating device was used to screen a wide range of Wnt-3a and R-spondin1 concentrations for their impact on a large number of colonoids. A Wnt-3a concentration of 60 ng/mL and R-spondin1 concentration of 88 ng/mL were identified as the critical concentrations

required for stem-cell renewal and colonoid expansion. The lower factor concentrations yielded the added benefit of a more morphologically appropriate colonoid possessing columnar cells surrounding a central lumen with active crypt-like bud formation.

In the final chapter, a gradient-generating device was used to introduce variable concentrations of the two key Wnt-signaling proteins along the length of a single colonoid. After 5 days in culture under a combination of Wnt-3a and R-spondin gradients, novel image analysis techniques leveraged the intrinsic fluorescence of the mouse model to quantify the levels of stem cell polarity across a colonoid. The microenvironment able to create a stem cell niche within a colonoid by applying external growth factors in a graded fashion across the colonoid.

ACKNOWLEDGEMENTS

Ammi, I want to let you know that the only reason I am in a position like this today is because you always demanded greatness out of me. Since a young child, this was not only expected, rather required, which set the tone for the rest of my life. Words cannot describe the impact that this little nuance had in my life. My brother is my best friend, confidant, punching bag, teammate and muse. We have developed an inseparable bond and watching you grow up over the years has been surreal. Our Chapel Hill summer adventure has been one of the most fortuitous gifts my life has bestowed upon me and I am very excited to see what the future has in store for you. My colleagues in and lab have played a major impact in my life as well. The most important and pivotal is Emilie Ruth-Anne Mainz. Thank you for showing me the graduate school ways and for calming me down when I thought I was wasting my life in the basement. If I died today, TOPS would be the most significant endeavor that I have done in my life – I am so proud of us for impacting so many lives. A special shout out to two of my colleagues: Pete Attayek for being a great roomie/MATLAB savant and Pavak Shah for illustrating what a true free thinker looks like. Thank you Nancy Allbritton for being the best academic advisor that I could ask for: providing me with the impetus to search for careers outside of academia and for truly wanting my success in life. To Chris Sims, thanks for your open door policy, that I perhaps exploited, and for helping me to cultivate my love affair with vinyls. Finally to Haoran Liu thank you for creating this monster and showing me the consulting way of the world.

TABLE OF CONTENTS

LIST OF FIGURES

LIST OF TABLES

LIST OF ABBREVIATIONS AND SYMBOLS

Abbreviation	Definition
°C	degrees celsius
µg	microgram
µL	microliter
µm	micrometer
1001F	Epon™ Resin 1001F
1002F	Epon™ Resin 1002F
BrdU	bromodeoxyuridine
CAG	cytomegalovirus/beta-actin/beta-globin
CBC	crypt base columnar
cDNA	complementary deoxyribonucleic acid
CNC	computer numerical control
CRC	colorectal cancer
DNA	nucleic acid
DSL	Delta/Serrate/Lag2
DI	deionized
DPBS	Dulbecco's phosphate-buffered saline

DMSO	dimethyl sulfoxide
ECM	extracellular matrix
EDTA	ethylenediaminetetraacetic acid
EdU	5-ethynyl-2’-deoxyuridine
EE	enteroendocrine
EGF	epidermal growth factor
EGFP	enhanced green fluorescent protein
EpCAM	epithelial cell adhesion molecule
ESC	embryonic stem cell
FACS	fluorescent activated cell sorting
FBS	fetal bovine serum
FSC	forward scatter
GBL	gamma-butyrolactone
GI	gastrointestinal
HBSS	Hank’s balanced salt solution
hr	hour
IBD	inflammatory bowel disease

IgG	immunoglobulin G
iPSC	induced pluripotent stem cell
ISC	intestinal stem cell
ISEMF	intestinal subepithelial myofibroblast
Lgr5	leucine-rich repeat-containing G-protein coupled receptor 5
LRC	label retaining cell
min	minute
mRNA	messenger ribonucleic acid
NDS	normal donkey serum
NGS	normal goat serum
OCT	optimal cutting temperature
PBS	phosphate-buffered saline
PC	paneth cell
PCA	principal component analysis
PCR	polymerase chain reaction
PDMS	polydimethylsiloxane
PEG	polyethylene glycol

PFA	paraformaldehyde
RNA	ribonucleic acid
RPM	revolutions per minute
RT-PCR	reverse transcriptase polymerase chain reaction
sec	second
SEM	standard error mean
SMA	smooth muscle actin
Sox	Sry Box-containing
Sry	Sex determining region Y
SSC	side scatter
TA	transit-amplifying cell
TGF-β	transforming growth factor β
Wnt	wingless-related integration site
wk	week
β-catenin	Beta cadherin associated protein

CHAPTER 1: INTRODUCTION

1.1 Intestinal Epithelial Structure & Function

1.1.1 Gastrointestinal tract and digestion

The digestive system is made up of the gastrointestinal (GI) tract, liver, pancreas and gallbladder. The GI tract is a series of conjoining, twisting tubes that consist of the follow organs: the mouth, esophagus, stomach, small intestine, large intestine and anus.[1] The GI tract is a vital organ system in the body and allows the replenishment of nutrients and dispelling of harmful by-products on a daily basis. The GI tract can be divided into two main components: with the upper tract consisting of primarily the esophagus and stomach and the lower tract consisting of the majority of the small intestine and the entire large intestine. The lower GI tract is crucial in the digestive process. Digestion is vital for breaking down food into nutrients, which the body can then use for energy, growth and cellular repair. Ingested food and drink is broken into smaller and smaller subunits as it matriculates through the GI tract. The large hollow organs of the GI tract contain a layer of muscle that enables their walls to move in a rhythmic fashion. This movement, called peristalsis, serves two major purposes: (i) to drive the food and liquid through the GI tract and (ii) to mix the contents within each organ. The muscle of the upper part of the stomach relaxes to accept large volumes of swallowed material from the esophagus and the muscle of the lower part of the stomach mixes the food and liquid. The stomach empties it slurried contents, called chyme, into the small intestine. In the small intestine, food is further broken down and the nutrients are absorbed into the bloodstream. The chyme is then passed onto

the large intestine where remaining nutrients and water are absorbed, changing the waste from liquid to solid. Finally, the rectum stores the stool until it is dispelled out of the body.[1, 2]

1.1.2 Colon structure and function

A key player in the digestive process is the large intestine, or colon, which extends 5 feet in length and about 2.5 inches in diameter. Although being only about a third the overall length of the small intestine, the colon derives its name from being considerably thicker in diameter. The intestines (both small and large), have the same basic structure and can be divided up into four concentric layers in the following order: the mucosa, submucosa, muscalaris externa and the serosa. The serosa is the outermost region and consists of a thin layer of simple squamous epithelial tissue that secretes watery fluid to lubricate the surface of the colon. This lubrication is key is protecting the colon from friction between abdominal organs and the muscle and bones of the lower torso. The muscularis externa layer surrounds the inner submucosa and houses the layers of visceral muscle cells that contract the colon. Next, the submucosa is a layer of dense irregular connective tissue that is comprised of blood vessels and nerves. Collectively, the outer layers of the colon contain the complex network of vasculature and nerves that regulate the movement of ingested matter down the GI, working to support the mucosa.[3, 4] Finally, the mucosa is the innermost layer and is made up of simple columnar epithelial tissue. A complex layer, the mucosa can be further segmented into three parts: the outer muscularis mucosa, the lamina propia and the inner-most colonic epithelium. Surrounded by a layer of smooth muscle, the lamina propria consists mainly of fibroblasts, myofibroblasts, capillaries and lymphocytes, which support the digestive and barrier function of the intestine. The colonic epithelium is a monolayer of simple columnar epithelium that lines the luminal surface of the organ and is responsible for a number of essential absorptive and digestive processes. Since the intestinal lumen is subjected to mechanical stress and potential toxics from ingested matters, the

epithelium provides the additional benefit of establishing a barrier between the lumen and the body. Found within the epithelium are small tubular invaginations called crypts, which is the central theme of this thesis.[5] Colon crypts are lined mostly with younger epithelial cells which are involved primarily in secretion of mucus and hormones. At the base of the crypts are stem cells which continually divide and provide the source of all the epithelial cells in the crypts.[6] The major differences between the otherwise similar small and large intestinal crypts are predicated on function. The small intestinal epithelium is arranged into villi composed mostly of mature enterocytes, increasing the overall surface area for absorptive purposes. On the other hand, the colonic epithelium is void of the presence of villi and contains more mucous-secreting goblet cells.[5]

While the colon is one functional unit, the organ demonstrates regional differences. In appearance, the proximal (upper) colon is more saccular while the distal (lower) colon is more tubular.[7] Short-chain fatty acids are principally synthesized in the more acidic environment of the proximal colon. The proximal colon serves as a reservoir, in contrast to the distal colon, which mainly performs as a conduit.[8] The short-chain fatty acids, present in the chyme entering the colon, are of integral importance in proper colon health. More than 95% of the short-chain fatty acids are created in and are immediately utilized by the colon with very little excreted in the stool.[2, 9] In fact, the retrieval of previously undigested matter in the colon as short-chain fatty acids provides 10-15% of the total caloric needs of an individual.[10] Although the least prevalent of the short chain fatty acids, butyrate has the greatest importance in colonic homeostasis. Butyrate best promotes the absorption functionalities of the colon and also advances the colonic cell proliferation and differentiation. In fact, butyrate supplies 75-90% of the energy requirements for colonic epithelial cells to perform their functions. The colon serves three main

functions: (i) complex carbohydrate processing, (ii) water/ electrolyte transport and (iii) recovery of sodium and chloride. The colon processes various complex carbs and, to a lesser extent, proteins that prove resistant to digestion in the small intestine.[5] Unlike the small intestine, the colon retrieves nutrients from these products via fermentation. Fermentation occurs by means of the over 400 species of bacteria, the majority of which are obligate anaerobes, present within the colon.[2] In total, approximately 10-15% of ingested carbohydrates enter the proximal colon as undigested material.[11] The colon maintains an appropriate hydration and electrolyte balance by means of the absorbtion and secretion of intestinal water and electrolytes. Generally, the surface epithelial cells are responsible for the absorption and the crypt cells are involved in fluid secretion. Under normal conditions, the colon is presented with 1.5-2 L of water daily, with approximately 90% of this water reclaimed by the organ.[12] Finally, the large intestine is essential to the recovery of sodium and chloride from the colonic lumen. The liquid chyme delivered to the colon contains roughly 130 mmol/L of sodium whereas the concentration in stool is 40 mmol/L.[8, 13]

1.1.3 Regulation of proliferation and differentiation in the colonic epithelium

The single cell- layer epithelium of the intestines characterizes the largest interface between the internal and external environment. The unparalleled cellular turnover capacity of the gut epithelium enables it to withstand modifications in the external milieu by renewing all the cells of the crypt-villus axis in 3-5 day.[14, 15] The epithelial cells are constantly being replaced by a stem-cell population located at the base of both small intestinal and colonic crypts, located within a complex microenvironment perfectly tailored for stem-cell proliferation. This stem-cell niche houses the most rapidly self-renewing tissue in the body, the colonic epithelium, with complete renewal occurring every 4-7 days. CSC give rise to transit amplifying progenitor cells,

which in turn differentiate into the three principal cell types of the gut epithelium as they migrate apically towards the lumen.[16-18] This process is tightly regulated by gradients of mitogens, morphogens and differentiation factors[16], which in turn rely upon the spatial organization of differentiated epithelial progeny, and the underlying pericryptal mesenchyme.[16, 17] Progenitor differentiation, regional architecture and intestinal homeostasis are orchestrated by a complex interplay of three main signaling pathways[6]: Wnt, Notch and BMP. The impact each of these pathways have on colon cell proliferation and differentiation will be explored here.[19-21]

The Wnt signaling pathway is one of the most comprehensively studied pathways, providing many of the critical proliferative signals to stem and progenitor cell populations throughout a wide range of cell types and tissues. Canonical Wnt signaling occurs when WNT ligands interact with FZD or LRP receptors. Binding of Wnt to its receptor activates the pathway with stabilization and nuclear translocation of β-catenin. β-catenin is crucial in blocking the pro-differentiation factors and recruits a number of co-factors to activate context-dependent targets, generally associated with cellular growth and proliferation.[6, 19] Because of its direct influence on proliferation in the intestinal epithelium, the Wnt-signaling pathway has been the subject of many studies aimed at understanding ISC biology. Early-stage studies demonstrated that WNT is essential for the maintenance of ISC populations. In fact, because many ISC biomarkers are downstream targets of WNT/β-catenin, early ISC biomarker discoveries were predicated upon genomic analyses of the effects of disruption in Wnt signaling.[19, 22, 23] These ISC biomarkers will be discussed in further detail in the next section. One of the most prominent results from these early studies was the observations that complete loss of Wnt signaling, resulted in a lack of proliferation *in vivo*.[24] In a following study by van de Wetering et al., the Wnt agonists Wnt-3, Wnt-6b and Wnt-9b were identified in cells located at the bottom of the crypt, indicating that

nuclear localization of β-catenin was restricted to the base of intestinal crypts.[22, 25] Recent studies have demonstrated that multiple sources in the intestinal epithelium produce WNT ligands: including Paneth cells (small intestine only) and mesenchymal cells of the lamina propria (small and large intestines).[26, 27] A series of *in vitro* co-culture experiments demonstrated that Wnt signaling can also be supplied to ISCs by subepithelial intestinal myofibroblasts (ISEMF), providing a partial explanation for the persistence of ISCs in the absence of Paneth cells.[28] Together, these data demonstrate that WNT provides a significant mitogenic and morphogenic signal in the intestinal epithelium that is critical to ISC survival and proliferation.

The current scope of knowledge suggests that the influence of Wnt-signaling on differentiation varies greatly from its effect on proliferation. Rather than an 'on-off' phenomenon, it is believed that an appropriate amount of Wnt activity is necessary for orderly differentiation, with variations in either direction leading to impaired differentiation. Overactive Wnt-signaling maintains cycling progenitor cell types resulting in increased proliferation, impeding differentiation. Induced by deletion of *Apc,* which triggers Wnt-hyperactivity, results in interrupted differentiation with the absence of alkaline phosphatase expression, an indicator for enterocytes, reduced goblet cell numbers and decreased enteroendocrine cells.[29, 30] Conversely, in the case of disrupted Wnt-signaling, progenitor cell depletion results in the absence of properly differentiated cells. In studies of decreased Wnt signaling, similar differentiation abnormalities are observed. In neonatal $Tcf4^{-/-}$ mice, enteroendocrine cells are absent but goblet cells develop normally.[24] Pinto and colleagues showed a disappearance of all secretory cells in a mouse model with ectopic overexpression of Dkk1[22], which correlated with the absence of the secretory cell master transcription factor, Atoh1.

Notch-signaling is based on direct cell-cell contact between neighboring cells exhibiting Notch ligands and receptors.[31-33] In the intestinal epithelium, Notch signaling is mainly restricted to the crypts, which express *Notch1* and *Notch2* receptors, as well as *Dll1*, *Dll4*, and *Jag1* ligands.[34] *Notch1/2* receptors are associated with ISCs, and appear to play important roles in ISC maintenance.[35] Ablation of Notch signaling in the intestine results in a complete loss of ISCs, and conversion of a majority of crypt cells into differentiated Goblet cells.[36] The two most widely accepted mechanisms proposed by which Notch signaling maintains the progenitor state, are the binding of *Hes1* to cyclin-depedant kinase inhibitors[37] and the downregulation of transcription factor *Atoh 1*.[35, 36, 38-40] Interestingly, there appears to be some redundancy in Notch receptors and ligands. Dual deletion of *Notch1* and *Notch2* is required to convert proliferating cells to secretory lineages, and dual deletion of *Dll1* and *Dll4* is required to achieve the same effect through modulation of ligand expression[37, 41] In fact, active Notch signaling results in the expression of the target gene *Hes1*, the loss of which results in increased secretory lineage differentiation and decreased production of absorptive enterocytes.[36, 37, 41-44] Loss of *Hes1* can be partially compensated for by *Hes3* and *Hes5*, and loss of all three intestinal *Hes* genes results in decreased proliferation, but does not fully ablate ISCs.[45] Taken together, these data suggest that other Notch targets may sustain ISC cell fate, while *Hes1* is more important for absorptive lineage commitment. In addition to participating in absorptive fate selection, expression of *Hes1* also results in the suppression of *Atoh1*, which drives cells toward enteroendocrine, goblet, or Paneth cell secretory fates in the absence of Notch signaling.[42, 43]

While much less is known about the role of Bmp signaling in the intestinal epithelium, the data suggests the pathway is critical in homeostasis by providing key pro-differentiation cues to prevent over-proliferation of the ISC compartment. BMP proteins belong to the TGF-β

cytokine family, and act by binding to type II and type I serine/threonine kinase receptors. This binding forms heteromeric complexes and activates downstream transcriptional effectors belonging to the Smad family.[46] BMP-signaling is believed to preserve 'stemness' and differentiation of intestinal progenitor cells acting both directly and indirectly. The pathway prevents stem cell proliferation by disruption of the Wnt-pathway via activation of PTEN and consequent inactivation of Akt mediated accumulation of β–catenin in the nucleas.[47] BMP predominantly has a role in differentiation of the epithelium. *Bmp4* is strongly expressed by the mesenchymal cells immediately underlying the epithelium, suggesting that these stromal cells play an important role in the induction of epithelial differentiation.[48] One of the most convincing studies employed the use of transgenic mice which over-expressed *Noggin*, a Bmp inhibitory protein, in epithelial cells.[48] When *Noggin* was over-expressed, *Bmp4* signals from the mesenchyme were essentially inactivated, resulting in *de novo* formation of crypts along the length of the intestinal villi. The authors likened this to the hyperplastic growth observed in patients with juvenile polyposis syndrome.[48] Taken together with a number of follow-up studies, the data suggests that the severe phenotypes associated with clinical polyposis disorders are the result of multiple mutations in the Bmp signaling pathway, which plays a major role in regulating intestinal epithelial proliferation through the induction of differentiation.[49-51] Genetic evidence indicates that the regulatory elements of Wnt and Bmp signaling may act through extensive crosstalk, as a number of loci containing response elements for both Wnt (*Tcf*/*Lef*) and Bmp (*Smad*) have been identified.[49, 52-55]

1.1.4 Diseases of the intestine

The majority of research on ISC biology in humans has been driven by the finding that mutations in the signaling pathways involved in ISC maintenance occur in the majority of

intestinal ailments and colon cancers. The two major ailments which affect the intestines are inflammatory bowel diseases (IBD), and colorectal cancer (CRC). Crohn's disease and ulcerative colitis (UC) are the principal types of IBD that can be classified as autoimmune diseases, in which the bodies own immune system attacks elements of the digestive system. Crohn's disease has the ability to effect both the small and large intestine, whereas UC primarily affects the colon and the rectum. In the United States alone, IBD resulted in 51,000 deaths in 2013, a slight decrease from the 55,000 deaths from 1990. The genetic basis behind the IBD is poorly understood and is currently believed to arise from small contributions of dozens of genes.[56] Recent studies have outlined the contributions of previously discussed signaling pathways in IBD. Crohn's disease has been linked to decreased expression of Tcf4 in the Wnt-signaling pathway and increased expression of *Notch1*, *Dll4* and *Hes1* in the Notch-signaling pathway.[57-59] UC has been linked to increased expression of *Notch1* and *Hes1* in the Notch- pathway and increased expression of *GL11* in the Hedgehog-pathway.[60-63]

Colorectal cancer (CRC) is the second leading cause of cancer-related deaths in the western world, responsible for nearly 50,000 deaths per year in the US alone.[64] The expansion of CRC in the Western world has provided impetus for the scientific community to uncover the histopathologic and molecular processes underlying the transformation from normal epithelium to invasive adenocarcinoma. It has been hypothesized that the pathological basis of tumorigenisis may be related to interruption of gradient signaling, mainly of the Wnt-pathway, leading to excessive proliferation of the stem cell niche.[23, 65, 66] Inactivating mutations in *Apc* are one of the most common mutations found in CRC, being detected in 85% of sporadic CRCs and resulting in the aberrant accumulation of β-catenin due to defective destruction complexes.[30, 67, 68] Unfortunately, CRC tumors exhibit heterogeneity in their proliferative capacity, cellular

morphology and therapeutic response, which make it extremely challenging to develop sophisticated treatments. Recent breakthroughs have refined previous models, to suggest the 'cancer stem cell theory' where tumorogenic capacity of an individual cancer cell may be influenced by distinct homeostatic signals derived directly from the microenvironment.[69, 70] Given that cancer stem cells are the compelling force for tumor formation, identifying the morphogenetic parameters regulating the 'cancer microenvironment' and identifying how this microenvironment differs from the normal ISC niche is of utmost importance in the disease. This thesis looks to address the current culture limitations that significantly hinder the ability to test the influence of fundamental morphogenetic cues in crypt homeostasis and cellular organization in healthy and diseased states.

1.2 Methods to Study the Intestine

1.2.1 Macroscopic techniques

In the past, due to the difficulties of reproducibly isolating and culturing healthy intestinal crypts, it has been impossible to develop in vitro models of the colonic epithelium. As a result previous investigations into intestinal pathophysiology have been restricted to an in vivo context, preventing detailed experimentation and restricting the scope of analysis. Although macroscopic examination of living tissue is made possible by endoscopy or noninvasive imaging, these techniques lack assessment at the cellular scale. Histological evaluation of fixed tissue samples has permitted study at the cellular level, but with the loss of the rich and dynamic qualities of the living tissue. Nevertheless, these studies have provided indirect evidence that there is a close interaction of several key signaling pathways, spatially present as protein gradients, in directing intestinal stem-cell renewal and differentiation.

1.2.2 Crypt as a functional subunit

The solid organ most extensively studied in respect to stem cell biology is the intestinal tract, because the presence of actively dividing stem cells that enable complete turnover every 5 days. More specifically, it is the intestinal epithelium where the unequaled regenerative potential of these stem cells are on display. The intestinal epithelium is organized along the crypt-villus axis, with the crypts containing the proliferative compartment of the epithelium.[71] A population of multipotent stem cells can be found located at the base of the crypts and maintains intestinal homeostasis in the most proliferative tissues in the body.[71] The intestinal crypt is routinely considered the functional subunit of the intestinal epithelium for two main reasons. The first is that the crypt houses the full repertoire of cell types present in the intestine, with highly-proliferative stem cells at the base, transit-ampliying progenitor cells above them[72, 73], and assortment of post-mitotic differentiated cells located at the apical end of the crypt. Because a single crypt has the regenerative horsepower to replenish the entire lining of the intestine, crypts can be considered to be 'building blocks' of the intestinal epithelium. The second reason has only been acknowledged recently, and is predicated on the fact that the crypt architecture offers the opportunity to track the entire lifetime of the colonic epithelial cell: from the foundational stem cells at the bottom of the crypts, to the temporary TA cells and lastly the post-mitotic differentiated cells at the top of crypts. Therefore, isolated crypts can be used to study the kinetics of intestinal epithelium proliferation, migration and differentiation of the intestinal epithelium.

1.2.3 Identification of colonic stem- and progenitor-cell populations

Somatic cells must possess the ability to self-renew, or produce daughter cells and must be multipotent to be considered stem cells: (i). The intestinal epithelium is an attractive tissue for the study of stem cell maintenance because of the tissue's high rate of physiologic renewal and

the well-defined post-mitotic lineages. Although the dynamics of intestinal epithelial turnover have been slowly uncovered for decades, the lack of specific genetic biomarkers has hampered direct studies on ISCs. Identification of stem cells has traditionally relied on three methods: label retention, transplantation and in vivo lineage tracing.[74] Before delving into the recent surge in ISC biomarker discovery, a brief discussion of the advantages and disadvantages of these identification methods will take place. Label retention involves the use of deoxynucleoside analogs such as bromodeoxyuridine (BrdU) or tritiated thymidine (3-thymidine). These analogs incorporate into DNA during S-phase replication and allow the detection of actively proliferating cells soon after incubation. As cells subsequently divide, the label is diluted and eventually becomes untraceable. In this way, actively proliferating cells loose the tag rapidly, whereas quiescent cells retain the label for much longer.[74] Although the method allows for real-time identification, a critical caveat of label-retention is that quiescence alone should not be used to define stemness. The second, which has been historically considered the gold-standard, is transplantation. Suitable stem cell populations are sorted and injected into an immunodeficient host and the host is eventually sacrificed for evidence of donor-derived tissue. Transgenic donor animals expressing fluorescent-tags are commonly used to distinguish between donor-derived and host-derived tissues. Transplantation is certainly an excellent *in vivo* method for assaying stem cell populations; however it is not always a true reflection of stem cell function under physiologic conditions (as was demonstrated by Bonfanti and colleagues in skin stem cells).[75] Finally, *in vivo* lineage tracing enables the visualization of the modified stem cell and its offspring over time via targeted introduction of a genetic marker into candidate stem cells *in situ*.[75]

Two philosophies currently exist regarding the exact location of the stem cells within the crypt. The classic model (+4 model) originated from elementary cell tracking experiments that predicted a cell or origin at position number 4 about the base of the crypt.[76] The theory was supported by two main pieces of evidence: cells in the +4 position are: (i) characteristically proliferative and label-retaining[26] and (ii) sensitive to X and γ radiation[14]. This radio-sensitivity was deemed beneficial to supporting the theory, as resistance to radiation could protect the stem cells from amassing potentially cancer-inducing genetic damage. The second school of thought was proposed in 1974 and is called the 'stem-cell zone model' that proposed that all of the crypt-base columnar cells (CBC) located at the basal end of the crypt represents the entire ISC population. These results were predicated upon observations made by light and electron microscopy and evidence of proliferation. [73, 77] Over the past couple of decades a number of studies have resulted in the overall acceptance of these two schools of thought: with an 'active' CBC population and a 'quiescent' reserve +4 population. The primary reason why the intestinal field has failed to reconcile these two theories has been the lack of well-validated markers for ISCs. Following is a discussion into the accepted stem cell markers of the intestinal epithelium.

In 2009, the G-protein coupled receptor Lgr5 became the first ISC biomarker to be validated by in vivo lineage tracing.[78] Investigation in expression patterns within normal intestinal epithelium revealed Lgr5 to be a highly specific indicator for proliferating CBC cells. [74, 79] Lineage tracing using the Lgr5EGFP-CreERT2 allele demonstrated that daughters of these cells were capable of developing into long-lived entities that contained all of the fully differentiated lineages of the intestinal epithelium. In addition to the biological implications of this study, the development of the Lgr5EGFP-CreERT2 allele was a significant technological contribution to the field, as it provided the first methodology for the isolation of ISCs. This

ground-breaking work, along with other seminal studies established Lgr5 as a specific marker of ISC, both in small and large intestine.[27, 78, 80, 81] It is important to know that a limiting factor of this mouse model is that the reporter gene is expressed in a mosaic manner, with only certain crypts exhibiting expression in spite of the fact that Lgr5 has been demonstrated to be expressed in all intestinal crypts.[79] The classification of Lgr5 as an ISC marker opened the floodgates with a subsequent surge in ISC biomarker discovery. The next marker characterized was Bmi1, and similar to Lgr5, lineage-tracing experiments in Bmi1CreERT2 mice revealed that Bmi1+ cells form long-lived clonal units that contain all of the appreciated differentiated lineages.[82] However unlike Lgr5, fate mapping studies revealed that Bmi1+ cells were primarily restricted to the +4 position in intestinal crypts.[18, 82] Nevertheless, there were some clear limitations that prevented Bmi1 from becoming a mainstay in ISC identification, primarily that Bmi1+ cells were only seen in 10% of crypts in the proximal small intestine.[82] Subsequent studies uncovered other genes related with the +4 position that also served as ISC biomarker, including mTert and Hopx. [83] Taken together with the limitations of each identified genetic marker, Lgr5 has provided compelling evidence as the premier ISC marker. My collaborator at UNC, Scott Magness, recently identified that Sox9, a member of the SRY family of transcription factors, was shown to be expressed within the proliferative compartment at the base of intestinal crypts.[27, 84, 85] Based on gene expression studies, it was demonstrated differential Sox9 expression correlated to different cell populations: with Sox9-SubLow marking TA cells, Sox9-Low marking actively cycling CBCs (ISC proxy) and the Sox9-High population correlated with markers of enteroendocrine cells.[27, 84] This work was further advanced with the demonstration that *in vitro* enteroid-forming capacity was restricted to the Sox9-Low population, consistent with the initial reports for Lgr5High cells[27]. Interestingly, for the first time, gene expression data revealed a

model in which CBC ISCs are distinct from +4 ISCs. Specifically, when crypt populations were isolated based on Sox9eGFP expression, (as opposed to Lgr5eGFP expression), the population expressing the highest levels of CBC ISC markers (Ascl2, Olfm4, and Lgr5) were genotypically distinct from the population expressing the highest levels of +4 ISC markers (Bmi1, mTert, and Hopx) .[27, 86] Taken together, the emerging data on ISC biomarker and reported similarities and differences between CBC and +4 ISCs support a much more complex model for stemness and potency in the intestinal epithelium than originally postulated.[21] Nonetheless, from these studies, Sox9 was revealed to be a reliable marker for identification of ISCs.

1.2.4 Identification of differentiated cell populations

Along with the recognized patterns of proliferation and migration in the intestine, the differentiated cells of the intestinal epithelium have been well characterized into cell structure and function of the GL tract.[73, 77, 87-89] The origin of cellular fate within the intestine can be considered at the +5 position, only one position away from ISCs.[6] Fully-differentiated lineages of the intestinal epithelium can be segmented into two main groups based on function: secretory cells and absorptive cells. Absorptive enterocytes constitute about 95% of the intestinal epithelium lining and serve to uptake ions, water and sugar. The Notch-signaling pathway is a key mediator of enterocyte differentiation and when the Math1 gene is repressed as a result of active Notch-signaling, cells are steered towards the enterocyte lineage.[6] There are two main populations of secretory cells in the intestine: goblet and enteroendocrine cells. Goblet cells primary function consists of secreting gel-forming mucins, which are the major components of mucus. Goblet cells are believed to be the default fate within the secretory lineage, as attenuated Notch levels differentiate actively proliferative cells into goblet cells.[6] The presence of the transcription factor SPDEF has been demonstrated to be crucial in goblet cell formation.[38, 908]

Enteroendocrine cells are hormone-secreting cells that comprise only about 1% of the cellular density of the crypt. Lineage specification requires the presence of the transcription factor Neurogenin along with SPDEF for enteroendocrine production.[6, 91] Although there are a handful of other post-mitotic cell types that can be found; enterocytes, goblet cells and enteroendocrine cells comprise ~99% of the differentiated cells present in the colon. Therefore, the collective presence of these cell types, along with ISCs is crucial in categorizing any *in vitro* generated organoid growth as physiologically similar to an *in vivo* intestinal epithelium. A number of monoclonal antibodies exist which are readily used to identify the presence of these differentiated lineages within in vitro developed organoids. Mucin-2 is the major secreted gel-forming mucin produced by goblet cells that form the protective mucus blanket covering the epithelium as the first line of innate host defense in the gut. A polyclonal immunoglobulin antibody specific to Mucin-2 is widely used to identify the presence of goblet cells[17, 92] and is used throughout the work presented in this thesis. The protein encoded by the Chromogranin A gene is a member of the chromogranin/secretogranin family of neuroendocrine secretory proteins and is found in secretory vesicles of neurons and endocrine cells. Similar to Mucin-2 for goblet cells, Chromogranin-A has been widely used in the intestinal field to identify the presence of enteroendocrine cells[92, 93] and it is used throughout this thesis for this purpose.

1.2.5 Studying colonic stem cells *in vitro*

For decades, the inability to expand primary intestinal tissue *in vitro* posed a significant barrier in uncovering the intricacies of intestinal biology. As a result of the lack of an *in vitro* model system for studying ISCs, a great deal of the initial data regarding biochemical and molecular signaling in the intestinal epithelium relied on *in vivo* mouse models or CRC cell lines. Besides being expensive and time-consuming, these avenues failed to accurately recapitulate

physiologically appropriate hallmarks of the intestine. Nevertheless, with improved understanding of signaling networks in the intestine over the past couple of decades, a novel, three-dimensional culture system for intestinal crypts and primary-isolated ISCs arose.[70] These culture conditions were first pioneered by Hans Clevers in 2009[70] and rely on the extensive use of growth factors targeting the Wnt, Bmp, and Notch pathways as well as small nutrient molecules. Clevers and colleagues demonstrated the ability of ISCs to produce complex, multicellular organotypic bodies without the need for co-culture with ISEMFs.[70] These organotypic bodies, termed enteroids, were long-lived in culture and produced crypt-like proliferative buds that contained all of the post-mitotic, differentiated lineages found in the intestinal epithelium.[70, 94, 95] The culture conditions were first successful in small intestinal epithelium of mice and since that time the technology has been expanded to the murine colonic crypts and single cells, human small intestinal and colonic crypts as well as murine stomach and adenomatous tissue[70, 96, 97].

The ISC culture system has proven to be an irreplaceable technology that has been applied to *in vitro* studies supporting observations made *in vivo*. As a result, the most common methodology used for mechanistic studies of the intestine the paradigm has shifted from *in vivo* animal studies to primary *in vitro* cultures, which allow unrivaled experimentalist control. Although lineage tracing is still a powerful, robust technique for elucidating stemness within populations of cells, it fails to distinguish between cell types based on gene expression levels. The *in vitro* assays enhance precision for promiscuous genes which exhibit broad expression levels. An example of this was recently done by our collaborators, the Magness group at UNC, who demonstrated that specific levels of the transcription factor *Sox9* are associated with ISCs, TAs, and enteroendocrine cells.[27, 72] Because *Sox9*$^{+}$ cells from the intestine could be expanded

into long-lived organotypic structures that were successfully maintained through multiple rounds of passaging, the *in vitro* culture techniques provided a secondary platform to establish stemness criteria and corroborate the in *vivo* findings.[27, 70] However, although the expansion technology has enabled a handful of functional ISC biology experiments, there are still some shortcomings of the technology hampering the ability towards more targeted molecular and genetic analysis, including the inability of quantification of organoid growth percentages.[17, 43, 98] This, as well as other, limitations will be addressed in the subsequent chapters of this thesis. Despite these limitations, the discovery of an *in vitro* culture system for ISCs has presented the field with an essential tool for examining the effect of external signaling on stemness and differentiation.

1.3 Microfluidic Gradient Generation

1.3.1 Principles of gradient-generation

In living organisms, cellular microenvironments are of great importance in maintaining homeostasis. Cells are surrounded by a milieu of physical and biochemical signals that comprise these microenvironments and elegantly orchestrate proliferation and differentiation. Specifically, biochemical signaling from growth factors, mitogens, morphogens and hormones exist in the form of gradients that vary in space and time depending on the organ.[99-101] These biochemical gradients are crucial to a number of biological processes including development[102-104], wound healing[105, 106], angiogenesis[107], cancer metastasis[108-111] and immune response.[112-114] Understanding the particular mechanisms behind these essential processes can yield deeper understanding into the influence of the chemical stimuli on signaling pathways in cells and how these pathways are implicated in cancer. Towards mimicking the in *vivo* chemical stimuli scientists have thought of methods to engineer *in vitro* devices, establishing what is known today as the microfluidic gradient-generating field. The early work in the field relied on makeshift *in*

vitro platforms such as the Boyden chamber (1962)[115], Zigmond chamber (1973)[116] and Dunn slide chamber (1991) .[117] Although these devices led to significant advances in biological understanding, the non-quantitative spatial gradients that were generated from these devices could not be manipulated or precisely controlled in a reproducible manner. Over the past decade, with a rapid boom in microfabrication techniques, research efforts directed at mirroring critical aspects of cellular microenvironments have gained momentum, as witnessed with the uptick in publications using gradient-generating devices. Indeed the paradigm has shifted within the biological community on how to study cellular gradient sensing responses: with the idea that concentration gradients of biomolecules can be introduced to cells and manipulated in time and space and disease progression and malignant conversion can be elegantly characterized and modeled. In this section, the basic mass transport phenomena in microfluidic generators will be covered with emphasis on free-diffusion based gradient generation. Additionally, the ability to combine 3D physiologic cues across hydrogels will be explained concluding with biological applications of microfluidic gradient generators.

The fluid flow that transports concentration gradients is governed by the Navier-Stokes (N-S) equation.[118, 119] In microfluidic conditions, the simplified equation becomes:

$$\nabla \mathrm{P} = \eta \nabla^2 v$$

where P is pressure, η is the viscosity and v is velocity. In order for the equation to be relevant, however, the equation assumes that the fluids used are both incompressible and Newtonian in nature. The assumption of incompressibility is fulfilled if liquids experience negligible volumetric changes upon pressure changes and a fluid can be considered Newtonian if its' viscosity does not vary with increased hydrodynamic shear. In the past, the large majority of liquids used within gradient generators have fulfilled these criteria including cell medium,[120]

growth factors[108], proteins[111, 112] and water-based dyes.[121] The fluids that are utilized in the work conducted for this thesis fulfill these criteria as well. With these conditions met, the N-S equation balances the fluidic rate of change with the externally applied forces on the system (ie, pressure, convective, electrical, viscous, etc.). Within microfluidic gradient generators, there is an overall absence of forces and the force term can be omitted from the N-S equation. Because of the small channel dimensions, fluid flow in microchannels is usually characterized as laminar. Fluid flow can be considered to be laminar if its Reynolds number is smaller than 2100-2300.[99, 118] Reynolds number, *Re*, is a dimensionless number than measures the relative importance between inertial and viscous forces and in a microfluidic sense is defined as:

$$Re = \frac{(\rho V L)}{\mu}$$

Where ρ is the fluid density, V is the velocity, L is the length of the fluidic channel and μ is the fluid viscosity.[118, 119, 122] Although linked to fluid mechanics, the Reynolds number is most often used to estimate the order of magnitude of flow velocities. Fluid flow velocities within microfluidic gradient generators can be solved by incorporating further assumptions to simplify the N–S equations[119, 122-124]. Further explanation into the two types of gradient generation modalities commonly utilized in microfluidic devices can be seen below.

1.3.2 Methods to establish gradient profiles in microfluidic devices

Microfluidic gradient generating devices can deliver spatial and temporal distributions of biochemical signaling molecules by precisely regulating advective and diffusive characteristics. Gradient generating devices can be broadly categorized into two main groups based on their gradient-generation principles: flow-based and diffusion-based. The key differentiator between these two groups is the method of forming the gradient-region: in flow-based devices molecular species are delivered to the region via convection (laminar flow streams). In diffusion-based

devices, gradients are established relying on diffusive transport of the molecular species across the convection-free gradient generating region.[125] The two gradient-generating modalities are explained in further detail below.

An important parameter in flow-based gradient generators is the maintenance of laminar flow.[126] In a laminar flow regime, streams of miscible liquids can flow side-by-side and only mix via diffusion, completely eliminating the occurrence of turbulent mixing. Therefore in these devices, flowing bodies containing different chemical concentrations (or species) are applied together within a microfluidic channel where the chemicals are allowed to diffuse across the culture interface as they flow down the microchannel. The 'first-generation' of flow-based gradient generation utilized a straightforward 'T-shaped' or Y-shaped' design to establish a gradient profile at the interface of two laminar flowing streams.[127-129] The flow characteristic of this design results in a low Reynolds number and as long as the flow is maintained at a constant rate, a gradient is created perpendicular to the flow direction. The strength and weaknesses of the 'T/Y-shaped' mixer as a gradient generator is predicated upon its simplicity. The device is very easy to fabricate and utilize, however it only permits formation of a basic gradient profiles (ie, sigmoid shape). Nonetheless, based on the experimental insight gleaned from the original device designs, subsequent generators were able to create a wide array of gradient profiles via microchannel networks to control input and output flows. First developed by Jeon et al.[130], an arrangement of microchannels resembling a 'Christmas tree' was the first example of this. The design consists of a series of bifurcated microchannels that continually divide and recombine, with input concentrations attenuated at each successive splitting and upon recombination multiple streams are produced, with each stream having different proportions of the original concentration. With more complex designs, the experimentalist must ensure that the generator is

performing as expected and by treating the microchannel network as an electronic circuit, each branching point can be calculated. As a result of the complexity of the design, gradient profiles can be considerably manipulated via tailoring the incoming flow rates, number of channels and geometry. For example, Dertinger et al. adapted the previous design and generated periodic, polynomial and overlapping gradient profiles utilizing novel combinations of microchannel networks.[130, 131] What was clearly demonstrated by this and subsequent reports was that novel construction of microchannel networks based on mathematical principles could essentially generate any complexity of gradient profile.

An alternative approach to microfluidic gradient generation utilizes free-diffusion of soluble molecules. Similar to how molecular species concentrations are kept constant with constant flowing streams, pure-diffusion based gradient generators utilize large, opposing 'sink' and 'source' reservoirs, with a gradient developing at the interface. The main difference in pure-diffusion generators versus flow-based generators is that the former uses microchannels with high fluidic resistance[110, 132, 133], hydrogels[134, 135] and/or semi-permeable membranes.[125, 136] Mass balance calculations specify that this developing gradient can only be steady state when the transport of the molecular species in equals the transport out and this is usually achieved at much later time scales than flow-based generators. There is therefore an inversely proportional relationship between the microchannel's fluidic resistance and the time it takes for the gradient to reach steady-state. The finite period before the input and output fluxes match and the time before the gradient is steady-state is defined by Fick's Second Law. Fick's second law essentially conveys two important concepts of the diffusion process: (i) diffusion is a time-evolving process which eventually results in equilibrium and (ii) diffusion always occurs from high to low concentrations. The diffusion of a simple molecular species is defined by the diffusion

coefficient, which can be understood as the measure of a molecule's ability to traverse through a specific medium over a specific amount time, usually cm^2/sec. Abhyankar and colleagues reported a pure-diffusion gradient generator composed of large reservoirs connected by a straight channel.[136] The device utilized two different porous polyester membranes sandwiched between the source and sink reservoirs. These membranes eradicated convective flow and allowed the gradient to develop via diffusion. Compared to the gradient-generating region, the device also used a very large sink reservoir to keep the concentrations constant and prolong the gradient profile. The 5-mm and 1-mm gradient generating device described in this thesis took a great deal of inspiration from this seminal work. Wu et al. took this concept one step further to incorporate a 3D gradient by developing a novel three part gradient generator: with a hydrogel layers surrounded between two layers of PDMS.[137] The lower layer was patterned with microchannels and concentration applied eventually reached steady-state as the species diffused across the hydrogel layer. The key insight that this work elegantly showed was that complex-shaped gradients over various time scales could be established via simple alterations of the organization or shape of the microchannels. Further advances in free-diffusion based gradient generators over the years have utilized various high fluidic resistance matrices and various microchannel architecture and combinations to generate an assortment of gradient profiles over a variety of time scales.[138]

1.3.3 Considerations for microfluidic gradient generation

When determining which microfluidic gradient generator to employ, a number of factors must be taken into account, as specific methods have intrinsic advantages and limitations, especially when considering application with live cells. Overall, of vital importance is to design the device so that operation is as straightforward as possible in a laboratory environment.

Broadly speaking, flow-based generators are the more commonly used and published methodology used for microfluidic gradient generation.[125] Flow-based generators can provide the experimentalist with spatially and temporally stable gradients with the additional bonus of tightly controlled and finely tuned concentration profiles. The concentration profiles of input molecular species can range from linear, monotonic functions to much more complex periodic and parabolic functions. As long as the flow streams can be maintained at stable velocities and within the laminar flow regime, molecular species can be presented as stable gradients over long periods of time. The principal differentiating quality of flow-based gradient generation over pure-diffusion is that dynamic adjustment of gradient profiles is possible with novel designs and arrangements, providing a unique opportunity to interrogate cellular response due to temporal changes in biochemical gradients. Nevertheless, the flow-based approach is not without limitations. Due to the constant flowing of media that is required to maintain stable streams, cells are continuously exposed to shear stresses on their surfaces and depending on the sensitivity of the cell type this can bias response results.[138] Taken together, flow-based gradient generation is most advantageous to implement when a firmly-controlled and fully-defined biochemical microenvironment is necessary.

Pure-diffusion based gradient generators provide a host of distinct advantages over flow-based devices. Employing static reservoirs in the place of actively flowing fluids, pure-diffusion is practical for cell types that are sensitive to mechanical stresses.[139] The use of ‘infinite’ source and sink reservoirs also eliminates the need for bulky, external equipment that is necessary for propelling convective flow.[140] Though pure-diffusion based gradient generators are less flexible to production of a variety of concentration profiles, they are frequently more straightforward to use, require less reagent volume and can be easily adapted for high-throughput experiments.

Diffusion-based gradient generation is not without its' limitations, however. Due to the principles of spontaneous diffusive transport, the shapes of the gradient profiles are limited in these gradient generators. There is also a lengthy delay in the time leading up to when the gradient reaches steady-state and once steady-state conditions are reached frequent replenishment of the reservoirs are necessary for long-term stability of the concentration profile. Recent reports have established that pneumatic actuation and incorporation of microvalves permits improved temporal control of the gradient profile.[141-143] With all things considered, pure-diffusion based approaches are best suited when effects of cell-secreted factors are experimentally required. Studies have utilized microfluidic gradient generation to create well-defined environmental cues that have led to novel insights across a number of insights across a number of different biological applications.[138]

1.4 *In Vitro* Model Systems

1.4.1 Importance of 3-dimenstional culture

For years, cellular-based experiments looking to progress fundamental knowledge into the intricacies of our organ systems, have relied on the unsound assumption that *in vitro* generated cell monolayers mimic physiological responses of real tissues. In reality, there is conclusive evidence that the highly simplified monolayer cultures fail to recapitulate the tissue-specific architecture, mechanical and chemical signals and cell-cell contact.[144] What is more, these 'petri-dish based' cultures are commonly developed on hard polystyrene or glass culture substrates that are far more rigid than environments found *in vivo*. To address this limitation, the paradigm has shifted away from conventional monolayer culture to 3D cultures. Growing research spanning the past two decades have demonstrated that culturing cells within 3D culture substrates is step towards reducing the gap between archaic 'petri-dish' cultures and live tissues.

Today scientists agree that a 3D approach to cell culture has the potential to improve the physiological significance of cell-based assays.[144, 145]

There are currently two available 3D models that researchers utilize to study the inner biological mechanisms: (i) intact animals and (ii) 3D tissue cultures. Both of these methodologies provide researchers with more physiologically-relevant tissue-specific information. Within intact animals, embryos have provided a great deal of data on the development of cells within their original, nascent physiological environment. Although the work is routinely conducted within an *in vivo* setting, culture of fruitfly and zebrafish embryos *in vitro* has provided researchers with a little flexibility in analysis. Nevertheless, the overall heterogeneity and low transparency of whole animal models can present significant limitations in imaging and reproducible data collection. 3D cell cultures offer a simplified model with a number of variables within the experimentalist's control. Cellular spheroids are 3D systems which leverage the intrinsic propensity of cells to aggregate. Spheroids generated from a number of different cell types are routinely being adopted by for use in therapeutically-relevant biomedical assays, with applications in biotechnology and high-throughput screening.[146-149] The symmetrical, spherical geometry of spheroids also lends itself for straightforward modelling of a number of dynamic cellular processes: including growth, proliferation and invasiveness of tumors.[150, 151] Because the genesis of 3D culture techniques traces back to the beginning of the decade, a streamlined collection of methods for spheroids culture is still lacking. A systematic collection of these methods is crucial to facilitate the transition from monolayer cultures to 3D systems.[152]

Advances in sample handling and imaging techniques have provided a crucial tool in comprehending the benefits of culturing cells in a 3D environment. Conventional microscopy

has its limitations in capturing cellular details of 3D tissues by virtue of samples being hundreds of microns thick and highly light-scattering. There are a number of important factors in achieving quantitative data via imaging: including field of view, extraordinary signal-to-noise ratio, suitable spatial resolution, a low fluorophore excitation rate and rapid image stacking rate.[144] The current state-of-the-art imaging modality for thick specimens is confocal microscopy. However, there are a few of limitations in the technique including: (i) whole planar illumination which increases photobleaching and phototoxic effects on the sample and (ii) restricted depth of penetration when implementing high numerical aperture objectives.[153] Two- or multi-photon microscopy provides a two-fold increase in penetration depth as compared to standard confocal, making it an attractive selection for 3D imaging.[154, 155] Nevertheless, the techniques' low resolution and risk of photobleaching limits the widespread utility of this technique.[156] Tomographic techniques including optical coherence tomography (OCT) and optical projection tomography (OPT) were designed for the imaging of 3D bodies. Using this technique, an object is imaged along multiple angles and the various images are merged together. Both OCT and OPT have been used to image tumor spheroids[157], developing embryos and organs it possesses limitations in terms of recording rate and spatial resolution.[158] In recent years, significant efforts have been placed on improving the spatial resolution of standard optical microscopy. Techniques such as 4Pi-confocal, confocal theta fluorescence and stimulated emission depletion (STED) microscopy have all demonstrated impressive subcellular resolving capabilities however have not yet been employed for 3D objects. Although progress in optical imaging techniques can now reliably capture details in a 3D setting, further advancements are needed to overcome the challenges that hinder high-resolution imaging of thick 3D samples.[159-161]

1.4.2 Hallmarks of tissue-level recapitulation

To fully understand how tissues form and function, it is imperative to study the way in which cells behave as a part of an entire organ system. Although transformation of 2D monolayer culture into 3D cultures represents advancement in the field, even the most elegant 3D culture model fails to recapitulate the microenvironment of living organs. As they currently stand, these 3D cultures fail to incorporate key parameters that are essential to the function of all living organs, including: proper function including spatiotemporal gradients of chemical, active mechanical forces and proper microarchitecture. Because of the inherent limitations in 2D and 3D culture systems, mechanistic analysis of disease processes remains almost wholly dependent on animal studies.[162, 163] Besides being extremely pricey and time-consuming, animal studies often fail to predict responses in humans, as the pharmaceutical industry has come to realize. To address these limitations, there is a new wave of culture platforms called 'organ-on-chip' that looks to bridge the gap between static monolayer cultures and living tissues. The burgeoning 'organ-on-chip' field looks to combine techniques from microfluidics, cell biology, organ physiology and tissue engineering to develop microchips on which human physiology can be studies in an organ-specific context.[145] In terms of engineering culture substrates, the field of microfabrication has proven to be extremely vital towards development of 3D culture platforms mimicking organ-level organization.

Recapitulating the physical microenvironment: Early efforts to microengineer cell culture substrates concentrated on fabricating substrates on which cells could readily adhere. Simply put, these early endeavors aimed to culture cells in such a way that bulk properties such as cell shape, growth, position and differentiation could be easily monitored.[164, 165] Additionally, the majority of these early efforts utilized silicon fabrication and machining techniques that are lengthy, pricey and not readily available. Not surprisingly, the genesis of the organ-on-chip field

coincided with the expansion of the microengineering: with the field enjoying great advancements over the past decade. Today, photolithography, replica molding and microcontact printing have made it possible to develop more complex cell culture platforms that closely resemble the 3D microarchitecture of living tissues and organs.[162, 166] The utilization of the silicone rubber, poly (dimethyl-siloxane) or PDMS, to create devices revolutionized the 'organ-on-chip' field in more ways than one. PDMS has several unique qualities that make it a perfect choice for the fabrication of microdevices for 3D cell cultures including: (i) high gas permeability, (ii) optical transparency for imaging, (iii) affordability and (iv) ease of fabrication.[162] Utilizing replica molding techniques (which is the transfer of topographical patterns from a microfabricated 'master' substrate to a 'mold'), a microfluidic liver chip was created with cell culture and flow chambers separated by a microfluidic barrier that separates hepatocytes from fluid flow in an attempt to recreate the hepatocyte-endothelial interface of the liver sinusoid.[167] A simplified pattern of the kidney was recently created by culturing rat renal tubular epithelial cells on a thin porous membrane and sandwiching them between two microfluidic chambers.[167] The human intestinal villus was architecturally replicated using laser ablation and hydrogel-based molding techniques to produce collagen scaffolds.[168] A similar approach was used to create a network of branched microchannels lined with human mammary epithelial cells in an attempt to recreate the ductal system of human mammary glands.[169] Efforts have been made into recreating an alveolar-capillary interface[170], microfluidic cornea[171] and even tissue interfaces of the brain.[172]

Recapitulating mechanical forces and stresses: A recent advancement in the microfluidic field has enabled a number of groups to tailor the physical microenvironment of the 3D substrates to mimic the physical microenvironment that tissues experience *in vivo*. Mechanical

forces in the form of shear stresses have long been appreciated as a key modulator of differentiated functions in our bodies and efforts made over the past couple of decades have demonstrated that cellular phenotype and genotype is drastically different when mechanical forces are introduced. What is key in incorporating mechanical forces into 3D culture platforms toward recapitulating *in vivo* function is to take organ-specific cues from the body. For example, a lung would require not only constant, but multiple types of mechanical cues simultaneously. A recent 'breathable' lung was fabricated from two PDMS membranes, where a central, horizontal microfluidic channel was home to human alveolar cells on one end and pulmonary vascular endothelial cells on the other.[170] To tailor the mechanical microenvironment of the device, culture medium was continuously flowed through the central channel to induce shear stresses at physiologically-relevant levels (1 dyne/cm^2). Cyclic strains and constant stresses were combined on-chip to create a customized 3D *in vitro* microenvironment. The integration of the strains and stresses on the lung-on-chip device not only encouraged cellular differentiation and multi-layered tissue formation, but it also resulted in the expression of complex functionalities that were never achieved in static monolayer cultures.[170] For one, the culture system demonstrated a number of complex organ-level functionalities including the response to bacteria and inflammatory cytokines: where the intercellular adhesion molecule-1 (ICAM-1) was induced on the endothelium surface. Additionally, the adhesion and transmigration of circulating human neutrophils across the capillary-alveolar interface and the phagocytosis of factious diseases could all be visualized in real time on the lung-on-chip device.

Recreating the chemical microenvironment: Microengineering principles have been applied to cell culture techniques to create chemical microenvironments towards mimicking the relevant chemical milieu towards recapitulation of cellular function. A number of groups have

generated gradients of varying complexities and cultured cells under them to comprehend the effects of variable chemical concentrations on cellular development. The overall goal of all of these efforts is to create an environment *in vitro* that most similarly mimics the environment *in vivo*. The first of these was generated with a microfluidic perfusion culture system equipped with hydrodynamic traps to preserve the morphology and function of murine-isolated pancreatic islet cells from mice.[173] Compared to 'petri-dish cultures', pancreatic islet cells cultures within the chamber resulted in a two-fold increase in endothelial cell density and increased diffusion of serum albumin into the central lumen of the cells.[173] Perfusion-based devices were also combined with 3D liver culture technologies to maintain the liver-specific function and viability the tissue. Oxygen gradients implemented on the device resulted in regional variations in hepatocyte function and transport along the liver sinusoids. These results closely mimicked those attributes of normal liver zonation.[174, 175] In another example, a multilayered chemotaxis of cancer cells during metastasis. These cells were hydrodynamically patterned within a microchannel at specific locations relative to 'source-cells' that secreted a specific chemoattractant and 'sink-cells' that scavenge the chemoattractant.[176] Studies of this system revealed some interesting findings: (i) migration induced by chemotactic factors depends the slope of the chemoattractant-gradient that was generated on the device which could be modulated depending on the distance between the sink and source cells and (ii) the device permitted chemotaxis to occur under much shallower gradients that previously possible.

1.4.3 Key limitations in current intestinal research

Microengineered systems can provide novel tools for studying intestinal crypt development and function. In the past, due to the difficulties of reproducibly isolating and culturing healthy intestinal crypts, it has not been impossible to develop *in vitro* models of the colonic epithelium. As a result previous investigations into intestinal pathophysiology have been

restricted to an *in vivo* context, preventing detailed experimentation and restricting the scope of analysis. With the advent of *in vitro* expansion of intestinal stem cells, what is now needed is an improved microengineered technology that can accurately recreate the complex crypt architecture and biochemical functionalities on an *in vitro* platform. Since microengineered systems possess the ability to dynamically control and monitor the microenvironment of cells and tissues, a novel device can provide an avenue to easily test mechanistic hypotheses in intestinal biology.[6, 70, 97, 177] Microfluidic devices, which permit tight spatial and temporal control on a cell's microenviroment[178-180], have been described for a number of assays on gut physiology however none have tried to replicate the complex 3-D culture environment.[27, 61, 181-184] These assays used tumor cell lines grown on the devices, to mimic a specific function of the gut. Examples of this include assays utilizing tumor cells grown in multiple, porous microchambers to approximate the transfer of a drug and its metabolite.[185-189] Only one of these assays used primary cells (jejunum tissue explants) housed in microperfusion chambers to investigate the metabolic fate of a variety of substances introduced over the explants.[190] Within 3 hours, however, the explants displayed detrimental changes consistent with loss of viability. Efforts have also been made to produce cell-culture substrates with comparable architectures to that of the intestinal crypt.[61, 191, 192] These studies have employed the use of the Caco-2 cell line as a surrogate for the intestinal epithelium. This human colon carcinoma cell line has been adapted for tissue culture and has little resemblance to normal intestine in terms of growth factor response, gene expression and susceptibility to apoptosis.[193] Additionally, these devices were made out of impermeable polymers preventing the possibility of gradient formation.[61, 191] To develop upon the previous assays, substrates produced from hydrogels have been fabricated with pillars and wells to somewhat mimic the topology of the intestine.[192, 194] Although a confluent

monolayer of Caco-2 cells have successfully been demonstrated on these substrates, they have yet to be assessed for the capacity to support primary cells, co-culture of cells or compatibility with a defined gradient across the substrate. To date, no effort has been made to produce a viable, multi-layered colonic epithelium utilizing primary cells with recapitulation of the crypt architecture, stem-cell microenvironment and overall function. Nevertheless, these studies have provided indirect evidence that there is a close interaction of several key signaling pathways, spatially present as protein gradients, in directing intestinal stem-cell renewal and differentiation. Yet how these different pathways coordinate in the specific anatomical compartment of the intestine remains unknown since currently there are no methods to dynamically manipulate the gradients and test mechanistic hypotheses. It is hypothesized that the random cellular distribution is likely due to the lack of defined luminal and basal polarity, resulting in a disorganized epithelium. Consequently, these limitations in culture technology significantly hinder the ability to test the influence of fundamental, morphogenetic cues in crypt homeostasis and cellular organization in healthy and diseased states.

1.5 Figures

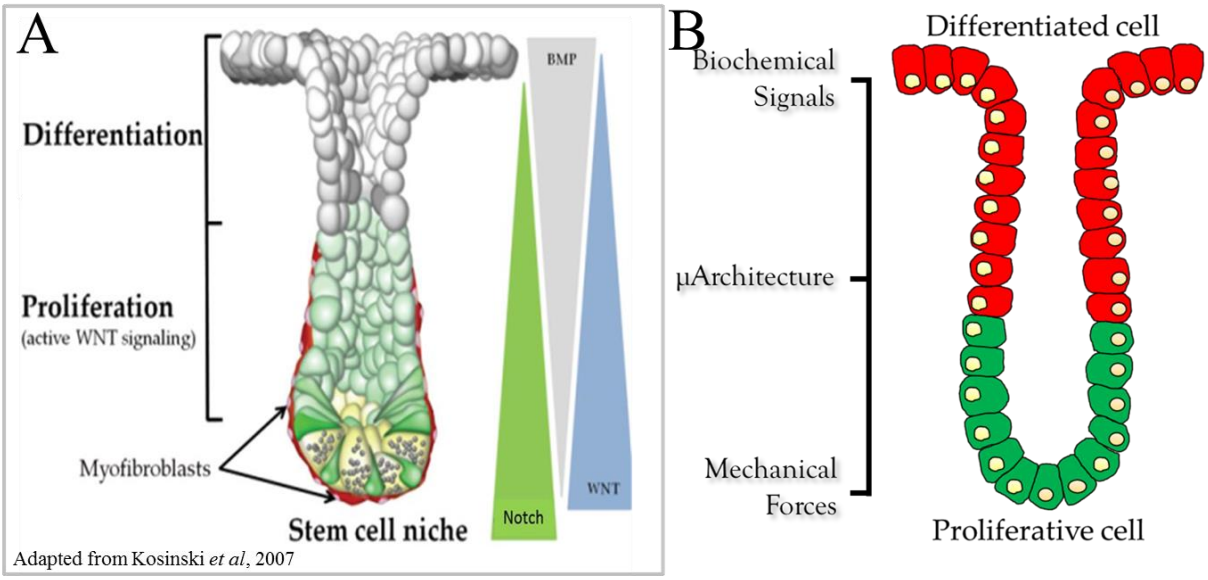

Figure 1.1 Regulation of intestinal homeostasis.

(A) The complex architecture, cell positioning, proliferating/differentiating patterns and overall gut homeostasis are elegantly orchestrated by interplay between mitogens, morphogens, and differentiation factors, which are present as gradients along the crypt axis. (B) To recreate the polarized regions of the intestinal crypt, efforts need to me be made to mimic the relevant biochemical signals, micro-architecture and mechanical forces of the tissue towards recapitulating colonic function.

1.6 REFERENCES

1. Montgomery RK, Mulberg AE, Grand RJ: Development of the human gastrointestinal tract: twenty years of progress. *Gastroenterology* 1999, 116:702-731.

2. Nordgaard I: Colon as a digestive organ - The importance of colonic support for energy absorption as small bowel failure proceeds. *Danish Medical Bulletin* 1998, 45:135-156.

3. Boulpaep EL, Boron WF, Caplan MJ, Cantley L, Igarashi P, Aronson PS, Moczydlowski EG: Medical Physiology a Cellular and Molecular Approach. *Signal Transduction* 2009, 48:27.

4. Gerbe F, Brulin B, Makrini L, Legraverend C, Jay P: DCAMKL-1 Expression Identifies Tuft Cells Rather Than Stem Cells in the Adult Mouse Intestinal Epithelium. *Gastroenterology* 2009, 137:2179-2180.

5. Szmulowicz UM, Hull TL: Colonic Physiology. *Ascrs Textbook of Colon and Rectal Surgery, Second Edition* 2011:23-39.

6. Clevers H: The Intestinal Crypt, A Prototype Stem Cell Compartment. *Cell* 2013, 154:274-284.

7. Jouet P, Coffin B, Lemann M, Gorbatchef C, Franchisseur C, Jian R, Rambaud JC, Flourie B: Tonic and phasic motor activity in the proximal and distal colon of healthy humans. *American Journal of Physiology-Gastrointestinal and Liver Physiology* 1998, 274:G459-G464.

8. Proano M, Camilleri M, Phillips SF, Brown ML, Thomforde GM: TRANSIT OF SOLIDS THROUGH THE HUMAN COLON - REGIONAL QUANTIFICATION IN THE UNPREPARED BOWEL. *American Journal of Physiology* 1990, 258:G856-G862.

9. Topping DL, Clifton PM: Short-chain fatty acids and human colonic function: Roles of resistant starch and nonstarch polysaccharides. *Physiological Reviews* 2001, 81:1031-1064.

10. Hamer HM, Jonkers D, Venema K, Vanhoutvin S, Troost FJ, Brummer RJ: Review article: the role of butyrate on colonic function. *Alimentary Pharmacology & Therapeutics* 2008, 27:104-119.

11. Camilleri M, Bharucha A, Di Lorenzo C, Hasler W, Prather C, Rao S, Wald A: American Neurogastroenterology and Motility Society consensus statement on intraluminal measurement of gastrointestinal and colonic motility in clinical practice. *Neurogastroenterology & Motility* 2008, 20:1269-1282.

12. Harrell L, Chang E: Intestinal water and electrolyte transport. *Sleisenger & Fordtran's gastrointestinal and liver disease: pathophysiology, disease, management 8th ed Philadelphia: Saunders Elsevier* 2006.

13. Phillips SF: Functions of the large bowel: an overview. *Scandinavian journal of gastroenterology Supplement* 1984, 93:1-12.

14. Potten CS, Loeffler M: STEM-CELLS - ATTRIBUTES, CYCLES, SPIRALS, PITFALLS AND UNCERTAINTIES - LESSONS FOR AND FROM THE CRYPT. *Development* 1990, 110:1001-1020.

15. Cheng H, Bjerknes M: CELL PRODUCTION IN MOUSE INTESTINAL EPITHELIUM MEASURED BY STATHMOKINETIC FLOW-CYTOMETRY AND COULTER PARTICLE COUNTING. *Anatomical Record* 1983, 207:427-434.

16. Gerbe F, van Es JH, Makrini L, Brulin B, Mellitzer G, Robine S, Romagnolo B, Shroyer NF, Bourgaux J-F, Pignodel C, et al: Distinct ATOH1 and Neurog3 requirements define tuft cells as a new secretory cell type in the intestinal epithelium. *Journal of Cell Biology* 2011, 192:767-780.

17. Sato T, van Es JH, Snippert HJ, Stange DE, Vries RG, van den Born M, Barker N, Shroyer NF, van de Wetering M, Clevers H, Toshiro S: Paneth cells constitute the niche for Lgr5 stem cells in intestinal crypts. *ArrayExpress Archive* 2012.

18. Yan KS, Chia LA, Li X, Ootani A, Su J, Lee JY, Su N, Luo Y, Heilshorn SC, Amieva MR, et al: The intestinal stem cell markers Bmi1 and Lgr5 identify two functionally distinct populations. *Proceedings of the National Academy of Sciences of the United States of America* 2012, 109:466-471.

19. Clevers H, Nusse R: Wnt/beta-Catenin Signaling and Disease. *Cell* 2012, 149:1192-1205.

20. Crosnier C, Stamataki D, Lewis J: Organizing cell renewal in the intestine: stem cells, signals and combinatorial control. *Nature Reviews Genetics* 2006, 7:349-359.

21. Noah TK, Shroyer NF: Notch in the Intestine: Regulation of Homeostasis and Pathogenesis. *Annual Review of Physiology, Vol 75* 2013, 75:263-288.

22. Gregorieff A, Pinto D, Begthel H, Destree O, Kielman M, Clevers H: Expression pattern of Wnt signaling components in the adult intestine. *Gastroenterology* 2005, 129:626-638.

23. Barker N, van de Wetering M, Clevers H: The intestinal stem cell. *Genes & Development* 2008, 22:1856-1864.

24. Korinek V, Barker N, Moerer P, van Donselaar E, Huls G, Peters PJ, Clevers H: Depletion of epithelial stem-cell compartments in the small intestine of mice lacking Tcf-4. *Nature Genetics* 1998, 19:379-383.

25. van de Wetering M, Sancho E, Verweij C, de Lau W, Oving I, Hurlstone A, van der Horn K, Batlle E, Coudreuse D, Haramis AP, et al: The beta-catenin/TCF-4 complex imposes a crypt progenitor phenotype on colorectal cancer cells. *Cell* 2002, 111:241-250.

26. Potten CS, Kovacs L, Hamilton E: CONTINUOUS LABELING STUDIES ON MOUSE SKIN AND INTESTINE. *Cell and Tissue Kinetics* 1974, 7:271-283.

27. Gracz AD, Ramalingam S, Magness ST: Sox9 expression marks a subset of CD24-expressing small intestine epithelial stem cells that form organoids in vitro. *American Journal of Physiology-Gastrointestinal and Liver Physiology* 2010, 298:G590-G600.

28. Farin HF, Van Es JH, Clevers H: Redundant Sources of Wnt Regulate Intestinal Stem Cells and Promote Formation of Paneth Cells. *Gastroenterology* 2012, 143:1518.

29. Sansom OJ, Reed KR, Hayes AJ, Ireland H, Brinkmann H, Newton IP, Batlle E, Simon-Assmann P, Clevers H, Nathke IS, et al: Loss of Apc in vivo immediately perturbs Wnt signaling, differentiation, and migration. *Genes & Development* 2004, 18:1385-1390.

30. Andreu P, Colnot S, Godard C, Gad S, Chafey P, Niwa-Kawakita M, Laurent-Puig P, Kahn A, Robine S, Perret C, Romagnolo B: Crypt-restricted proliferation and commitment to the Paneth cell lineage following Apc loss in the mouse intestine. *Development* 2005, 132:1443-1451.

31. Mumm JS, Kopan R: Notch signaling: From the outside in. *Developmental Biology* 2000, 228:151-165.

32. Artavanis-Tsakonas S, Rand MD, Lake RJ: Notch signaling: Cell fate control and signal integration in development. *Science* 1999, 284:770-776.

33. Vooijs M, Liu Z, Kopan R: Notch: Architect, Landscaper, and Guardian of the Intestine. *Gastroenterology* 2011, 141:448-459.

34. Schroeder N, Gossler A: Expression of Notch pathway components in fetal and adult mouse small intestine. *Gene Expression Patterns* 2002, 2:247-250.

35. Fre S, Bardin A, Robine S, Louvard D: Notch signaling in intestinal homeostasis across species: the cases of Drosophila, Zebrafish and the mouse. *Experimental Cell Research* 2011, 317:2740-2747.

36. van Es JH, van Gijn ME, Riccio O, van den Born M, Vooijs M, Begthel H, Cozijnsen M, Robine S, Winton DJ, Radtke F, Clevers H: Notch/gamma-secretase inhibition turns proliferative cells in intestinal crypts and adenomas into goblet cells. *Nature* 2005, 435:959-963.

37. Riccio O, van Gijn ME, Bezdek AC, Pellegrinet L, van Es JH, Zimber-Strobl U, Strobl LJ, Honjo T, Clevers H, Radtke F: Loss of intestinal crypt progenitor cells owing to

inactivation of both Notch1 and Notch2 is accompanied by derepression of CDK inhibitors p27(Kip1) and p57(Kip2). *Embo Reports* 2008, 9:377-383.

38. Kazanjian A, Noah T, Brown D, Burkart J, Shroyer NF: Atonal Homolog 1 Is Required for Growth and Differentiation Effects of Notch/gamma-Secretase Inhibitors on Normal and Cancerous Intestinal Epithelial Cells. *Gastroenterology* 2010, 139:918-U299.

39. Yang Q, Bermingham NA, Finegold MJ, Zoghbi HY: Requirement of Math1 for secretory cell lineage commitment in the mouse intestine. *Science* 2001, 294:2155-2158.

40. Zheng X, Tsuchiya K, Okamoto R, Iwasaki M, Kano Y, Sakamoto N, Nakamura T, Watanabe M: Suppression of Hath1 Gene Expression Directly Regulated by Hes1 Via Notch Signaling Is Associated with Goblet Cell Depletion in Ulcerative Colitis. *Inflammatory Bowel Diseases* 2011, 17:2251-2260.

41. Pellegrinet L, Rodilla V, Liu Z, Chen S, Koch U, Espinosa L, Kaestner KH, Kopan R, Lewis J, Radtke F: Dll1- and Dll4-Mediated Notch Signaling Are Required for Homeostasis of Intestinal Stem Cells. *Gastroenterology* 2011, 140:1230.

42. Jensen J, Pedersen EE, Galante P, Hald J, Heller RS, Ishibashi M, Kageyama R, Guillemot F, Serup P, Madsen OD: Control sf endodermal endocrine development by Hes-1. *Nature Genetics* 2000, 24:36-44.

43. VanDussen KL, Carulli AJ, Keeley TM, Patel SR, Puthoff BJ, Magness ST, Tran IT, Maillard I, Siebel C, Kolterud A, et al: Notch signaling modulates proliferation and differentiation of intestinal crypt base columnar stem cells. *Development* 2012, 139:488-497.

44. Wu Y, Cain-Hom C, Choy L, Hagenbeek TJ, de Leon GP, Chen Y, Finkle D, Venook R, Wu X, Ridgway J, et al: Therapeutic antibody targeting of individual Notch receptors. *Nature* 2010, 464:1052-U1122.

45. Ueo T, Imayoshi I, Kobayashi T, Ohtsuka T, Seno H, Nakase H, Chiba T, Kageyama R: The role of Hes genes in intestinal development, homeostasis and tumor formation. *Development* 2012, 139:1071-1082.

46. Itoh S, Itoh F, Goumans MJ, ten Dijke P: Signaling of transforming growth factor-beta family members through Smad proteins. *European Journal of Biochemistry* 2000, 267:6954-6967.

47. He XC, Zhang JW, Tong WG, Tawfik O, Ross J, Scoville DH, Tian Q, Zeng X, He X, Wiedemann LM, et al: BMP signaling inhibits intestinal stem cell self-renewal through suppression of Wnt-beta-catenin signaling. *Nature Genetics* 2004, 36:1117-1121.

48. Haramis APG, Begthel H, van den Born M, van Es J, Jonkheer S, Offerhaus GJA, Clevers H: De novo crypt formation and juvenile polyposis on BMP inhibition in mouse intestine. *Science* 2004, 303:1684-1686.

49. Howe JR, Roth S, Ringold JC, Summers RW, Jarvinen HJ, Sistonen P, Tomlinson IPM, Houlston RS, Bevan S, Mitros FA, et al: Mutations in the SMAD4/DPC4 gene in juvenile polyposis. *Science* 1998, 280:1086-1088.

50. Howe JR, Bair JL, Sayed MG, Anderson ME, Mitros FA, Petersen GM, Velculescu VE, Traverso G, Vogelstein B: Germline mutations of the gene encoding bone morphogenetic protein receptor 1A in juvenile polyposis. *Nature Genetics* 2001, 28:184-187.

51. Auclair BA, Benoit YD, Rivard N, Mishina Y, Perreault N: Bone morphogenetic protein signaling is essential for terminal differentiation of the intestinal secretory cell lineage. *Gastroenterology* 2007, 133:887-896.

52. Itasaki N, Hoppler S: Crosstalk Between Wnt and Bone Morphogenic Protein Signaling: A Turbulent Relationship. *Developmental Dynamics* 2010, 239:16-33.

53. Wice BM, Gordon JI: Forced expression of Id-1 in the adult mouse small intestinal epithelium is associated with development of adenomas. *Journal of Biological Chemistry* 1998, 273:25310-25319.

54. Chan ASW, Tsui WY, Chen X, Chu KM, Chan TL, Chan ASY, Li R, So S, Yuen ST, Leung SY: Downregulation of ID4 by promoter hypermethylation in gastric adenocarcinoma. *Oncogene* 2003, 22:6946-6953.

55. Houlston R, Bevan S, Williams A, Young J, Dunlop M, Rozen P, Eng C, Markie D, Woodford-Richens K, Rodriguez-Bigas MA, et al: Mutations in DPC4 (SMAD4) cause juvenile polyposis syndrome, but only account for a minority of cases. *Human Molecular Genetics* 1998, 7:1907-1912.

56. Hubbard JM, Grothey A: COLORECTAL CANCER IN 2014 Progress in defining first-line and maintenance therapies. *Nature Reviews Clinical Oncology* 2015, 12:73-74.

57. Ireland H, Kemp R, Houghton C, Howard L, Clarke AR, Sansom OJ, Winton DJ: Inducible Cre-mediated control of gene expression in the murine gastrointestinal tract: effect of loss of β-catenin. *Gastroenterology* 2004, 126:1236-1246.

58. Koslowski MJ, Kuebler I, Chamaillard M, Schaeffeler E, Reinisch W, Wang G, Beisner J, Teml A, Peyrin-Biroulet L, Winter S, et al: Genetic Variants of Wnt Transcription Factor TCF-4 (TCF7L2) Putative Promoter Region Are Associated with Small Intestinal Crohn's Disease. *Plos One* 2009, 4.

59. Wehkamp J, Wang G, Kübler I, Nuding S, Gregorieff A, Schnabel A, Kays RJ, Fellermann K, Burk O, Schwab M: The Paneth cell α-defensin deficiency of ileal Crohn's disease is linked to Wnt/Tcf-4. *The Journal of Immunology* 2007, 179:3109-3118.

60. Fre S, Huyghe M, Mourikis P, Robine S, Louvard D, Artavanis-Tsakonas S: Notch signals control the fate of immature progenitor cells in the intestine. *Nature* 2005, 435:964-968.

61. Koo B-K, Stange DE, Sato T, Karthaus W, Farin HF, Huch M, van Es JH, Clevers H: Controlled gene expression in primary Lgr5 organoid cultures. *Nature Methods* 2012, 9:81-U197.

62. Katz JP, Perreault N, Goldstein BG, Lee CS, Labosky PA, Yang VW, Kaestner KH: The zinc-finger transcription factor Klf4 is required for terminal differentiation of goblet cells in the colon. *Development* 2002, 129:2619-2628.

63. Fukaya M, Isohata N, Ohta H, Aoyagi K, Ochiya T, Saeki N, Yanagihara K, Nakanishi Y, Taniguchi H, Sakamoto H, et al: Hedgehog signal activation in gastric pit cell and in diffuse-type gastric cancer. *Gastroenterology* 2006, 131:14-29.

64. Lipkin M: GROWTH AND DEVELOPMENT OF GASTROINTESTINAL CELLS. *Annual Review of Physiology* 1985, 47:175-197.

65. van der Flier LG, Clevers H: Stem Cells, Self-Renewal, and Differentiation in the Intestinal Epithelium. *Annual Review of Physiology* 2009, 71:241-260.

66. Kosinski C, Li VSW, Chan ASY, Zhang J, Ho C, Tsui WY, Chan TL, Mifflin RC, Powell DW, Yuen ST, et al: Gene expression patterns of human colon tops and basal crypts and BMP antagonists as intestinal stem cell niche factors. *Proceedings of the National Academy of Sciences of the United States of America* 2007, 104:15418-15423.

67. Schonhoff SE, Giel-Moloney M, Leiter AB: Neurogenin 3-expressing progenitor cells in the gastrointestinal tract differentiate into both endocrine and non-endocrine cell types. *Developmental Biology* 2004, 270:443-454.

68. Wang Y, Giel-Moloney M, Rindi G, Leiter AB: Enteroendocrine precursors differentiate independently of Wnt and form serotonin expressing adenomas in response to active beta-catenin. *Proceedings of the National Academy of Sciences of the United States of America* 2007, 104:11328-11333.

69. Mariadason JM, Nicholas C, L'Italien KE, Zhuang M, Smartt HJM, Heerdt BG, Yang WC, Corner GA, Wilson AJ, Klampfer L, et al: Gene expression profiling of intestinal epithelial cell maturation along the crypt-villus axis. *Gastroenterology* 2005, 128:1081-1088.

70. Sato T, Vries RG, Snippert HJ, van de Wetering M, Barker N, Stange DE, van Es JH, Abo A, Kujala P, Peters PJ, Clevers H: Single Lgr5 stem cells build crypt-villus structures in vitro without a mesenchymal niche. *Nature* 2009, 459:262-U147.

71. Wright N, Alison M: The biology of epithelial cell populations. Volume 1. *The biology of epithelial cell populations Volume 1* 1984:i-xviii, 1-536.

72. Potten CS: EXTREME SENSITIVITY OF SOME INTESTINAL CRYPT CELLS TO X AND GAMMA-IRRADIATION. *Nature* 1977, 269:518-521.

73. Cheng H, Leblond CP: ORIGIN, DIFFERENTIATION AND RENEWAL OF 4 MAIN EPITHELIAL-CELL TYPES IN MOUSE SMALL INTESTINEUNITARIAN THEORY OF ORIGIN OF 4 EPITHELIAL-CELL TYPES. *American Journal of Anatomy* 1974, 141:537-&.

74. Lin SA, Barker N: Gastrointestinal stem cells in self-renewal and cancer. *Journal of Gastroenterology* 2011, 46:1039-1055.

75. Bonfanti P, Claudinot S, Amici AW, Farley A, Blackburn CC, Barrandon Y: Microenvironmental reprogramming of thymic epithelial cells to skin multipotent stem cells. *Nature* 2010, 466:978-U105.

76. Cairnie AB, Lamerton LF, Steel GG: CELL PROLIFERATION STUDIES IN INTESTINAL EPITHELIUM OF RAT .I. DETERMINATION OF KINETIC PARAMETERS. *Experimental Cell Research* 1965, 39:528-&.

77. Cheng H, Leblond CP: ORIGIN, DIFFERENTIATION AND RENEWAL OF 4 MAIN EPITHELIAL-CELL TYPES IN MOUSE SMALL INTESTINE .1. COLUMNAR CELL. *American Journal of Anatomy* 1974, 141:461-&.

78. Furuyama K, Kawaguchi Y, Akiyama H, Horiguchi M, Kodama S, Kuhara T, Hosokawa S, Elbahrawy A, Soeda T, Koizumi M, et al: Continuous cell supply from a Sox9-expressing progenitor zone in adult liver, exocrine pancreas and intestine. *Nature Genetics* 2011, 43:34-U52.

79. Barker N, van Es JH, Kuipers J, Kujala P, van den Born M, Cozijnsen M, Haegebarth A, Korving J, Begthel H, Peters PJ, Clevers H: Identification of stem cells in small intestine and colon by marker gene Lgr5. *Nature* 2007, 449:1003-U1001.

80. Van der Flier LG, Haegebarth A, Stange DE, Van de Wetering M, Clevers H: OLFM4 Is a Robust Marker for Stem Cells in Human Intestine and Marks a Subset of Colorectal Cancer Cells. *Gastroenterology* 2009, 137:15-17.

81. van der Flier LG, van Gijn ME, Hatzis P, Kujala P, Haegebarth A, Stange DE, Begthel H, van den Born M, Guryev V, Oving I, et al: Transcription Factor Achaete Scute-Like 2 Controls Intestinal Stem Cell Fate. *Cell* 2009, 136:903-912.

82. Sangiorgi E, Capecchi MR: Bmi1 is expressed in vivo in intestinal stem cells. *Nature Genetics* 2008, 40:915-920.

83. Montgomery RK, Carlone DL, Richmond CA, Farilla L, Kranendonk MEG, Henderson DE, Baffour-Awuah NY, Ambruzs DM, Fogli LK, Algra S, Breault DT: Mouse telomerase reverse transcriptase (mTert) expression marks slowly cycling intestinal stem cells. *Proceedings of the National Academy of Sciences of the United States of America* 2011, 108:179-184.

84. Formeister EJ, Sionas AL, Lorance DK, Barkley CL, Lee GH, Magness ST: Distinct SOX9 levels differentially mark stem/progenitor populations and enteroendocrine cells of the small intestine epithelium. *American Journal of Physiology-Gastrointestinal and Liver Physiology* 2009, 296:G1108-G1118.

85. Blache P, van de Wetering M, Duluc I, Domon C, Berta P, Freund JN, Clevers H, Jay P: SOX9 is an intestine crypt transcription factor, is regulated by the Wnt pathway, and represses the CDX2 and MUC2 genes. *Journal of Cell Biology* 2004, 166:37-47.

86. Ramalingam S, Daughtridge GW, Johnston MJ, Gracz AD, Magness ST: Distinct levels of Sox9 expression mark colon epithelial stem cells that form colonoids in culture. *American Journal of Physiology-Gastrointestinal and Liver Physiology* 2012, 302:G10-G20.

87. Cheng H: ORIGIN, DIFFERENTIATION AND RENEWAL OF 4 MAIN EPITHELIAL-CELL TYPES IN MOUSE SMALL INTESTINE .2. MUCOUS CELLS. *American Journal of Anatomy* 1974, 141:481.

88. Cheng H, Leblond CP: ORIGIN, DIFFERENTIATION AND RENEWAL OF 4 MAIN EPITHELIAL-CELL TYPES IN MOUSE SMALL INTESTINE .3. ENTERO-ENDOCRINE CELLS. *American Journal of Anatomy* 1974, 141:503-&.

89. Cheng H: ORIGIN, DIFFERENTIATION AND RENEWAL OF 4 MAIN EPITHELIAL-CELL TYPES IN MOUSE SMALL INTESTINE .4. PANETH CELLS. *American Journal of Anatomy* 1974, 141:521.

90. Gregorieff A, Stange DE, Kujala P, Begthel H, Van den Born M, Korving J, Peters PJ, Clevers H: The Ets-Domain Transcription Factor Spdef Promotes Maturation of Goblet and Paneth Cells in the Intestinal Epithelium. *Gastroenterology* 2009, 137:1333-1345.

91. Jenny M, Uhl C, Roche C, Duluc I, Guillermin V, Guillemot F, Jensen J, Kedinger M, Gradwohl G: Neurogenin3 is differentially required for endocrine cell fate specification in the intestinal and gastric epithelium. *Embo Journal* 2002, 21:6338-6347.

92. Ahmad AA, Wang Y, Gracz AD, Sims CE, Magness ST, Allbritton NL: Optimization of 3-D organotypic primary colonic cultures for organ-on-chip applications. *Journal of Biological Engineering* 2014, 8:9 1754-1611.

93. Barker N, Tan S, Clevers H: Lgr proteins in epithelial stem cell biology. *Development* 2013, 140:2484-2494.

94. Stelzner M, Helmrath M, Dunn JCY, Henning SJ, Houchen CW, Kuo C, Lynch J, Li LH, Magness ST, Martin MG, et al: A nomenclature for intestinal in vitro cultures. *American Journal of Physiology-Gastrointestinal and Liver Physiology* 2012, 302:G1359-G1363.

95. Wang F, Scoville D, He XC, Mahe MM, Box A, Perry JM, Smith NR, Lei NY, Davies PS, Fuller MK, et al: Isolation and Characterization of Intestinal Stem Cells Based on Surface Marker Combinations and Colony-Formation Assay. *Gastroenterology* 2013, 145:383.

96. Jung P, Sato T, Merlos-Suarez A, Barriga FM, Iglesias M, Rossell D, Auer H, Gallardo M, Blasco MA, Sancho E, et al: Isolation and in vitro expansion of human colonic stem cells. *Nature Medicine* 2011, 17:1225-1227.

97. Sato T, Stange DE, Ferrante M, Vries RGJ, van Es JH, van den Brink S, van Houdt WJ, Pronk A, van Gorp J, Siersema PD, Clevers H: Long-term Expansion of Epithelial Organoids From Human Colon, Adenoma, Adenocarcinoma, and Barrett's Epithelium. *Gastroenterology* 2011, 141:1762-1772.

98. Van Landeghem L, Santoro MA, Krebs AE, Mah AT, Dehmer JJ, Gracz AD, Scull BP, McNaughton K, Magness ST, Lund PK: Activation of two distinct Sox9-EGFP-expressing intestinal stem cell populations during crypt regeneration after irradiation. *American Journal of Physiology-Gastrointestinal and Liver Physiology* 2012, 302:G1111-G1132.

99. Gurdon JB, Bourillot PY: Morphogen gradient interpretation. *Nature* 2001, 413:797-803.

100. Goodman CS: Mechanisms and molecules that control growth cone guidance. *Annual Review of Neuroscience* 1996, 19:341-377.

101. Bogenrieder T, Herlyn M: Axis of evil: molecular mechanisms of cancer metastasis. *Oncogene* 2003, 22:6524-6536.

102. Chung BG, Flanagan LA, Rhee SW, Schwartz PH, Lee AP, Monuki ES, Jeon NL: Human neural stem cell growth and differentiation in a gradient-generating microfluidic device. *Lab on a Chip* 2005, 5:401-406.

103. Park JY, Hwang CM, Lee SH, Lee S-H: Gradient generation by an osmotic pump and the behavior of human mesenchymal stem cells under the fetal bovine serum concentration gradient. *Lab on a Chip* 2007, 7:1673-1680.

104. Gupta K, Kim D-H, Ellison D, Smith C, Kundu A, Tuan J, Suh K-Y, Levchenko A: Lab-on-a-chip devices as an emerging platform for stem cell biology. *Lab on a Chip* 2010, 10:2019-2031.

105. Lin F: A MICROFLUIDICS-BASED METHOD FOR ANALYZING LEUKOCYTE MIGRATION TO CHEMOATTRACTANT GRADIENTS. *Methods in Enzymology, Vol 461: Chemokines, Part B* 2009, 461:333-347.

106. Meier M, Lucchetta EM, Ismagilov RF: Chemical stimulation of the Arabidopsis thaliana root using multi-laminar flow on a microfluidic chip. *Lab on a Chip* 2010, 10:2147-2153.

107. Heo YS, Cabrera LM, Bormann CL, Shah CT, Takayama S, Smith GD: Dynamic microfunnel culture enhances mouse embryo development and pregnancy rates. *Human Reproduction* 2010, 25:613-622.

108. Wang SJ, Saadi W, Lin F, Nguyen CMC, Jeon NL: Differential effects of EGF gradient profiles on MDA-MB-231 breast cancer cell chemotaxis. *Experimental Cell Research* 2004, 300:180-189.

109. Saadi W, Wang SJ, Lin F, Jeon NL: A parallel-gradient microfluidic chamber for quantitative analysis of breast cancer cell chemotaxis. *Biomedical Microdevices* 2006, 8:109-118.

110. Saadi W, Rhee SW, Lin F, Vahidi B, Chung BG, Jeon NL: Generation of stable concentration gradients in 2D and 3D environments using a microfluidic ladder chamber. *Biomedical Microdevices* 2007, 9:627-635.

111. Nandagopal S, Wu D, Lin F: Combinatorial Guidance by CCR7 Ligands for T Lymphocytes Migration in Co-Existing Chemokine Fields. *Plos One* 2011, 6.

112. Lin F, Nguyen CMC, Wang SJ, Saadi W, Gross SP, Jeon NL: Effective neutrophil chemotaxis is strongly influenced by mean IL-8 concentration. *Biochemical and Biophysical Research Communications* 2004, 319:576-581.

113. Li GN, Liu J, Hoffman-Kim D: Multi-molecular gradients of permissive and inhibitory cues direct neurite outgrowth. *Annals of Biomedical Engineering* 2008, 36:889-904.

114. Kothapalli CR, van Veen E, de Valence S, Chung S, Zervantonakis IK, Gertler FB, Kamm RD: A high-throughput microfluidic assay to study neurite response to growth factor gradients. *Lab on a Chip* 2011, 11:497-507.

115. Boyden S: CHEMOTACTIC EFFECT OF MIXTURES OF ANTIBODY AND ANTIGEN ON POLYMORPHONUCLEAR LEUCOCYTES. *Journal of Experimental Medicine* 1962, 115:453-&.

116. Zigmond SH, Hirsch JG: LEUKOCYTE LOCOMOTION AND CHEMOTAXIS NEW METHODS FOR EVALUATION, AND DEMONSTRATION OF A CELL-DERIVED CHEMOTACTIC FACTOR. *The Journal of experimental medicine* 1973, 137:387-410.

117. Zicha D, Dunn GA, Brown AF: A NEW DIRECT-VIEWING CHEMOTAXIS CHAMBER. *Journal of Cell Science* 1991, 99:769-775.

118. Purcell EM: Life at low Reynolds number. *Am J Phys* 1977, 45:3-11.

119. Walker GM, Zeringue HC, Beebe DJ: Microenvironment design considerations for cellular scale studies. *Lab on a Chip* 2004, 4:91-97.

120. Park JY, Kim S-K, Woo D-H, Lee E-J, Kim J-H, Lee S-H: Differentiation of Neural Progenitor Cells in a Microfluidic Chip-Generated Cytokine Gradient. *Stem Cells* 2009, 27:2646-2654.

121. Morel M, Galas J-C, Dahan M, Studer V: Concentration landscape generators for shear free dynamic chemical stimulation. *Lab on a Chip* 2012, 12:1340-1346.

122. Atencia J, Beebe DJ: Controlled microfluidic interfaces. *Nature* 2005, 437:648-655.

123. Santiago JG, Wereley ST, Meinhart CD, Beebe D, Adrian RJ: A particle image velocimetry system for microfluidics. *Experiments in fluids* 1998, 25:316-319.

124. Berthier E, Beebe D: Gradient generation platforms: new directions for an established microfluidic technology. *Lab Chip* 2014.

125. Kim S, Kim HJ, Jeon NL: Biological applications of microfluidic gradient devices. *Integrative Biology* 2010, 2:584-603.

126. Squires TM, Messinger RJ, Manalis SR: Making it stick: convection, reaction and diffusion in surface-based biosensors. *Nature Biotechnology* 2008, 26:417-426.

127. Hatch A, Kamholz AE, Hawkins KR, Munson MS, Schilling EA, Weigl BH, Yager P: A rapid diffusion immunoassay in a T-sensor. *Nature Biotechnology* 2001, 19:461-465.

128. Kamholz AE, Schilling EA, Yager P: Optical measurement of transverse molecular diffusion in a microchannel. *Biophysical Journal* 2001, 80:1967-1972.

129. Ismagilov RF, Stroock AD, Kenis PJA, Whitesides G, Stone HA: Experimental and theoretical scaling laws for transverse diffusive broadening in two-phase laminar flows in microchannels. *Applied Physics Letters* 2000, 76:2376-2378.

130. Jeon NL, Dertinger SKW, Chiu DT, Choi IS, Stroock AD, Whitesides GM: Generation of solution and surface gradients using microfluidic systems. *Langmuir* 2000, 16:8311-8316.

131. Dertinger SKW, Chiu DT, Jeon NL, Whitesides GM: Generation of gradients having complex shapes using microfluidic networks. *Analytical Chemistry* 2001, 73:1240-1246.

132. Shamloo A, Ma N, Poo M-m, Sohn LL, Heilshorn SC: Endothelial cell polarization and chemotaxis in a microfluidic device. *Lab on a Chip* 2008, 8:1292-1299.

133. Atencia J, Morrow J, Locascio LE: The microfluidic palette: A diffusive gradient generator with spatio-temporal control. *Lab on a Chip* 2009, 9:2707-2714.

134. Cheng S-Y, Heilman S, Wasserman M, Archer S, Shuler ML, Wu M: A hydrogel-based microfluidic device for the studies of directed cell migration. *Lab on a Chip* 2007, 7:763-769.

135. Haessler U, Kalinin Y, Swartz MA, Wu M: An agarose-based microfluidic platform with a gradient buffer for 3D chemotaxis studies. *Biomedical Microdevices* 2009, 11:827-835.

136. Abhyankar VV, Lokuta MA, Huttenlocher A, Beebe DJ: Characterization of a membrane-based gradient generator for use in cell-signaling studies. *Lab on a Chip* 2006, 6:389-393.

137. Wu HK, Huang B, Zare RN: Generation of complex, static solution gradients in microfluidic channels. *Journal of the American Chemical Society* 2006, 128:4194-4195.

138. Toh AGG, Wang ZP, Yang C, Nam-Trung N: Engineering microfluidic concentration gradient generators for biological applications. *Microfluidics and Nanofluidics* 2014, 16:1-18.

139. Paliwal S, Iglesias PA, Campbell K, Hilioti Z, Groisman A, Levchenko A: MAPK-mediated bimodal gene expression and adaptive gradient sensing in yeast. *Nature* 2007, 446:46-51.

140. Kim M, Kim T: Diffusion-Based and Long-Range Concentration Gradients of Multiple Chemicals for Bacterial Chemotaxis Assays. *Analytical Chemistry* 2010, 82:9401-9409.

141. Irimia D, Geba DA, Toner M: Universal microfluidic gradient generator. *Analytical Chemistry* 2006, 78:3472-3477.

142. Keenan TM, Frevert CW, Wu A, Wong V, Folch A: A new method for studying gradient-induced neutrophil desensitization based on an open microfluidic chamber. *Lab on a Chip* 2010, 10:116-122.

143. Herzmark P, Campbell K, Wang F, Wong K, El-Samad H, Groisman A, Bourne HR: Bound attractant at the leading vs. the trailing edge determines chemotactic prowess. *Proceedings of the National Academy of Sciences of the United States of America* 2007, 104:13349-13354.

144. Pampaloni F, Reynaud EG, Stelzer EHK: The third dimension bridges the gap between cell culture and live tissue. *Nature Reviews Molecular Cell Biology* 2007, 8:839-845.

145. Huh D, Torisawa Y-s, Hamilton GA, Kim HJ, Ingber DE: Microengineered physiological biomimicry: Organs-on-Chips. *Lab on a Chip* 2012, 12:2156-2164.

146. Mueller-Klieser W: Three-dimensional cell cultures: From molecular mechanisms to clinical applications. *American Journal of Physiology* 1997, 273:C1109-C1123.

147. Kale S, Biermann S, Edwards C, Tarnowski C, Morris M, Long MW: Three-dimensional cellular development is essential for ex vivo formation of human bone. *Nature Biotechnology* 2000, 18:954-958.

148. Zhang XL, Wang W, Yu WT, Xie YB, Zhang XH, Zhang Y, Ma XJ: Development of an in vitro multicellular tumor spheroid model using microencapsulation and its application in anticancer drug screening and testing. *Biotechnology Progress* 2005, 21:1289-1296.

149. Ivascu A, Kubbies M: Rapid generation of single-tumor spheroids for high-throughput cell function and toxicity analysis. *Journal of Biomolecular Screening* 2006, 11:922-932.

150. Stein AM, Demuth T, Mobley D, Berens M, Sander LM: A mathematical model of glioblastoma tumor spheroid invasion in a three-dimensional in vitro experiment. *Biophysical Journal* 2007, 92:356-365.

151. Jiang Y, Pjesivac-Grbovic J, Cantrell C, Freyer JP: A multiscale model for avascular tumor growth. *Biophysical journal* 2005, 89:3884-3894.

152. Griffith LG, Swartz MA: Capturing complex 3D tissue physiology in vitro. *Nature Reviews Molecular Cell Biology* 2006, 7:211-224.

153. Verveer PJ, Swoger J, Pampaloni F, Greger K, Marcello M, Stelzer EHK: High-resolution three-dimensional imaging of large specimens with light sheet-based microscopy. *Nature Methods* 2007, 4:311-313.

154. Gilbert RJ, Hoffman M, Capitano A, So PT: Imaging of three-dimensional epithelial architecture and function in cultured CaCo2a monolayers with two-photon excitation microscopy. *Microscopy research and technique* 2000, 51:204-210.

155. Hadjantonakis AK, Dickinson ME, Fraser SE, Papaioannou VE: Technicolour transgenics: Imaging tools for functional genomics in the mouse. *Nature Reviews Genetics* 2003, 4:613-625.

156. Hell S, Stelzer EHK: PROPERTIES OF A 4PI CONFOCAL FLUORESCENCE MICROSCOPE. *Journal of the Optical Society of America a-Optics Image Science and Vision* 1992, 9:2159-2166.

157. Sharma M, Verma Y, Rao KD, Nair R, Gupta PK: Imaging growth dynamics of tumour spheroids using optical coherence tomography. *Biotechnology Letters* 2007, 29:273-278.

158. Dickinson ME: Multimodal imaging of mouse development: Tools for the postgenomic era. *Developmental Dynamics* 2006, 235:2386-2400.

159. Willig KI, Kellner RR, Medda R, Hein B, Jakobs S, Hell SW: Nanoscale resolution in GFP-based microscopy. *Nature Methods* 2006, 3:721-723.

160. Klar TA, Jakobs S, Dyba M, Egner A, Hell SW: Fluorescence microscopy with diffraction resolution barrier broken by stimulated emission. *Proceedings of the National Academy of Sciences of the United States of America* 2000, 97:8206-8210.

161. Alanentalo T, Asayesh A, Morrison H, Loren CE, Holmberg D, Sharpe J, Ahlgren U: Tomographic molecular imaging and 3D quantification within adult mouse organs. *Nature Methods* 2007, 4:31-33.

162. Huh D, Hamilton GA, Ingber DE: From 3D cell culture to organs-on-chips. *Trends in Cell Biology* 2011, 21:745-754.

163. Kim HJ, Huh D, Hamilton G, Ingber DE: Human gut-on-a-chip inhabited by microbial flora that experiences intestinal peristalsis-like motions and flow. *Lab on a Chip* 2012, 12:2165-2174.

164. Chen CS, Mrksich M, Huang S, Whitesides GM, Ingber DE: Geometric control of cell life and death. *Science* 1997, 276:1425-1428.

165. Singhvi R, Kumar A, Lopez GP, Stephanopoulos GN, Wang DIC, Whitesides GM, Ingber DE: ENGINEERING CELL-SHAPE AND FUNCTION. *Science* 1994, 264:696-698.

166. El-Ali J, Sorger PK, Jensen KF: Cells on chips. *Nature* 2006, 442:403-411.

167. Nakao Y, Kimura H, Sakai Y, Fujii T: Bile canaliculi formation by aligning rat primary hepatocytes in a microfluidic device. *Biomicrofluidics* 2011, 5.

168. Sung JH, Yu J, Luo D, Shuler ML, March JC: Microscale 3-D hydrogel scaffold for biomimetic gastrointestinal (GI) tract model. *Lab on a Chip* 2011, 11:389-392.

169. Grafton MMG, Wang L, Vidi P-A, Leary J, Lelievre SA: Breast on-a-chip: mimicry of the channeling system of the breast for development of theranostics. *Integrative Biology* 2011, 3:451-459.

170. Huh D, Matthews BD, Mammoto A, Montoya-Zavala M, Hsin HY, Ingber DE: Reconstituting Organ-Level Lung Functions on a Chip. *Science* 2010, 328:1662-1668.

171. Puleo CM, Ambrose WM, Takezawa T, Elisseeff J, Wang T-H: Integration and application of vitrified collagen in multilayered microfluidic devices for corneal microtissue culture. *Lab on a Chip* 2009, 9:3221-3227.

172. Peyrin J-M, Deleglise B, Saias L, Vignes M, Gougis P, Magnifico S, Betuing S, Pietri M, Caboche J, Vanhoutte P, et al: Axon diodes for the reconstruction of oriented neuronal networks in microfluidic chambers. *Lab on a Chip* 2011, 11:3663-3673.

173. Sankar KS, Green BJ, Crocker AR, Verity JE, Altamentova SM, Rocheleau JV: Culturing Pancreatic Islets in Microfluidic Flow Enhances Morphology of the Associated Endothelial Cells. *Plos One* 2011, 6.

174. Goral VN, Hsieh Y-C, Petzold ON, Clark JS, Yuen PK, Faris RA: Perfusion-based microfluidic device for three-dimensional dynamic primary human hepatocyte cell culture in the absence of biological or synthetic matrices or coagulants. *Lab on a Chip* 2010, 10:3380-3386.

175. Domansky K, Inman W, Serdy J, Dash A, Lim MHM, Griffith LG: Perfused multiwell plate for 3D liver tissue engineering. *Lab on a Chip* 2010, 10:51-58.

176. Torisawa Y-s, Mosadegh B, Bersano-Begey T, Steele JM, Luker KE, Luker GD, Takayama S: Microfluidic platform for chemotaxis in gradients formed by CXCL12 source-sink cells. *Integrative Biology* 2010, 2:680-686.

177. Sato T, Clevers H: Growing Self-Organizing Mini-Guts from a Single Intestinal Stem Cell: Mechanism and Applications. *Science* 2013, 340:1190-1194.

178. Rosenberg DW, Giardina C, Tanaka T: Mouse models for the study of colon carcinogenesis. *Carcinogenesis* 2009, 30:183-196.

179. Barker N, Ridgway RA, van Es JH, van de Wetering M, Begthel H, van den Born M, Danenberg E, Clarke AR, Sansom OJ, Clevers H: Crypt stem cells as the cells-of-origin of intestinal cancer. *Nature* 2009, 457:608-U119.

180. Takayama T, Miyanishi K, Hayashi T, Kukitsu T, Takanashi K, Ishiwatari H, Kogawa T, Abe T, Niitsu Y: Aberrant crypt foci: detection, gene abnormalities, and clinical usefulness. *Clinical gastroenterology and hepatology : the official clinical practice journal of the American Gastroenterological Association* 2005, 3:S42-45.

181. Ootani A, Li XN, Sangiorgi E, Ho QT, Ueno H, Toda S, Sugihara H, Fujimoto K, Weissman IL, Capecchi MR, Kuo CJ: Sustained in vitro intestinal epithelial culture within a Wnt-dependent stem cell niche. *Nature Medicine* 2009, 15:1-U140.

182. Kim HJ, Ingber DE: Gut-on-a-Chip microenvironment induces human intestinal cells to undergo villus differentiation. *Integrative Biology* 2013, 5:1130-1140.

183. Miyoshi H, Stappenbeck TS: Counteracting stem cell expansion during wound repair Distinct roles of non-canonical Wnt and TGF-beta. *Cell Cycle* 2013, 12:387-388.

184. de Lau W, Barker N, Low TY, Koo B-K, Li VSW, Teunissen H, Kujala P, Haegebarth A, Peters PJ, van de Wetering M, et al: Lgr5 homologues associate with Wnt receptors and mediate R-spondin signalling. *Nature* 2011, 476:293-U257.

185. Sodhi CP, Neal MD, Siggers R, Sho S, Ma C, Branca MF, Prindle T, Jr., Russo AM, Afrazi A, Good M, et al: Intestinal Epithelial Toll-Like Receptor 4 Regulates Goblet Cell Development and Is Required for Necrotizing Enterocolitis in Mice. *Gastroenterology* 2012, 143:708-U234.

186. Ruffner H, Sprunger J, Charlat O, Leighton-Davies J, Grosshans B, Salathe A, Zietzling S, Beck V, Therier M, Isken A, et al: R-Spondin Potentiates Wnt/beta-Catenin Signaling through Orphan Receptors LGR4 and LGR5. *Plos One* 2012, 7.

187. Mustata RC, Van Loy T, Lefort A, Libert F, Strollo S, Vassart G, Garcia M-I: Lgr4 is required for Paneth cell differentiation and maintenance of intestinal stem cells ex vivo. *Embo Reports* 2011, 12:558-564.

188. Barry ER, Morikawa T, Butler BL, Shrestha K, de la Rosa R, Yan KS, Fuchs CS, Magness ST, Smits R, Ogino S, et al: Restriction of intestinal stem cell expansion and the regenerative response by YAP. *Nature* 2013, 493:106.

189. Fafilek B, Krausova M, Vojtechova M, Pospichalova V, Tumova L, Sloncova E, Huranova M, Stancikova J, Hlavata A, Svec J, et al: Troy, a Tumor Necrosis Factor Receptor Family Member, Interacts With Lgr5 to Inhibit Wnt Signaling in Intestinal Stem Cells. *Gastroenterology* 2013, 144:381-391.

190. Mizutani T, Nakamura T, Morikawa R, Fukuda M, Mochizuki W, Yamauchi Y, Nozaki K, Yui S, Nemoto Y, Nagaishi T, et al: Real-time analysis of P-glycoprotein-mediated drug transport across primary intestinal epithelium three-dimensionally cultured in vitro. *Biochemical and Biophysical Research Communications* 2012, 419:238-243.

191. Yui S, Nakamura T, Sato T, Nemoto Y, Mizutani T, Zheng X, Ichinose S, Nagaishi T, Okamoto R, Tsuchiya K, et al: Functional engraftment of colon epithelium expanded in vitro from a single adult Lgr5(+) stem cell. *Nature Medicine* 2012, 18:618-623.

192. Schwitalla S, Fingerle AA, Cammareri P, Nebelsiek T, Goektuna SI, Ziegler PK, Canli O, Heijmans J, Huels DJ, Moreaux G, et al: Intestinal Tumorigenesis Initiated by Dedifferentiation and Acquisition of Stem-Cell-like Properties. *Cell* 2013, 152:25-38.

193. van der Meer AD, van den Berg A: Organs-on-chips: breaking the in vitro impasse. *Integrative Biology* 2012, 4:461-470.

194. Schepers AG, Snippert HJ, Stange DE, van den Born M, van Es JH, van de Wetering M, Clevers H: Lineage Tracing Reveals Lgr5(+) Stem Cell Activity in Mouse Intestinal Adenomas. *Science* 2012, 337:730-735.

CHAPTER 2: OPTIMIZATION OF 3-D ORGANOTYPIC PRIMARY COLONIC CULTURES FOR ORGAN-ON-CHIP APPLICATIONS

2.1 Introduction

Self-renewal of the colonic epithelium is driven by the proliferation of epithelial stem cells located at the base of the functional tissue subunit called the colon crypt. The rapid regeneration to renew the epithelium is driven by colonic epithelial stem cells (CESCs). Understanding the CESC biology and conditions impacting their growth and differentiation is an active area of research.[1-3] The colonic epithelium is negatively impacted by a number of inflammatory diseases, cancer and acute injuries. The high incidence of colorectal cancer (CRC) in the Western World is believed to be in part due to the high proliferation rate of the epithelial lining, and increasing evidence strongly suggests CRC may arise at the level of the stem cell.[4,5] Inflammatory bowel diseases including ulcerative colitis and Crohn's disease result from attack on the crypt cells by inflammatory infiltrates.[6,7] Due to technical challenges for the *in vitro* assessment of colonic mucosa and crypts, studies of colonic physiology and pathophysiology have been restricted primarily to *in vivo* inspection. *In vivo* studies by endoscopy or noninvasive imaging have enabled examination of living colonic tissue at a macroscopic, but not cellular scale. Histological evaluation of fixed tissue has permitted study at the cellular level, but with the loss of the rich and dynamic qualities of the living tissue.

Recent breakthroughs in the understanding of fundamental morphogenetic pathways and their contributions to intestinal homeostasis have enabled culture methods to be devised that successfully generate 3-D crypt-like cellular spheroids, or 'colonoids', from isolated crypts or

purified stem cells.[3,8-11] Colonoids are sustainable *in vitro* for long periods up to a year. Rapid *ex vivo* establishment of colonoids in culture is potentiated by three factors: Wnt-3A, the Wnt-agonist R-spondin1 and the BMP-antagonist Noggin. *In vivo*, Wnt-3A is essential for stem cell maintenance;[8] excess R-spondin1 induces hyperplasia; Noggin at supraphysiologic concentrations produces an expansion in crypt numbers.[11] In the colonoid-culture system, CESCs, progenitors and differentiated cell lineages are present, and their composition can be adjusted by the concentration of these and other growth factors.[3] The availability of the colonoid culture system is expected to open the door to future investigations into the CESC niche and the contribution of morphogenetic cues in crypt homeostasis and organization.[12] These organotypic culture methods will have widespread impact on studies of intestinal biology, host-pathogen interactions, neoplasia and regenerative medicine. Furthermore, a better understanding of the optimal crypt isolation and culture conditions may enable the creation of novel microscale devices to recapitulate gut function *in vitro* using primary cells.

While three-dimensional (3-D) cell culture systems better mimic the microstructure of intact organs relative to 2-D cultures, the 3-D systems still fail to fully recapitulate organ-level physiologic functions presumably due to an inability to fully control the microenvironment of the organoid. Consequently, a growing trend is to build 'organ-on-chip' devices which integrate the 3-D tissue culture systems with microdevice technologies to offer enhanced control of both surface and fluidic conditions.[13-16] However due to the difficulty in obtaining and isolating primary tissue, these 'organ-on-chip' devices often utilize tumor cell lines which are incapable of demonstrating organ-level physiologic function. For example, 'gut-on-chips' devices are frequently assembled by placing Caco-2 tumor cells within microdevices.[17-19] The Caco-2 tumor cell line has been adapted for tissue culture and poorly mimics the intestinal epithelium in terms

of architecture, growth factor response, differentiation, gene expression and susceptibility to apoptosis.[20,21] A significant challenge to the 'organ-on-chip' community is the development of optimized strategies to isolate high-quality primary cells for culture within a microdevice.

Although recent work has enhanced *in vitro* intestinal culture, isolation of the crypts and propagation of the colonoids has not been systematically optimized. Existing protocols fail to quantify overall yield and viability of the isolated crypts over time. The current work focuses on maximizing the yield of viable, high-quality crypts obtained from resected colon and enhancing the overall culture efficiency to produce large numbers of living colonoids from the isolated crypts. Since the cell microenvironment impacts colon cell fate and function, further characterization of the matrix concentration and identification of biocompatible substrates for colonoid culture were also performed. Microengineered environments are increasingly used to direct tissue and stem cell organization so that commonly used materials for microfabrication (including glass, polydimethoxysilane, polystyrene and epoxy photoresists) were assessed for their ability to support colonoid formation. This paper focuses on three major points of emphasis: 1) standardization of crypt isolation protocol, 2) optimization of Matrigel concentration for colonoid formation, and 3) crypt cell interaction with various substrates. We believe this research will support future development of intestinal studies and 'organ-on-chip' endeavors.

2.2 Materials and Methods

2.2.1 Materials

N2 and B27 supplements, GlutaMAX, Advanced DMEM/F12 base media, 5-ethynyl-2′-deoxyuridine (EdU) kit and α-goat-Alexa Fluor 488 were purchased from Invitrogen (Carlsbad, CA). Y27632 Rock inhibitor, HEPES buffer, N-acetylcysteine (NAC), ethyl-enediaminetetraacetic acid (EDTA, 0.5 M, pH 8.0), bis-Benzimide (Hoescht 33342), and α–rabbit-Cy3 were obtained from Sigma-Aldrich (St. Louis, MO). Cell-culture-grade bovine serum

albumin (BSA), dithiothreitol (DTT) and a pulse vortex-mixer were purchased from Thermo-Fisher (Fairlawn, NJ). Recombinant mouse Wnt-3a, recombinant human R-Spondin1 and recombinant mouse EGF were acquired from R&D Systems (Minneapolis, MN). Growth-factor reduced Matrigel was obtained from BD Biosciences (Bedford, MA). Recombinant mouse Noggin was purchased from Peprotech (Rocky Hill, NJ). Sylgard 184 silicone elastomer kit was procured from Dow Corning (Midland, MI). EPON epoxy resin 1002 F (fusion solids) was purchased from Miller Stephenson Chemical Co. (Sylmar, CA). Primary antibodies α -mucin2 and α-chromogranin A were purchased from Santa Cruz Biotechnology (Santa Cruz, CA).

2.2.2 Transgenic mouse model and isolation of colonic crypts

The *Sox9*eGFP-CAGDsRed mouse model on a CD-1 background was used for experimental analysis. The CAGDsRed mouse line ubiquitously expresses the red fluorescent protein DsRed under the control of a chicken beta-actin promoter (CAG). The DsRed-expressing mice were bred with *Sox9*eGFP mice, which possessed the *Sox9* promoter controlling eGFP (enhanced green fluorescent protein) expression on a modified bacterial artificial chromosome (BAC).[3] Previous work demonstrated that *Sox9* is expressed in the stem and progenitor cells of the colon so that the *Sox9*eGFP mouse possesses eGFP expression in the stem/proliferative cell compartment at the crypt base. For stem/progenitor cell quantification within fresh crypts, monolayers and colonoids, eGFP fluorescence was used as a measure of *Sox9* expression After resecting the distal colon from a 6–9 week-old mouse, the colon was cut longitudinally, flushed of its contents and washed with chilled rinse buffer (5.6 mM Na_2HPO_4, 8.0 mM KH_2PO_4, 96.2 mM NaCl, 1.6 mM KCl, 43.4 mM sucrose, 54.9 mM D-sorbitol, pH 7).[20] The distal colon was then incubated in isolation buffer (rinse buffer + 2.0 mM EDTA + 0.5 mM DTT), for 30, 60 or 90 min at 22ºC as indicated in the text. The tissue was washed by transferring to 3 separate vials

containing chilled rinse buffer. The sample was then agitated at 2.7 × g for 5 seconds using a pulsing vortex mixer, unless stated otherwise in the text. The crypts were inspected by brightfield microscopy for the presence of a defined lumen. The overall yield was determined by adding a 250 μL crypt-suspension to a 12-well plate and using a 4× objective to count the number of crypts per field of view. This number was then used to calculate the number of crypts in the total volume of crypt-suspension.

2.2.3 Culture of colonic crypts for matrigel optimization

A microwell fabricated from thick 1002 F photoresist was used for facile tracking of the colonoids to optimize the Matrigel concentration. To assess the effect of Matrigel on colonoid formation, Matrigel was diluted in complete culture medium (CCM: advanced DMEM-F12 with N2 supplement, B27 supplement, 1× GlutaMAX, 10 μM HEPES buffer, 1 μg/mL penicillin, 1 μg/mL streptomycin, 3.2 mg/mL Y27632 and 163.2 mg/mL NAC) at 4 °C to yield 25, 50, 75 and 100 vol% concentrations. The microwells were sterilized with ethanol, washed × 3 in rinse buffer, and placed at 4ºC before plating the crypts. A 400-μL suspension of crypts was added to each microwell (5000 crypts/mL) and the crypts were allowed to settle into the wells for 2 min. The supernatant was then carefully removed and ice-cold Matrigel (400 μL) was overlaid. The Matrigel was supplemented with the following growth factor concentrations: 5 ng/mL Wnt-3a, 50 ng/mL EGF, 100 ng/mL Noggin and 1 μg/mL R-spondin1.[3] Matrigel was polymerized for 15 min at 37ºC. After polymerization, 1.6 mL of complete culture medium was overlaid onto the Matrigel. Growth factors were replenished by direct addition to the medium every 2 days and the medium was changed every 4 days. R-spondin1 was used at 1 μg/mL for the initial plating and 500 ng/mL for the duration of the culture. Y27632 and NAC were only included in the CCM at the time of initial plating and were removed from subsequent culture media.

2.2.4 Calculation of acceleration intensity

The pulsing vortex mixer (Fisher Scientific, Catalog # 02-215-375) produced acceleration profiles in the x-, y-, and z-directions. The acceleration of 6 different settings on the vortex mixer (800–1800 rpm) was measured over time using a 3-D accelerometer (Gulf Coast Data Concepts, Catalog# X16-1C). The magnitude of the x-, y-, and z-direction acceleration vectors was calculated from these measurements. The average magnitude over time was then used as the average accelerated intensity for each direciton.

2.2.5 Culture of crypts on microfabrication substrates

Five different common microfabrication substrates were tested for the culture of crypts on their surface: PDMS, polystyrene (tissue-culture treated), glass, and the photoresists SU-8 and 1002 F. Round glass coverslips (#1, diameter = 25 mm) were spin-coated with PDMS, SU-8 or 1002 F, baked and cured, sterilized with ethanol, and placed in a 6-well plate. Before culturing, the substrates were coated with 50% Matrigel at 4°C for 8 h. A 200 μL crypt suspension (5000 crypts/mL) in Matrigel (50% in CCM unless otherwise stated) was added to each of the 6 wells. The plate was then placed at 4°C for 10 min to ensure that the crypts traveled through the liquid gel and settled onto the experimental substrate. Subsequently, the gel was polymerized at 37°C for 15 min. After polymerization, the crypts were overlaid with CCM. Growth factor and media exchange was performed as described above.

2.2.6 EdU analysis and immunostaining

Crypts and colonoids from wild-type mice were used for EdU analysis[22] and immunostaining. 5-ethynyl-2′-deoxyuridine (EdU) nucleoside was used to assess proliferation as per manufacturer's instructions: EdU (10 μM) was added to the culture medium and allowed to become incorporated into the cells for 4 h. The culture medium was then removed, and the entire

culture was fixed using 3.7% paraformaldehyde in phosphate-buffered saline (PBS) for 20 min at room temperature. Cells in the fixed colonoids were permeabilized using 0.5% Triton X-100 in PBS for 20 min, followed by washing × 3 with PBS containing 3% BSA. Each quadrant of the microwell was then incubated with 250 μL of click-it reaction cocktail (containing the Alexa Fluor-555 azide) for 30 min at room temperature, followed by rinsing × 3 with PBS. The samples were stored in PBS at 4ºC until visualization by fluorescence microscopy. For immunostaining, colonoids were fixed, rinsed with PBS and permeabilized using 0.3% Triton X-100 in PBS for 20 min. Following rinsing × 3 with PBS containing 100 mM glycine, the colonoids were incubated in immunofluorescence (IF) wash (0.2% Triton X-100, 0.1% BSA, 0.05% Tween-20, 7.7 mM NaN_3 in PBS and 5% normal goat serum) for 90 min to block nonspecific binding. Primary-antibodies (α-chromogranin A and α-mucin2) were applied in IF wash (1:100) for 12 h at 4ºC. Secondary antibodies (α-rabbit-Cy3 and α-goat-Alexa Fluor 488) were applied in IF wash (1:500) for 45 min. All nuclei were stained with bis-benzimide (10 μg/mL in PBS) using a 30 min incubation.[3]

2.2.7 Image Analysis of Monolayers and Freshly Isolated Crypts

Epifluorescence images were captured on a Nikon Eclipse TE2000-U microscope fitted with a Photometrics CoolSNAP HQ2 digital camera. Objective lenses used were 10×, 20× and 40× with numerical apertures of 0.30, 0.55 and 1.40, respectively. Prior to quantification, image acquisition and preprocessing of raw images was necessary to reduce background noise. This was done using a custom script implemented in MATLAB (MathWorks; Natick, MA) for each fluorescence image acquired. Background was first reduced using a top-hat filter followed by application of a median filter to smooth the images and further reduce noise. The images were then thresholded and ‘holes’ were filled to create a binary image which was used to define the

image area with measurable fluorescence. The total number of pixels in this masked area was then summed for each image. Quantification for the regions of stem/proliferative cell area within monolayers and freshly isolated crypts were assessed by dividing the number of $eGFP^+$ pixels by the total number of $DsRed^+$ pixels in the image. All data points represent the average ± standard deviation of at least four separate experiments. Statistical analysis was conducted by one-way ANOVA pairwise tests. A p-value of < 0.05 was considered statistically significant.

2.2.8 Image analysis for the colonoids

Confocal images were captured on a Zeiss CLSM 710 Spectral Confocal Laser Scanning Microscope, using objective lenses of either 20× or 40× magnifications (numerical apertures of 0.80 and 0.95, respectively). Preprocessing of the raw images, thresholding and masking was performed for each confocal slice as described in the previous section. eGFP was quantified relative to DsRed in each slice as described in the prior section and then averaged over all slices possessing colonoids to yield the percentage colonoid volume positive for eGFP. To quantify the Muc2- and ChgA-expression or EdU-staining regions in each image slice, the number of pixels positive for these markers was divided by the number of pixels positive for Hoechst 33342. The average ratio for every slice in a sample was then calculated to yield the average volume of sample positive for Muc2, ChgA, or EdU relative to that positive for Hoechst 33342.

2.3 Results and Discussion

2.3.1 Optimization of incubation time with chelating agents to remove epithelium from basement membrane

In the initial step of crypt isolation, the colon is incubated in a buffer to chelate divalent cations and reduce disulfide bonds. Chelation of divalent cations reduces crypt-stromal adhesion by binding the calcium and magnesium ions required for receptor interactions between the

basement membrane and stromal cells.[3,20] The chelation-buffer, incubation time was optimized by varying the time (30, 60, 90 min) in which the colon was placed in a standard buffer with EDTA and DTT, initially described by Booth *et al.* (Fig. 1A).[20] This buffer was chosen due to its past usage and reported high cell viability. All other isolation steps were held constant. Isolated crypts were assayed for the total yield of intact and broken crypts. The presence of intact crypts was used as an indicator of the extent of tissue trauma since these structures are easily fragmented when subjected to significant stress or harsh chemical conditions. Liberated crypts were considered to be intact if they were at least 150 μm in length. Utilization of a distal colon from the *Sox9*eGFP-CAGDsRed mouse model permitted facile evaluation of the viability of stem cell/progenitor (green plus red fluorescence) and differentiated lineages (red fluorescence) of the liberated crypts immediately after retrieval from the tissue.[3] The CAGDsRed mouse line, which ubiquitously expresses the red fluorescent protein DsRed, was bred with *Sox9*eGFP mice, which expresses eGFP under control of the *Sox9* promoter.[3] Previous work has demonstrated that the presence of the *Sox9* transcription factor is a distinguishing characteristic of colonic stem and progenitor cells.

Incubation of a single distal colon for 30 min in the EDTA-containing buffer resulted in a total yield of 139,000 ± 22,000 crypts of which 69.7% were intact. The 60-min incubation yielded 280,000 ± 28,000 crypts with 79.3% intact and 90-min incubation produced 360,000 ± 41,000 crypts with 65.9% intact. The 30-min incubation period provided the lowest yield of intact and total crypts, probably as a result of inadequate time for the chelating agents to be effective in disrupting submucosal adhesion. Although 90-min incubation produced a higher overall yield, the 60-min incubation retrieved a higher percentage of intact crypts and resulted in

more than double the number of intact crypts relative to that after 30-min incubation. Therefore, 60-min incubation was chosen for all subsequent experiments.

2.3.2 Optimization of acceleration intensity required to release crypts

Following chelation of divalent ions and disruption of the adhesion between the epithelium and the basement membrane, mechanical agitation is use to remove crypts from the underlying tissue. Most protocols instruct "vigorous agitation of the tissue" to retrieve crypts, without quantification of the force or accelerative intensities involved.[3,8,9,11,20] To develop a reproducible protocol, varying average acceleration intensities were quantified for mechanically agitating the tissue in releasing crypts from the underlying stroma. Initially the average acceleration intensity achieved during agitation for 5 s was varied (1.5, 2.0, 2.7, 3.7, 5.0 and 6.3 × g) to optimize the agitation step (Fig. 4). To minimize the number of animals used, the colon was agitated for 5 s at the lowest acceleration intensity followed by settling of the tissue remnant and collection of the crypt-containing supernatant. Fresh isolation buffer was then added to the colon and the tissue was agitated at the next higher acceleration intensity after which the supernatant was again collected. This procedure was repeated until 6 crypt-containing supernatants were collected (Fig. 1B). Each fraction was assayed for the total number of crypts, the number of intact crypts and crypt quality. Crypt quality was quantified by measuring the percentage of crypts that were both intact and retained an identifiable lumen. Identification of the lumen insured that the crypts possessed the basic morphology present *in vivo*. Utilization of the *Sox9*eGFP-CAGDsRed mouse model permitted verification of the quality, as only crypts possessing intact stem-cells possessed green fluorescence at the crypt base (Fig. 1C). The total number of undamaged crypts with an identifiable lumen was greatest for acceleration intensities of 1.5, 2.0 and 2.7 × g (52,000 ± 15,000, 87,000 ± 17,000 and 90,000 ± 21,000 crypts,

respectively) (Figure 1d). An ANOVA comparison revealed that the 1.5, 2.0 and 2.7 × g agitation acceleration intensities produced statistically different yields ($p < 0.01$) of intact versus broke crypts. The percentage of crypts with the appropriate morphology was optimal when the acceleration intensities were 1.5 × g (85.7%) and 2.0 × g (84.3%). At increased acceleration intensities (>3.7 × g), the lumens collapsed (Fig.1E). While progressively higher acceleration intensities liberated more crypts, the apparent quality of the crypts was also diminished as the acceleration intensities increased. For these measurements, the optimal compromise between crypt yield and quality was thus determined to be 1.5 and 2.0 × g. Since an untested combination of chelation-buffer incubation times and agitation conditions might have proved superior, a broad range of combinations of incubation times and acceleration intensities were assessed (Table 1). Of the conditions tested, 60-min incubation in chelation buffer and an acceleration intensity of 1.5 × g yielded the greatest percentage of crypts with high-quality morphology. eGFP was expressed in 36 ± 4% of the crypt area, demonstrating that crypts isolated under these conditions possessed intact stem/proliferative cells (Fig. 5). Since the intended application of this work was the culture of viable crypts with formation of colonoids, these conditions were used for all subsequent experiments. When a higher yield of crypts is required without regard to quality, for example in gene expression studies, longer incubation times and greater acceleration intensities would generate significantly larger sample sizes and might be preferable.

2.3.3 Optimization of matrigel concentration for colonoid culture

Laminin-rich Matrigel is believed to provide the required matrix contacts for crypt cells mimicking that supplied by the underlying stroma *in vivo*.[3,8,10] Additionally, it is likely that Matrigel contains critical growth factors to maintain the crypt cells. In all past reports, crypts were cultured in 100% Matrigel, although it is unknown if this is the optimal concentration for

colonoid growth. At 100%, Matrigel is extremely viscous, quick to gel and difficult to load into confined spaces such as those in microfabricated devices (*e.g.* microfluidic channels). For these reasons, four concentrations of Matrigel (25%, 50%, 75% and 100 vol% in complete culture medium (CCM) plus growth factors) were assessed for the ability to support colonoid formation. Crypts were isolated using the optimized protocol described above and were then plated on a microwell formed from native 1002 F such that the crypts remained suspended in Matrigel and not in contact with the 1002 F surface. The Matrigel-encapsulated crypts were imaged daily by brightfield and fluorescence microscopy (Fig. 2A). The percentage of crypts forming colonoids was quantified as the number of budding crypts divided by the number of total crypts plated (n = 4 experiments for each Matrigel concentration with an average of 113 ± 32 crypts/experiment). Interestingly, 100% Matrigel was the least effective in yielding colonoid growth (18 ± 1%) after 7 days of culture in microwells (Fig. 2B). 50% Matrigel supported the highest percentage of colonoid formation (33 ± 5%) followed by 75% and 25% Matrigel (23 ± 3% and 20 ± 7%, respectively) at day 7, as determined by colonoid morphology. To verify that crypts isolated under the optimal conditions and cultured in 50% Matrigel formed colonoids which possessed all of the differentiated cell lineages, immunostaining for the post-mitotic lineage markers Muc2 (mucus-producing goblet cells) and ChgA (hormone-secreting enteroendocrine cells) was performed (Fig. 2D,E) . For colonoids cultured in 50% Matrigel, eGFP was expressed in 49 ± 14% of the colonoid volume compared to 49 ± 12% in 100% Matrigel, suggesting similar numbers of stem/progenitor cells at one week under both conditions (Fig. 2F). The colonoid volume positive for Muc2 or ChgA was 14 ± 3 and 0.6 ± 0.2 times the volume staining positive for Hoechst 33342 when cultured in 50% Matrigel for 7 days. In the presence of 100% Matrigel for 7 days, $Muc2^+$ or $ChgA^+$ regions occupied 16 ± 4 and 0.5 ± 0.2 times more volume than that

of Hoechst 33342 suggesting that the density of these differentiated cell types was similar for the two conditions. Colonoids in 50% and 100% Matrigel possessed EdU^+ positive regions (43 ± 12 and 47 ± 10 times greater in volume than that positive for Hoechst 33342) suggesting that comparable numbers of cells were actively synthesizing DNA when cultured in the two different Matrigel concentrations (Fig. 2G).[22] Thus colonoids cultured in 50% Matrigel were nearly identical to that in 100% Matrigel with respect to these measured cell properties. Since the use of 50% Matrigel was superior to the other concentrations at forming colonoids and was also able to support both stem/proliferative and differentiated cells, 50% Matrigel was employed in all subsequent experiments. Given the high cost of Matrigel, reduction in the concentration to 50% will substantially reduce future experimental costs. The mechanistic impact of Matrigel concentration on the cells is unknown; however, the optimal concentration identified in this study suggest that 50% Matrigel may provide the optimal stiffness, the proper concentrations of growth and differentiating factors, and/or the appropriate density of extracellular matrix contacts to maximize colonoid cell growth.

2.3.4 Assessment of crypt interaction with microfabricated substrates

Surface biochemical properties are known to modulate the growth and differentiation of stem cells.[23-26] Thus, the property of solid surfaces in contact with the crypts is likely to impact the efficiency of colonoid formation and potentially the fate of the crypt cells. Along with the 3-D colonoids, it was noticed that the intestinal crypt cells also formed 2-D monolayers when in contact with the well substrate. Conditions promoting monolayer formation from primary cells for this monolayer have not been well described.[9,11, 27,28] For this reason, five commonly used transparent, microfabrication substrates were assessed for their impact on cell growth and phenotype: glass, polystyrene, PDMS, and the epoxy photoresists SU-8 and 1002 F. Glass and

polystyrene have long been the gold standard for cell culture, and devices can be microfabricated by a variety of methods from all of these materials. PDMS is the most popular material for prototyping microdevices and it can be readily microfabricated by soft lithography.[13,29,30] The epoxy-based, transparent, negative SU-8 photoresist is used in building high-aspect ratio microstructures by standard photolithography.[31] 1002 F photoresist is closely related to SU-8 in molecular structure, and prior work has demonstrated that 1002 F is biocompatible, supporting cell attachment and growth, and exhibits significantly lower autofluorescence than SU-8.[31-33] Non-transparent or opaque substrates (*e.g.* silicon) were not assessed here due to their incompatibility with many light microscopy methods.

Crypts were cultured in contact with the microfabrication substrates and monolayer expansion efficiency was calculated by dividing the number of crypts that successfully expanded into monolayers by the total number of crypts plated. 95.5 ± 2.5% of crypts plated on glass developed into monolayers, the highest average percentage of any of the experimental materials. After one week, 46.3 ± 3.4% of crypts cultured on native PDMS substrates developed into monolayers, the lowest percentage of the experimental materials (p-value of 5.67×10^{-6}) (Fig.3A). However, monolayer-formation percentage for crypts on glass was not statistically different than that on polystyrene, 1002 F and SU-8 (p-values of 0.33, 0.10 and 0.052, respectively) (Fig. 3B). Immunohistochemical staining for the goblet-cell and enteroendocrine lineages demonstrated the presence of differentiated cells throughout the monolayers on the PDMS surfaces (Fig. 3C,D).

The monolayers forming on the various surveyed substrates possessed very little eGFP fluorescence, suggesting little to no *Sox9* expression. Monolayers on 1002 F and PDMS substrates possessed the most eGFP expression after a week of culture (covering 1.3 ± 0.8% and

3.7 ± 3.0% of the monolayer surface area, respectively). To determine whether cells in the monolayers were proliferating but without eGFP expression, an EdU-based cellular proliferation assay was performed on the cells grown for 7 days on PDMS substrates. EdU^+ cells were infrequent in the monolayers suggesting that most of the cells within the monolayer were not actively proliferating (compare Fig. 3E to 2G). These data suggested that crypt-cells rapidly differentiated upon adherence to glass, oxidized polystyrene and epoxy photoresists. All of these materials are hydrophilic displaying charged oxygen groups on their surface. It may be necessary to avoid cell contact with these surfaces to maintain stem/progenitor cells. PDMS was an exception likely because the intrinsic hydrophobic properties of PDMS[30] discouraged surface attachment by cells. PDMS may be attractive for microfabricated devices constructed to house stem/progenitor cells. Further studies will be required to understand how the surface property of a substrate modulates the fate of crypt cells. While monolayer formation was critically dependent on the surface properties of the culture vessel, monolayer dependence on the overlaid Matrigel concentration was less pronounced as long as a concentration threshold of 50% Matrigel was utilized (Fig. 6).

2.4 Conclusions

The current work established a reproducible, standardized isolation protocol for isolating intact murine colonic crypts with high proliferative capacity. In a step-wise fashion, the incubation duration of the tissue in chelating buffer and mechanical acceleration intensities required for crypt release were optimized to retrieve the maximal number of high quality crypts. The concentration of Matrigel, a costly reagent used for *in vitro* expansion of intestinal stem cells, was optimized to maximize the development of colonoids from the isolated crypts while minimizing reagent use. Crypts were isolated from a genetically engineered *Sox9*eGFP-

CAGDsRed reporter mouse, enabling fluorescent measurements to be used as functional readouts of stem-cell proliferation and differentiation. The microwell provided an efficient platform for facile screening and quantification of colonoid formation while further reducing the amounts of expensive reagents including such as Wnt-3a, EGF, Noggin, and R-spondin1. Immunohistochemical staining demonstrated the presence of the differentiated intestinal cellular lineages (goblet and enteroendocrine) in these colonoids. The type of growth (2-D monolayer *vs.* 3-D colonoid) was dependent on the culture substrate properties. Crypts plated on PDMS substrates demonstrated the highest percentage of 3-D colonoid formation and most stem cells, while crypts plated on glass, polystyrene, 1002 F and SU-8 surfaces produced the highest percentages of 2-D monolayer formation with few identifiable stem cells. By standardizing the isolation process and optimizing the matrix concentrations on different surfaces, reproducible crypt isolation and robust culture protocols were established to facilitate the use of colonoid-based assays by the intestinal stem-cell community. Common microfabricated substrates were surveyed to identify substrates that are compatible with maintenance of stem and differentiated cells. This research provides a clear isolation and culture protocol for colonic crypts supporting future development of intestinal studies and ‘organ-on-chip’ endeavors.

2.5 Figures

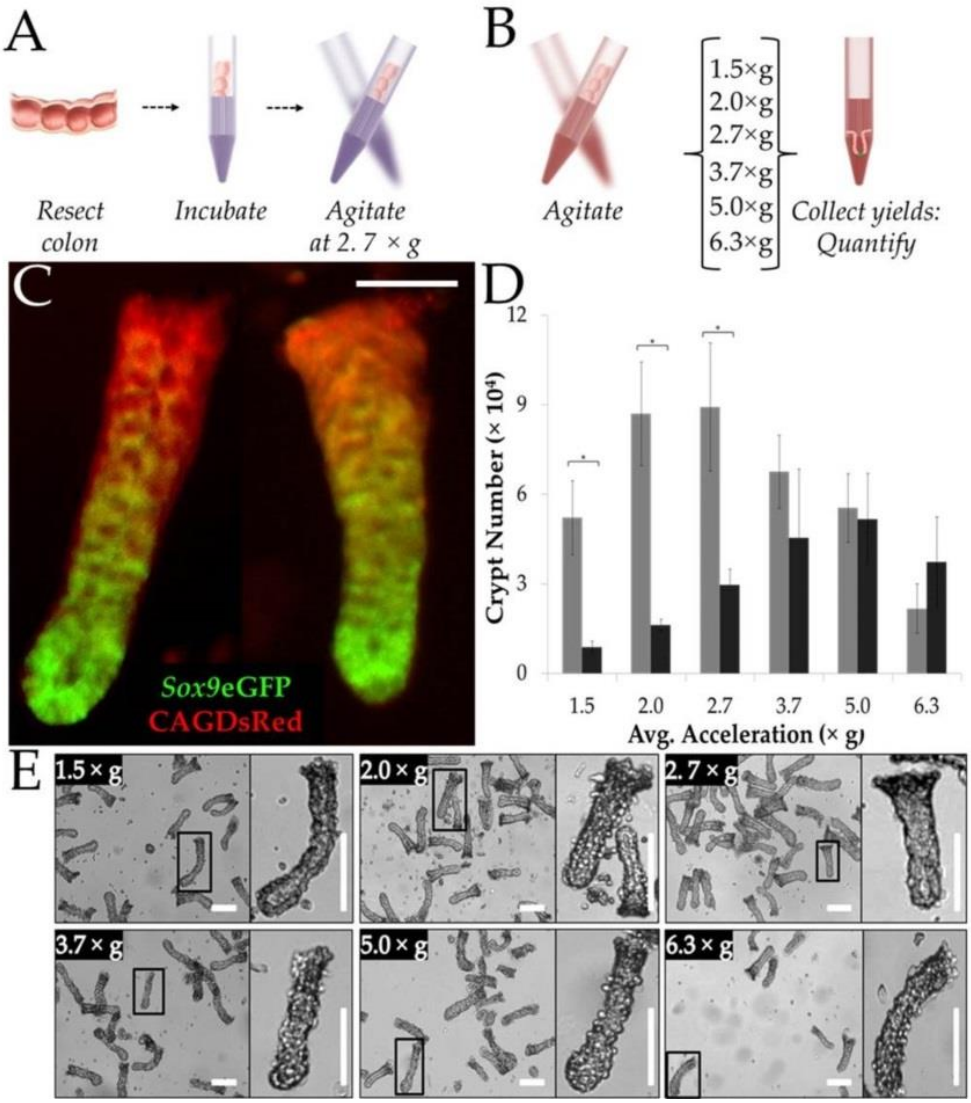

Figure 2.1 Isolation of crypts from a mouse colon. Isolation of crypts from a mouse colon (A) Schematic of crypt isolation. The resected colon was incubated in chelating buffer, washed and then mechanically agitated. (B) Schematic of the strategy to identify the optimal acceleration intensity needed to retrieve crypts: the tissue was incubated in chelating buffer, rinsed and then sequentially agitated at different acceleration intensities. After each agitation, the crypt-rich supernatant was collected and assayed. (C) Fresh crypts isolated using an acceleration intensity

of 1.5 × g displaying eGFP fluorescence, indicating Sox9 expression (green). Scale bar = 40 μm. (D) Quantification of the number of intact and broken crypts at each of the six acceleration intensities tested. Grey bars indicate intact-crypt yield and black bars indicate broken-crypt yield. (E) Brightfield images of isolated crypts isolated at different accelerations intensities. Crypts isolated using an acceleration intensity of 1.5 × g display a visible lumen, indicating unperturbed crypt morphology. Scale bar = 150 μm.

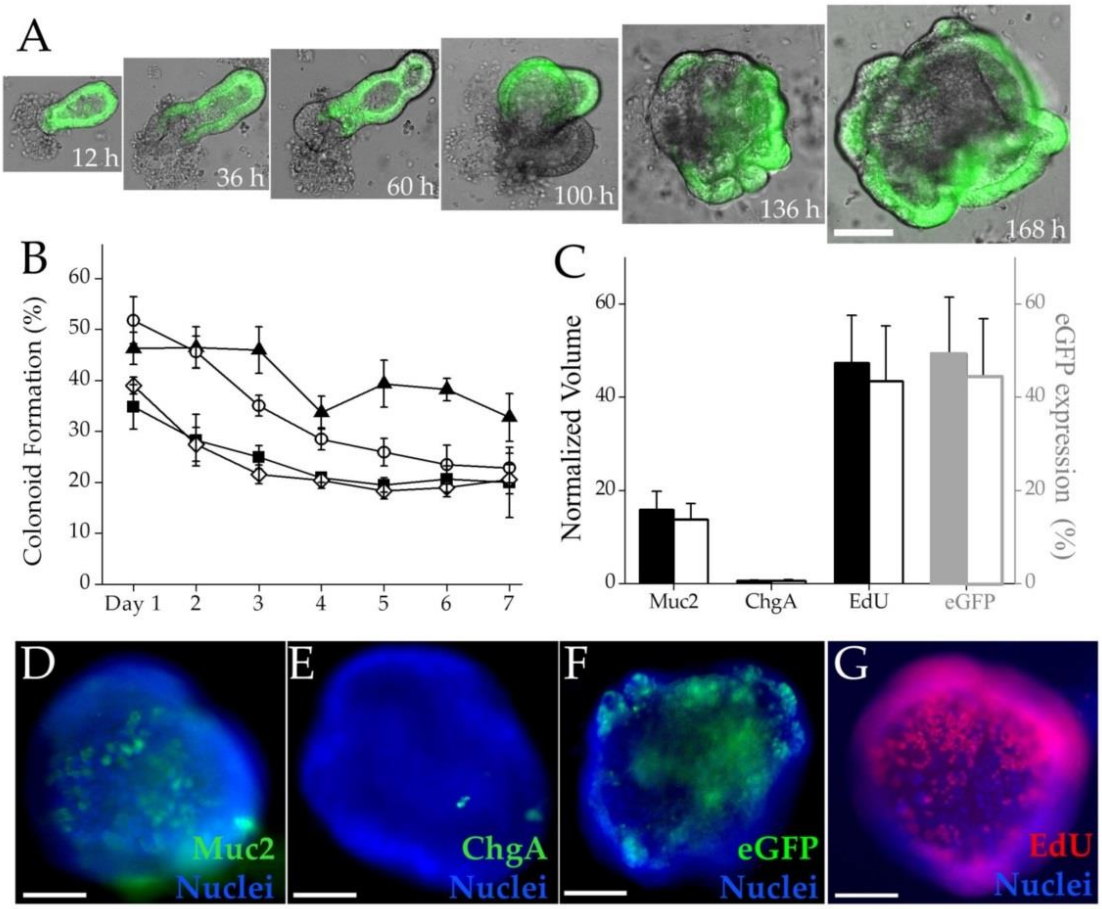

Figure 2.2 Effect of Matrigel concentrations on in vitro expansion of colonic crypts into 3-D colonoids. (A) Serial overlaid brightfield and eGFP fluorescence images of the same colonoid over 1 week in culture. Scale bar = 50 μm. (B) Effect of Matrigel concentration on the percentage of crypts growing into colonoids over 1 week of culture. Squares, triangles, circles and diamonds represent 25%, 50%, 75% and 100% Matrigel, respectively. 50% Matrigel provides the optimum 3-D growth environment for the colonoids. (C) Quantification of the cell properties in the colonoids. Shown is the colonoid volume (left y axis, black) staining positive for Muc-2, ChgA or EdU divided by that positive for Hoechst 33342 when colonoids were cultured in 100% (filled bars) or 50% (open bars) Matrigel. The volume of the colonoid expressing eGFP relative to that expressing dsRed is shown on the right y-axis (grey) for colonoids cultured in 100% (filled bars) or 50% (open bars) Matrigel. (D-E) Colonoids were

cultured for 1 week and then stained by immunohistochemistry for: (D) mucin-2 (goblet cell marker: green) and (E) chromogranin-A (enteroendocrine marker: green). (F) A crypt obtained from a Sox9eGFP-CAGDsRed mouse was cultured for 1 week and then imaged for eGFP fluorescence. (G) Fluorescence image of a colonoid (1 week culture) after an 8-hour EdU pulse (red). Hoescht 33442 was used as a nuclear stain (blue) in panels C-G. Scale bar = 75 μm.

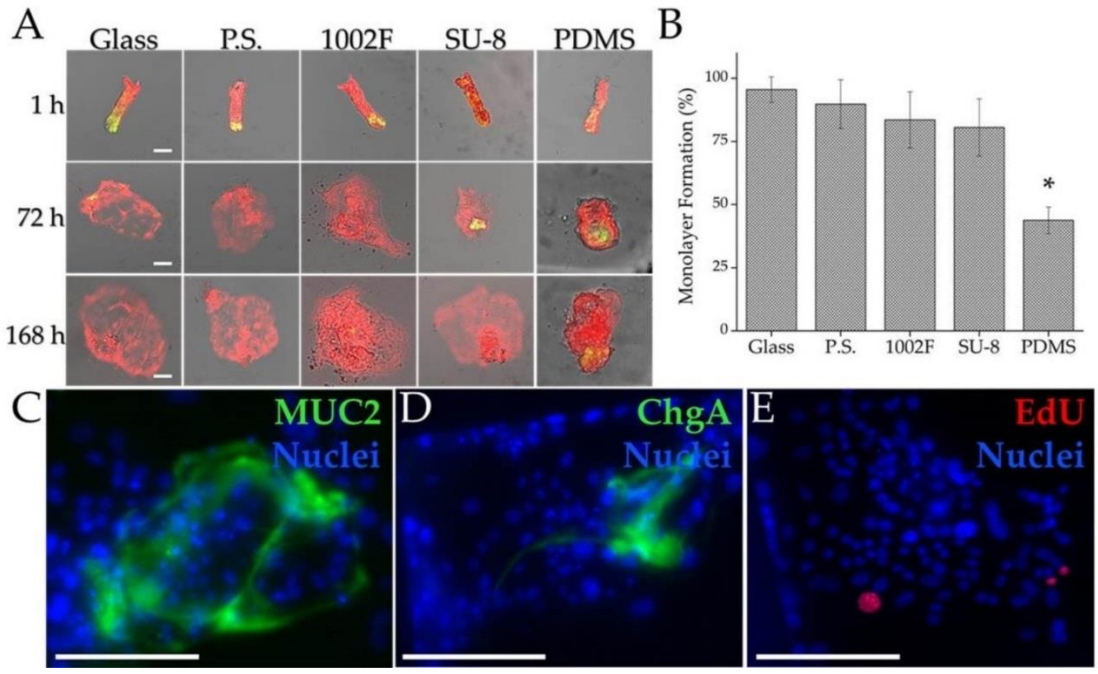

Figure 2.3 Crypt-substrate interaction. (A) Representative time-lapse images of monolayer formation on the experimental substrates from crypts isolated from a Sox9eGFP-CAGDsRed mouse. eGFP and DsRed fluorescence was overlaid on brightfield microscopy images. Upon adherence to glass, oxidized polystyrene and epoxy photoresist, crypt-cells rapidly differentiate. (B) Quantification of the percentage of crypts forming a monolayer when crypts were cultured on the microfabrication substrates over 1 week. (C, D) Whole-mount immunohistochemical staining of a monolayer after 1 week in culture. Fluorescence images are shown for: mucin-2 (green, C) and chromogranin-A (green, D). (E) Fluorescence image after an 8-hour EdU pulse (red). Hoescht 33442 was used as a nuclear stain (blue) in panels C-E. Scale bars = 50 μm.

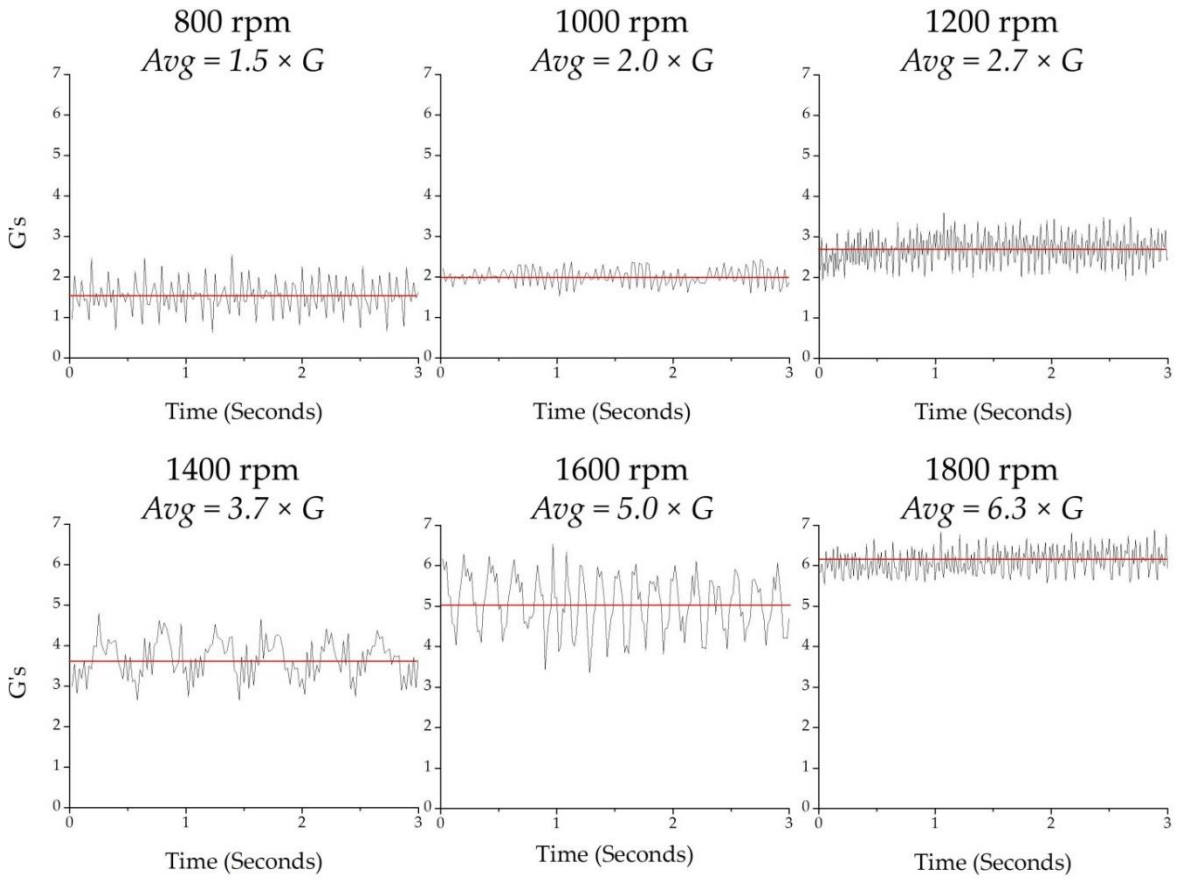

Figure 2.4 Accelerometer measurements of the acceleration vector magnitudes applied to the colonic tissue.

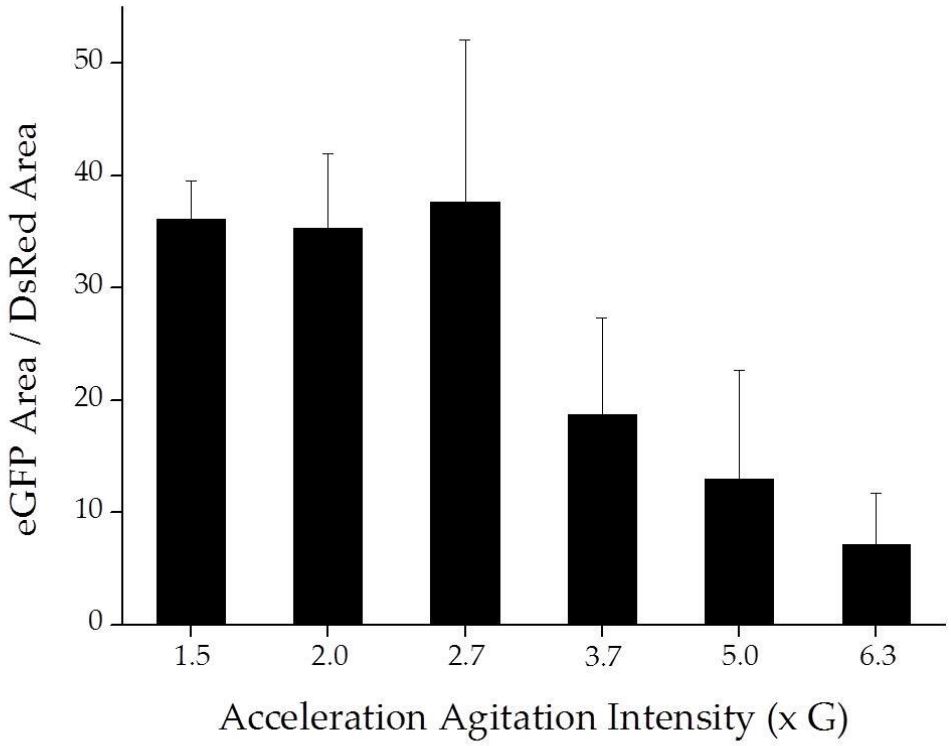

Figure 2.5 Effect of increased accelerated agitation intensity on eGFP expression.

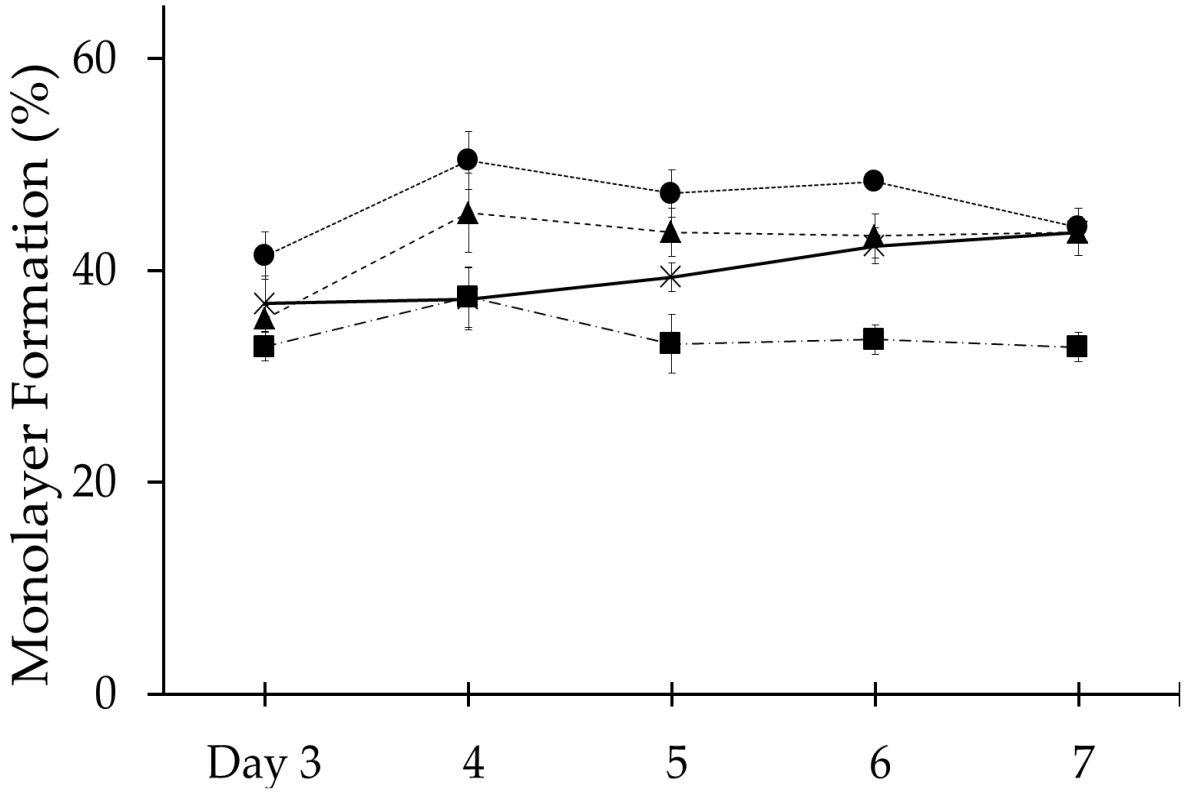

Figure 2.6 Effect of Matrigel concentration on monolayer expansion.

Data collected on native PDMS surfaces. Squares, circles, triangles, and x's represent 25%, 50%, 75% and 100% Matrigel, respectively.

2.6 Tables

A Number of Whole Crypts Isolated

Incubation Duration \ Average Acceleration Intensity	1.5 × g	2.0 × g	2.7 × g	3.7 × g	5.0 × g	6.3 × g
30 min	44,700 ± 10,300	74,500 ± 18,600	66,200 ± 17,300	102,700 ± 31,600	72,900 ± 22,700	19,900 ± 11,200
60 min	60,800 ± 17,200	103,100 ± 19,200	118,900 ± 22,800	112,900 ± 43,700	107,100 ± 26,100	59,000 ± 23,300
90 min	109,300 ± 22,000	178,900 ± 52,100	172,300 ± 46,900	67,900 ± 28,100	54,700 ± 20,100	23,200 ± 15,400

B Percent of Crypts with Intact Morphology

Incubation Duration \ Average Acceleration Intensity	1.5 × g	2.0 × g	2.7 × g	3.7 × g	5.0 × g	6.3 × g
30 min	74.8 %	70.4 %	63.9 %	59.5 %	58.2 %	68.3 %
60 min	85.7 %	84.3 %	75.1 %	59.8 %	51.7 %	36.8 %
90 min	77.6 %	68.8 %	63.6 %	66.3 %	62.6 %	44.7 %

Table 2.1 Crypt isolation data.

(A) Number of isolated, intact crypts obtained at the various agitation intensity shake-steps and incubation times. (B) Percent of crypts with intact morphology at each of these steps.

2.7 REFERENCES

1. Barker N, van de Wetering M, Clevers H: The intestinal stem cell. *Genes & Development* 2008, 22: 1856-1864.

2. Ramalingam S, Daughtridge GW, Johnston MJ, Gracz AD, Magness ST: Distinct levels of Sox9 expression mark colon epithelial stem cells that form colonoids in culture. *American Journal of Physiology-Gastrointestinal and Liver Physiology* 2012, 302: G10-G20.

3. Medema JP, Vermeulen L: Microenvironmental regulation of stem cells in intestinal homeostasis and cancer. *Nature* 2011, 474: 318-326.

4. Humphries A, Wright NA: Colonic crypt organization and tumorigenesis. *Nature Reviews Cancer* 2008, 8: 415-424.

5. Sato T, Vries RG, Snippert HJ, van de Wetering M, Barker N, Stange DE, van Es JH, Abo A, Kujala P, Peters PJ, Clevers H: Long-term expansion of epithelial organoids from human colon, adenoma, adenocarcinoma, and Barrett's epithelium. *Nature*, 2009, 459: 262-U147.

6. Garrison AP, Helmrath MA, Dekaney CM: Intestinal Stem Cells. *Journal of Pediatric Gastroenterology and Nutrition* 2009, 49: 2-7.

7. Yantiss RK and Odze RD: Diagnostic difficulties in inflammatory bowel disease pathology. *Histopathology* 2006, 48: 116-132.

8. Booth C, O'Shea JA, Potten CS: Maintenance of functional stem cells in isolated and cultured adult intestinal epithelium. *Experimental Cell Research* 1999, 249: 359-366.

9. Ootani A, Li XN, Sangiorgi E, Ho QT, Ueno H, Toda S, Sugihara H, Fujimoto K, Weissman IL, Capecchi MR, Kuo CJ: Sustained in vitro intestinal epithelial culture within a Wnt-dependent stem cell niche. *Nature Medicine* 2009, 15: 1-U140.

10. Jung P, Sato T, Merlos-Suarez A, Barriga FM, Iglesias M, Rossell D, Auer H, Gallardo M, Blasco MA, Sancho E, Clevers H, Batlle E: Isolation and in vitro expansion of human colonic stem cells. *Nature Medicine* 2011, 17: 1225-1227.

11. Sato T, Stange DE, Ferrante M, Vries RG, Van Es JH, van den Brink S, Van Houdt WJ, Pronk A, Van Gorp J, Siersema PD, Clevers H: Single Lgr5 stem cells build crypt-villus structures in vitro without a mesenchymal niche. *Gastroenterology* 2011, 141: 1762-1772.

12. Barker N, van Es JH, Kuipers J, Kujala P, van den Born M, Cozijnsen M, Haegebarth A, Korving J, Begthel H, Peters PJ, Clevers H: Identification of stem cells in small intestine and colon by marker gene Lgr5. *Nature* 2007, 449: 1003-U1001.

13. Haramis APG, Begthel H, van den Born M, van Es J, Jonkheer S, Offerhaus GJA, Clevers H: De novo crypt formation and juvenile polyposis on BMP inhibition in mouse intestine. *Science* 2004, 303: 1684-1686.

14. Madara JL, Stafford J, Dharmsathaphorn K, Carlson S: Structural-analysis of a human intestinal epithelial cell line. *Gastroenterology* 1987, 92: 1133-1145.

15. Danielson KG, Oborn CJ, Durban EM, Butel JS, Medina D: Epithelial mouse mammary cell-line exhibiting normal morphogenesis *in vivo* and functional differentiation *in vitro*. *Proceedings of the National Academy of Sciences of the United States of America-Biological Sciences* 1984, 81: 3756-3760.

16. Madara JL, Dharmsathaphorn K: Occluding junction structure funtion relationships in a cultured epithelial monolayer. *Journal of Cell Biology* 1985, 101: 2124-2133.

17. Dharmsathaphorn K, McRoberts JA, Mandel KG, Tisdale LD, Masui H: Human colonic tumor-cell line that maintains vectoral electrolyte transport. *American Journal of Physiology* 1984, 246: G204-G208.

18. Hakala, Rajala K, Ojala M, Panula S, Areva S, Kellomaki M, Suuronen R, Skottman H: Comparison of Biomaterials and Extracellular Matrices as a Culture Platform for Multiple Independently Derived Human Embryonic Stem Cell Lines. *Tissue Engineering Part A* 2009, 15: 1775-1785.

19. Phillips JE, Petrie TA, Creighton FP, Garcia AJ: Human mesenchymal stem cell differentiation on self-assembled monolayers presenting different surface chemistries. *Acta Biomaterialia* 2010, 6: 12-20.

20. Kaivosoja E, Barreto G, Levon K, Virtanen S, Ainola M, Konttinen YT: Chemical and physical properties of regenerative medicine materials controlling stem cell fate. *Annals of Medicine* 2012, 44: 635-650.

21. Basson MD, Turowski G, Emenaker NJ: Regulation of human (Caco-2) intestinal epithelial cell differentiation by extracellular matrix proteins. *Experimental Cell Research* 1996, 225: 301-305.

22. Jorissen M, Vanderschueren B, Vandenberghe H, Cassiman JJ: The preservation and regeneration of cilia on human nasal epithelial-cells cultures *in vitro*. *Archives of Oto-Rhino-Laryngology* 1989, 246: 308-314.

23. Murakami H, Masui H: Hormonal-control of human-colon carcinoma cell growth in serum-free media. *Proceedings of the National Academy of Sciences of the United States of America-Biological Sciences* 1980, 77: 3464-3468.

24. Duffy DC, McDonald JC, Schueller OJA, Whitesides GM: Rapid prototyping of microfluidic systems in poly(dimethylsiloxane). *Analytical Chemistry* 1998, 70: 4974-4984.

25. Abgrall P, Conedera V, Camon H, Gue AM, Nguyen NT: SU-8 as a structural material for labs-on-chips and microelectromechanical systems. *Electrophoresis* 2007, 28: 4539-4551.

26. Pai JH, Wang Y, Salazar GT, Sims CE, Bachman M, Li GP, Allbritton NL: Photoresist with low fluorescence for bioanalytical applications. *Analytical Chemistry* 2007, 79: 8774-8780.

27. Wang YL, Phillips C, Xu W, Pai JH, Dhopeshwarkar R, Sims CE, Allbritton NL: Micromolded arrays for separation of adherent cells. *Lab on a Chip* 2010, 10: 2917-2924.

28. Mata A, Fleischman AJ, Roy S: Characterization of polydimethylsiloxane (PDMS) properties for biomedical micro/nanosystems. *Biomedical Microdevices* 2005, 7: 281-293.

CHAPTER 3: OPTIMIZING WNT-3A AND R-SPONDIN1 CONCENTRATIONS FOR INTESTINAL ORGANOIDS USING A GRADIENT-FORMING MICRODEVICE

3.1 Introduction

The health of the colon is partly dependent on the chemical milieu surrounding the colonic stem-cell niche. The epithelial monolayer lining the colon is supplied by constantly renewing cells migrating from the stem-cell niche. This niche resides at the base of colonic crypts, local invaginations that harbor the intestinal stem cells, their immediate progeny and supporting cells.[1] The stem cells give rise to transit-amplifying cells that proliferate and differentiate into absorptive colonocytes, mucus-producing goblet cells, and hormone-producing enteroendocrine cells. These non-dividing cells migrate to the luminal surface where they undergo apoptosis and exfoliate. This process drives complete replacement of the colonic epithelium every 4-7 days making this tissue the most actively self-renewing tissue in the body.[2] Stem-cell self-renewal and differentiation are known to be modulated by the interplay of intrinsic gradients of mitogens, morphogens, and differentiation factors.[3] Much remains to be understood as to how these various chemical factors control the process of epithelial homeostasis in health and disease including their threshold concentrations for activity. To better study these processes, *in vitro* model systems that enable precise control of the stem-cell environment are needed.

In vitro models of cell proliferation and differentiation in the colon have been hampered by the inability to recapitulate the key features of normal intestinal epithelial tissue. Most studies have been restricted to *in vivo* inspection, histological assessment, or cancer cell lines that are incapable of normal differentiation.[4,5] Recent advances in organotypic culture techniques now

enable the culture of primary stem cells derived from colonic crypt tissue.[6] Under specific culture conditions, both single intestinal stem cells and isolated crypts grow into self-organizing, functional 3D epithelial organoids or "mini-guts" containing stem cells and the full repertoire of differentiated colonic epithelial cell types.[2,7-9] When these *in vitro* cultured mini-guts are derived from colon tissue they are referred to as colonoids. Colonoid culture requires explicit growth conditions in which the cells are suspended in Matrigel, a 3D laminin and collagen-rich matrix similar to the basal *lamina propria*, which is further supplemented with a mixture of growth factors including Wnt-3a, R-spondin1, epidermal growth factor (EGF), Noggin, and Jagged. These conditions maintain stem-cell multipotency and enable culture of the colonoids for greater than 1 year while maintaining a normal karyotype.[1,10] Colonoids generated either from isolated crypts or individual stem cells grow into cystic structures with multiple crypt-like buds projecting outward from a central lumen.[11] Remarkably, cell-renewal kinetics, differentiation and crypt patterning characteristics recapitulate those seen *in vivo.* Stem cells in the colonoids give rise to transit-amplifying cells that proliferate, differentiate, undergo apoptosis and are shed into the central lumen 3-5 days later.[10,12] This 3D culture system has enabled a rapidly growing number of studies elucidating molecular mechanisms involved in stem-cell renewal and differentiation, membrane transport, intestinal regeneration, and carcinogenesis.[8,13,14]

In vitro cell-based screens using these types of primary organotypic tissue mimics are poised to greatly improve our understanding of the biological effects of intrinsic and extrinsic factors on cell renewal and physiology.[12,15] The combination of these 3D culture systems with microfabricated platforms will be a powerful combination in compound screening and in the understanding of concentration-dependent biological effects while reducing cost and speeding discovery. Microfabricated systems offer the opportunity to grow cells under carefully controlled

environmental conditions, for instance with gradients of growth and differentiation factors. A burgeoning number of microfluidic devices have been described for studying stem-cell renewal and differentiation, creating 3D spheroids, and drug testing.[16-28] Most devices have utilized tumor cells grown in one or multiple chambers to mimic a limited aspect of gut function, such as absorption.[29-32] The development of a microfluidic device compatible with the 3D culture of primary colonic epithelium remains a critical need for growth factor screening especially that involved in stem-cell renewal.

This report focuses on the adaptation, characterization, and implementation of a simple gradient-generating microfluidic device to assess the required concentration of Wnt-signaling factors on stem/transit-amplifying cell renewal and differentiation, and viability of primary colonic epithelial tissue in the colonoid system. Colonic crypts were loaded into the microdevice and developing colonoids were exposed to varying concentrations of the Wnt-pathway agonists, Wnt-3a and R-spondin1. The colonoids were characterized *in situ* over time by monitoring endogenously expressed fluorescent proteins and by immunochemistry to identify the presence of proliferative and differentiated cell types. The impact of the growth factors at varying concentrations and at varying culture times was quantified for large numbers of colonoids to provide statistically relevant data while minimizing reagent usage.

3.2 Materials and Methods

3.2.1 Transgenic mouse models and isolation of colonic crypts

Crypts were isolated from either *Sox9*EGFP mice or *Sox9*EGFP-CAGDsRed mice (6-9 weeks old) using previously described methods. The *Sox9*EGFP and *Sox9*EGFP-CAGDsRed mouse models were developed on a CD-1 background. The CAGDsRed mouse line ubiquitously expresses the red fluorescent protein DsRed under the control of a chicken beta-actin promoter

(CAG). To create the *Sox9*EGFP-CAGDsRed mice, the DsRed-expressing mice were bred with *Sox9*EGFP mice, which possessed the *Sox9* promoter controlling EGFP (enhanced green fluorescent protein) expression on a modified bacterial artificial chromosome.[34-35] Mice genetically engineered with this construct express EGFP in intestinal stem cells and transit-amplifying cells. The colonic tissues were harvested from mice that were bred, handled and sacrificed under protocols approved by the UNC Institutional Animal Use and Care Committee.

3.2.2 Colonoid culture

Colonoid culture media, CCM, consisted of a mixture of advanced DMEM/F12 medium (Invitrogen), Wnt-3A (120 ng/mL) and R-spondin1 (175 ng/mL) unless otherwise specified (Table 13). CCM also contained Noggin (100 ng/mL), EGF (50 ng/mL), Y27632 ROCK inhibitor (10 μM), NAC (1 mM), GlutaMAX (1×), HEPES (10 mM), penicillin (100 unit/mL), and streptomycin (100 μg/mL). Wnt-3A and R-spondin1 were prepared from conditioned medium as described previously or purchased purified from a supplier (Table 13).[36] The CCM was prepared in a bulk volume of 500 mL, split into 6-mL aliquots, and stored at -80 °C until use. For crypt/colonoid culture, Matrigel was diluted 50% in CCM. A 1 mL suspension of freshly isolated crypts (5000 crypts/mL) was added to standard 12-well plates at 4 °C. The Matrigel was then polymerized for 15 min at 37 °C. After polymerization, 1.6 mL of CCM was overlaid onto the Matrigel. The isolated crypts typically formed colonoids within 24 h under these culture conditions. The CCM was changed every 24 h during the course of the experiment.

3.2.3 Placement and culture of crypts and Matrigel on the gradient device

Before use, the device was sterilized with 70% ethanol and rinsed with phosphate buffered saline (PBS) ×5. The gradient-generating region of the device was coated by overnight incubation with 3% Matrigel in PBS for 12 h at 4 °C, and then rinsed with PBS ×3 prior to

loading crypts or colonoids. This step resulted in deposition of a thick coat (35 ± 5 μm, n=3) of Matrigel (Dow Corning, Midland, MI) on the channel walls (Figure 5) that improved adhesion of the subsequently loaded Matrigel plug, improved loading of the crypt/Matrigel suspension (see below) and centered subsequently loaded crypts/colonoids along the z axis of the device. Crypts were isolated from the distal colon of a mouse as previously described. The crypts were pelleted by centrifugation at 300 × G for 90 s. The supernatant was aspirated and the crypts were mixed with cold liquid Matrigel (50% in CCM, 4 °C). A 25 μL aliquot of this suspension containing 100 ± 10 crypts was pipetted into the device's gradient-generating region. The Matrigel pre-coat layer enabled the crypt/Matrigel solution to quickly enter the central channel by surface tension. Excess gel entering the reservoirs was removed and the gel was polymerized by incubation at 37 °C for 15 min. Once the Matrigel solidified, CCM (500 μl) was immediately added to each reservoir. For experiments in which a gradient was formed, Wnt-3A and/or R-spondin1 were omitted from the CCM added to the sink as appropriate for the specific experiment.

3.2.4 Diffusion based gradient generation and characterization

Gradient formation through the Matrigel layer on the device was characterized by imaging the movement of a 40 kDa FITC-dextran (Sigma-Aldrich, St. Louis, MO) in 50% Matrigel by time-lapse imaging using an Olympus MVX10 Macroview microscope. Fluorescence images were acquired every 15 min over 24 h to measure gradient formation. The volume of the source and sink was 500 μL and that of the channel was 5 μL. Gradient formation over time was modeled using Fick's Law:[37]

$$C(x,t) = A + \frac{1}{2} C_O \, erfc\left(\frac{x}{2\sqrt{(Dt)}}\right)$$

where A is an integration constant, x ranges from 0 to 5 mm corresponding to the positions along

the length of the channel, *t* is time, *D* is the diffusion coefficient, *erfc* is the complementary error function, and C_O is the concentration of the species of interest loaded into the source. COMSOL Multiphysics with finite-element analysis (FEA) was used to model the data and calculate *D*. For experiments applying gradients to colonoids, the media in both the source and sink were replaced every 24 h.

3.2.5 Microscopy

Colonoid formation and growth over time was tracked by wide-field imaging of the entire device using an Olympus MVX10 research macro zoom fluorescence microscope with a 1.0×, 0.25N.A. objective and 0.63× demagnification that provided a depth-of-focus of 91 μm. The MVX-10 was equipped with Chroma 49002 FITC/Cy2 and Chroma 49008 mCherry/Texas Red filter sets. Digital images were collected with a Hamamatsu Orca-flash 4.0 CCD camera. Confocal images of isolated crypts and colonoids were obtained using a Zeiss CLSM 710 Spectral Laser Scanning Microscope equipped with 405, 488 and 543 nm lasers to image Hoechst 33342, EGFP and DsRed, respectively. A Nikon Eclipse TE2000 microscope fitted with a Photometrics CoolSNAP HQ2 digital camera was used to quantify colonoid buds.

3.2.6 On-chip fluorescence staining

Crypts isolated from a *Sox9*EGFP-only mouse were used for immunofluorescence staining to avoid interference from the DsRed fluorescence of the CAG-DsRed/*Sox9*EGFP mouse. For immunofluorescence staining, freshly isolated crypts, and colonoids on the device and on tissue-culture plates were fixed with 4% paraformaldehyde for 20 min, followed by permeabilization with 0.5% Triton X-100 (Thermo-Fisher, Waltham, MA) for 20 min. Following rinsing ×3 with PBS containing 100 mM glycine, the colonoids were incubated in immunofluorescence wash (0.2% Triton X-100, 0.1% BSA, 0.05% Tween-20, 7.7 mM NaN3 in

PBS and 5% normal goat serum) for 90 min to block nonspecific binding. Primary-antibodies (polyclonal rabbit α-Muc2 (1:200) and polyclonal goat α-chromogranin A (1:1000)) were applied in immunofluorescence wash for 12 h at 4ºC (Invitrogen, Carlsbad, CA). Secondary antibodies (α-rabbit-Cy3 or α-goat-Cy3) were applied in immunofluorescence wash (1:500) for 45 min (Invitrogen, Carlsbad, CA). All nuclei were stained with Hoechst 33342 (10 μg/mL in PBS) using a 30 min incubation. Microdevices were imaged by brightfield and fluorescence microscopy. An EdU-based assay was also used to measure proliferating cells (Life Technologies, product #10640).

3.2.7 On-chip quantification of colonoid fluorescence and area

For imaging colonoid formation under each of the gradient conditions, fluorescence images were acquired every 24 h for a total of 5 days. Microscopy with a large depth-of-focus of 91 μm was used so that the majority of the colonoid volume resided within the image plane. A custom script was written in MATLAB (MathWorks; Natick, MA) to quantify the number of DsRed-positive pixels and the EGFP fluorescence intensity of pixels in each colonoid in the 2D image. Prior to quantitation, images from the DsRed channel were pre-processed to reduce background noise using top-hat filtering.[38] The images were then thresholded using Otsu's method[39] and "holes" were closed to identify the number of pixels occupied by each colonoid in the device. The number of pixels was then converted to the area occupied by the colonoid in the 2-D image. When manually reexamined, this strategy yielded zero false negatives (missed colonoids) and 2% false positives (structures misidentified as a colonoid) for n=1,050 colonoids. In addition to identifying the colonoids, the number of DsRed-positive pixels or colonoid area was also used as a proxy for colonoid size or total cell number. The images from the EGFP channel were pre-processed to reduce background noise (top-hat filtering) and the fluorescence

intensity of each pixel previously identified as being within the boundaries of colonoid (using the DsRed mask) was summed. The MATLAB script also included code to bin data from each of the devices according to the location on the device. For data analysis, the images of the gradient channel were divided into 4 regions each corresponding to a 1.25-mm length of the channel. The region adjacent to the source was always designated "region 1" while that nearest the sink was designated "region 4".

Boxplots were used to represent the non-normal distribution of colonoid area and EGFP fluorescence intensity of the developing colonoids. Within the boxplots, stars represented the mean, a bar represented the median, and the upper and lower boxes showed the 75% and 25% percentile of the data, respectively. The whiskers extended to the 5^{th} and 95^{th} percentile with outlying data shown as individual points. The data are presented in the text as medians, first- and third-quartile values for colonoid DsRed area and colonoid EGFP fluorescence intensity within the regions. For statistical comparison, the data were converted to a normal distribution using a logarithmic transform and assessed using an ANOVA mixed model (Fig. 10, Table 15). Data are also presented as average ± standard deviation where appropriate.

3.2.8 Off-chip quantification of colonoids possessing different fluorescent signatures

Crypts isolated from wild-type, *Sox9*EGFP mice were cultured in CCM at the indicated Wnt-3A and R-spondin1 concentrations in 12-well plates. After 5 days in culture, colonoids were fixed, and stained with a fluorescent marker as described above. Hoechst 33442 staining was used to identify nuclei. Imaging was performed at low resolution (91 μm depth of field) so that the entire colonoid was captured in a single image plane. Blue Hoechst fluorescence was used to identify and segment colonoids. All other image processing was as described above. Based on percentages obtained when freshly isolated crypts were stained and assayed, a colonoid was

judged to possess goblet cells if the number of pixels positive for Muc-2 was greater than 10% of the total colonoid pixel number. A colonoid was considered to possess enteroendocrine cells if the pixels positive for Chg-A was greater than 0.5% the total colonoid pixel number. All data sets reflect $n \geq 20$ colonoids.

3.2.9 Off-chip quantification of the colonoid volume displaying a fluorescent signature

Crypts isolated from wild-type, *Sox9*EGFP mice were cultured in CCM at the indicated Wnt-3A and R-spondin1 concentrations in 12-well plates. After 5 days in culture, colonoids were fixed, and stained with a fluorescent marker (immunofluorescence, EdU or other) as described above. Hoechst 33442 staining was used to identify nuclei and segment the colonoids in three dimensions. The colonoids were imaged confocally to obtain a set of image slices covering the entire volume of the colonoid. Thresholding and masking were performed for each confocal slice as described in the prior section. To quantify the percentage of pixels in a colonoid possessing a fluorescent marker, the number of pixels positive for the fluorescence marker in every image slice of that colonoid was divided by the total number of pixels in the colonoid. This was then reported as the percentage of colonoid volume positive for the fluorescent marker. All data sets reflect at least $n = 5$ colonoids.

3.3 Results and Discussion

3.3.1 Gradient characterization

The current work focused on the adaptation, characterization and utilization of a simple, gradient-generating microdevice to assess the dose-dependent effects of the two principle Wnt-signaling proteins, Wnt-3a and R-spondin1, on colonic stem/transit-amplifying-cell activity using the colonoid as an in vitro model system. PDMS was selected as the material of choice for the device since PDMS microdevices can be readily prepared on a benchtop, are gas permeable,

and are compatible with colonic stem cells.[41] The device design was simple, incorporating a central 5-mm-long microchannel with a large reservoir at either end. The gradient was formed across the microchannel which was filled with Matrigel (Fig 5). The reservoir volumes were 100× that of the gradient forming region.[42, 43]

FITC-dextran (40 kDa) was used as a model analyte to characterize the gradient formed on the device as it is similar in molecular weight to Wnt-3a (39.7 kDa) and R-spondin1 (40.0 kDa). The microchannel was imaged over time by fluorescence microscopy after addition of a solution of the fluorescent dextran to the source reservoir. At times after 24 h, the measured fluorescence through the microchannel displayed a linear decrease from the source to the sink reservoirs (Fig. 1B). The temporal evolution of the fluorescence intensity across the microchannel was fit to Fick's Law. The experimentally measured molecular diffusion coefficient of the FITC-dextran was 7.4±0.5 × 10-11 m^2/sec, which is similar to that measured for vascular epithelial growth factor (42 kDa) through Matrigel (7.0 × 10-11 m^2/sec).[44, 45] To maintain this linear gradient over long time scales, the source and sink solutions were replaced every 24 h. Construction of a model incorporating these solution changes indicated that the concentration of a 40 kDa analyte across the microchannel will vary by no more than 0.3% over a 5 day period. These data indicated that a stable, linear gradient was successfully established across the Matrigel plug within the microchannel between the source and sink reservoirs. Similar gradient strategies have been employed successfully by others.[42, 43]

3.3.2 Comparison of colonoids culture on the microdevice to that cultured under standard conditions

To determine whether culture within the PDMS device altered colonoid formation and growth, freshly isolated crypts were mixed with Matrigel and loaded into the microchannel.

CCM containing typical concentrations of both Wnt-3a (120 ng/mL) and R-spondin1 (175 ng/mL) for colonoid culture was placed into both the source and sink reservoirs of the microdevice and replenished every 24 h during culture. In parallel, crypts were cultured in a conventional Matrigel patty overlaid with the identical CCM which was also replaced every 24 h. Crypts from a Sox9EGFP-CAGDsRed mouse were used since the expression of DsRed in all cells and EGFP in stem/transit-amplifying cells enabled rapid assessment of both colonoid size (DsRed+) and the relative number of proliferative cells (EGFP+).[35] Of the crypts plated in the microdevice, 62.0±12.5% (avg.±s.d.) developed into colonoids with a median DsRed area of 15,010 μm^2 after 5 days in culture (Table 2). In comparison, 63.5±7.5% of crypts plated and cultured for 5 days in the Matrigel patties under standard conditions developed into colonoids with a median DsRed area of 16,240 μm^2 (Table 2). The percentage of colonoids possessing EGFP expression was similar under both conditions with 82.0±7.0% (microdevice) and 80.5±6.0% (control) of colonoids positive for EGFP. The average EGFP fluorescence intensity per colonoid on the entire device increased from day 1 to day 5. The median integrated EGFP fluorescence per colonoid on day 1 and day 5 was 23,250 and 62,830 RFUs, respectively, suggesting that the colonoids possessed actively dividing populations of colonic stem cells (Table 3). In comparison, colonoids cultured for 5 days in the Matrigel patties under standard conditions developed into colonoids with an average EGFP fluorescence similar to that of colonoids cultured on the microdevice. The median EGFP fluorescence per colonoid on day 1 and day 5 was 26,810 and 66,610 RFUs, respectively (Table 3). These data demonstrated that the rate of colonoid formation and growth and the numbers of stem/transit-amplifying cells increased within expanding colonoids in the microdevice in a manner similar to that in conventional Matrigel patties.

The presence of differentiated cell lineages, goblet and enteroendocrine cells, in colonoids on the microdevice was also compared to that of colonoids under conventional culture conditions (Fig. 1A-C). At 5 days after plating freshly isolated crypts, the colonoids in the microchannel were assayed for these lineages and compared with controls cultured under standard conditions. The percentage of colonoids on the microdevice expressing goblet cells (Muc-2+) was 95.0±3.5%, compared to 92.5±5.5% in the Matrigel patty (Fig. 1D). The percentage of colonoids containing enteroendocrine cells (ChgA+) was 38.5±10.0% on the microdevice, which was similar to that for colonoids in standard culture (34.5±13.5%) (Fig. 1D). These data demonstrated that colonoids cultured on the microdevice and in the Matrigel patty developed similarly in terms of the presence of differentiated cell types.

3.3.3 Comparison of colonoids cultured in different regions of the microchannel in the absence of a gradient.

Due to the length of the microchannel, it was important to determine whether colonoids developed identically throughout the length of the channel in the absence of a gradient. Crypts from a *Sox9*EGFP-CAGDsRed mouse were loaded and cultured in Matrigel on the microdevice with CCM containing Wnt-3a (120 ng/mL) and R-spondin1 (175 ng/mL) in both the source and sink reservoirs. The properties of the colonoids in each of the 4 regions of the channel were quantified from images acquired daily over 5 days (Fig. 2A). To compare colonoid size in each region, the DsRed area per colonoid was determined for each of the 4 regions. Ten separate devices were assayed (n=253, 277, 266, 254 total number of colonoids after 5 days in regions 1-4, respectively). Colonoids expanded in all regions of the microdevice and the median DsRed area per colonoid was 15,731 μm^2 (region 1), 12,767 μm^2 (region 2), 13,930 μm^2 (region 3) and 13,320 μm^2 (region 4) (Fig. 2C, D and Table 4). To assess stem/transit-amplifying cell renewal

and expansion in each of the four regions across the device, EGFP fluorescence was measured. At day 5, the median EGFP fluorescence per colonoid was 56,157 RFUs (region 1), 66,039 RFUs (region 2), 58,758 RFUs (region 3) and 58,766 RFUs (region 4) (Fig. 2E, F and Table 5). Based on these data, colonoid growth and stem/transit-amplifying cell number was similar in all regions of the microchannel.

3.3.4 Effect of wnt-3a concentration on colonoid expansion and stem/transit-amplifying cell number

Crypts were loaded into the microchannel as above, but Wnt-3a (120 ng/mL) was placed in the source reservoir while medium lacking Wnt-3a was placed in the sink reservoir. The R-spondin1 concentration was held constant at 175 ng/mL in both reservoirs. Seven separate devices were assayed to examine the effect of the Wnt-3a concentration on the colonoids (Table 1). After 24 h in culture, the differences in the DsRed area per colonoid were not statistically significant across the four device regions suggesting that at this early time the size of colonoids developing from the crypts was similar at all Wnt-3A concentrations (Fig. 6A, C). However, after 5 days in culture, the average DsRed area per colonoid (n=181, 173, 194, 179 colonoids in regions 1-4, respectively) varied considerably between regions (Fig. 3B, D and Table 6). The largest colonoids were present in regions 1 and 2 ((Wnt-3a) > 60 ng/mL) with median areas of 10,721 μm^2 and 8,960 μm^2, respectively. The area of colonoids cultured in regions 3 and 4 ((Wnt-3a) < 60 ng/mL) demonstrated median areas of 8,566 and 4,610μm^2, respectively. A comparison of colonoids cultured at Wnt-3a concentrations above (regions 1 and 2) and below (regions 3 and 4) 60 ng/mL showed that colonoids expanded significantly more at the higher concentration ($p=0.022$). These data suggested a critical concentration for Wnt-3a of 60 ng/mL for colonoid maintenance when the R-spondin1 concentration was constant at 175 ng/mL.

The impact of Wnt-3a concentration on the stem/transit amplifying cell number within the colonoids was then assessed. After 5 days in culture, the colonoids in regions 1 and 2 possessed much greater EGFP fluorescence per colonoid than those in regions 3 and 4 with median EGFP fluorescence of 68,773, 39,738, 20,605 and 12,082 RFUs, for regions 1-4, respectively (Fig. 7 and Table 7). The colonoids cultured in regions 3 and 4 demonstrated a lower EGFP fluorescence that was statistically significant compared with that in regions 1 and 2 ($p=0.001$). These data revealed a dose-dependent impact on stem/transit-amplifying cell proliferation in response to (Wnt-3a), consistent with a minimal required concentration of 60 ng/mL. This concentration is well below that used for colonoid culture in the vast majority of publications (250-500 ng/mL).[1,35] Thus, current accepted *in vitro* culture conditions appear to be utilizing a vast excess of Wnt-3a well above the threshold needed for stem-cell renewal and maintenance.

3.3.5 Effect of R-Spondin1 Concentration on Colonoid Expansion and Stem/Transit-Amplifying Cell Number.

Crypts were cultured in the microchannel under a linear R-spondin1 gradient (0-175 ng/ml). At 24 h, the DsRed area per colonoid was similar across the 4 regions of the microchannel (Fig. 7A, C). After 5 days in culture, the largest colonoids developed in regions 1-3 at (R-spondin1) > 44 ng/mL with median DsRed areas per colonoid of 9,870, 11,798, 8,857, and 5,569 μm^2, for regions 1-4, respectively (Figure 7B, D and Table 8). The areas of colonoids in regions 1 and 2 were statistically different compared to that of region 4 colonoids ($p=0.042$). The impact of R-spondin1 concentration on stem/transit-amplifying cell numbers was also assessed by measuring colonoid EGFP fluorescence. After 5 days in culture, colonoids in regions 1 and 2 possessed statistically significant greater levels of EGFP fluorescence per colonoid relative to regions 3 and 4 with median values of 54,298, 59,967, 34,149 and 43,982 RFUs,

respectively in regions 1-4 (Fig. 7B, F and Table 9, p=0.011). Six separate devices were assayed for these data (n=162, 152, 181, 164 total number of colonoids after 5 days in regions 1-4, respectively). Taken together, the data on colonoid area and stem/transit-amplifying cell proliferation support a minimal concentration for the bioactivity of R-spondin1 near 88 ng/mL *i.e.* that concentration occurring near the interface of regions 2 and 3. This R-spondin1 concentration is well below that which has been empirically used in colonoid culture systems (500-1000 ng/mL),[1,35] again suggesting that current *in vitro* culture conditions utilize an R-spondin1 concentration well above that needed to support stem-cell renewal.

3.3.6 Colonoid Growth in the Presence of Combined Wnt-3a and R-spondin1 Gradients.

In the prior experiments, the concentration of one of the growth factors was held constant at a supra-threshold concentration while the other was varied. To understand whether colonoids could expand and maintain stem cells when cultured in the presence of both Wnt-3a and R-spondin1 at lower concentrations, colonoids were cultured on the gradient device under conditions in which the minimal required concentrations of Wnt-3a and R-spondin1 coincided at the interface of regions 2 and 3. Wnt-3a (120 ng/mL) and R-spondin1 (175 ng/mL) were added to the source reservoir, but were excluded from the sink (Table 1). Six separate devices were assayed (n=147, 163, 152, 148 total number of colonoids after 5 days in regions 1-4, respectively). At 24 h of culture, the 4 channel regions possessed similar DsRed area per colonoid (Figure 3A, C, and Table 10). After 5 days in culture, colonoids in region 1 experienced a >3-fold increase in area with the median value of 13,923 μm^2 (Fig. 3 and Table 10). Over this same timescale, colonoids cultured in regions 2, 3, and 4 increased their median areas by 1.8, 1.5 and 1.1-fold, respectively. The differences between colonoid sizes in region 1 and each of regions 2-4 were statistically significant (p=0.004); however, the area of colonoids in region 2

was not statistically different from that of the colonoids in regions 3-4 ($p=0.045$). When the EGFP fluorescence was examined, the colonoids in regions 1 and 2 increased their median integrated EGFP fluorescence intensity by 4.0- and 1.6-fold, respectively between days 1 and 5. Regions 3 and 4 on the other hand displayed an overall decrease in EGFP fluorescence, with a 0.7- and 0.3-fold decrease in EGFP fluorescence per colonoid, respectively, between days 1 and 5 (Table 11). The differences in EGFP fluorescence per colonoid between region 1-2 and that of regions 3-4 were statistically significant ($p=0.001$). Taken together these data suggested that the threshold concentrations of Wnt-3a (>60 ng/mL) and R-spondin1 (>88 ng/mL) were independent of each other. A minimum concentration of each factor (independent of the concentration of the other factor under these conditions) was required to support proliferation and growth of the stem/transit amplifying cells in the colonoids.

3.3.7 Comparison of growth factor reduced to conventional culture conditions

In the current literature, a wide range of growth factor concentrations are employed for colonoid maintenance during experimentation, with the majority of groups utilizing a (Wnt-3a) > 100 ng/mL[46] and R-spondin1 > 1,000 ng/mL.[6,12,34,35,47,48] In contrast, the gradient-device data suggests that significantly lower concentrations of these factors (Wnt-3a (60 ng/mL) and R-spondin1 (88 ng/mL)) will maintain stem cells and sustain colonoid cultures. For this reason, these growth-factor concentrations were compared to those used in conventional culture to determine whether colonoid attributes were similar under the two conditions. *Sox9*EGFP-CAGDsRed crypts were cultured within a Matrigel patty in 12-well plates and six parameters were compared: *i)* growth based on change in colonoid area over time, *ii)* differentiation based on presence of goblet and enteroendocrine cells, *iii)* stem cell maintenance/support based on

renewal of stem/transit amplifying cells, *iv)* cell proliferation based on Edu staining, *v)* maintenance in culture based on passaging efficiency, and *vi)* morphologic characteristics based on colonoid bud formation.

At 24 h in culture, the average colonoid area was 6,271 ± 852 and 6,818 ± 930 μm^2 for growth factor reduced and conventional conditions, respectively.[35] After 5 days in culture, colonoids continued to maintain similar areas, 28,129 ± 2,309 and 29,621 ± 2,957 μm^2 under both conditions (Fig. 4A). The presence of goblet cells (Muc2), enteroendocrine cells (ChgA), stem/transit amplifying cells (EGFP-Sox9) and actively proliferating cells (EdU-based assay) in the colonoids were also similar at day 5 (Fig. 4C and Fig. 9). A greater percentage of the colonoid volume was occupied by enteroendocrine cells (ChgA+) than that of colonoids under conventional culture (1.2 ± 0.2% *versus* 0.6 ± 0.2%, $p \leq 0.047$). The numbers of these rare cells were still low compared to normal crypts which possess ~6% ChgA+ cells. When all assays were considered, the two culture systems yielded similar numbers of stem/transit amplifying and differentiated cells.

To compare the morphological characteristics of the colonoids grown under both conditions, the presence of buds or multi-cellular protrusions around the central lumen of individual colonoids was assessed. These buds house collections of stem cells and previous work by Sato and colleagues suggests that budding might be an early stage of crypt formation.[12] Thus colonoids with greater budding profiles are likely to be more representative of a normal phenotype. Two colonoid attributes (solidity and area divided by perimeter) were utilized as a metric for the presence of bud formation around a central lumen. The solidity defined as the colonoid area divided by the convex hull area in the 2D image measured the extent to which the colonoid area was studded with concave cavities such as might occur between buds. Whereas the

area divided by perimeter is more reflective of how convoluted the colonoid surface is. A training data set of manually identified budding and nonbudding colonoids combined with support vector machine learning was used to classify test colonoids grown under the different culture conditions as either budding or non-budding (Fig. 8). The majority of colonoids cultured under the reduced growth factor conditions (92 ± 6 %, n = 3 experimental replicates of 25 colonoids each) were classified as possessing buds, whereas only 8 ± 4 % of colonoids (n = 3 experimental replicates of 25 colonoids each) cultured under the conventional conditions were scored as possessing buds (Fig. 4D). The much greater number of colonoids possessing buds under the reduced factor conditions suggested that these conditions promoted more appropriate gut morphologic patterning than the higher concentrations of Wnt-3a and R-spondin1.[49,50] These data are also consistent with the greater number of ChgA+ cells in the reduced-factor conditions observed previously. Colonoids cultured under the conventional factor conditions also displayed a more cystic morphology with thin outer walls relative to that under conventional conditions (Fig. 4B). Gracz and colleagues recently characterized the genotypic differences between the cystic and noncystic colonoid morphologies.[51] While both phenotypes possess a central lumen, the noncystic phenotype displays a greater mRNA expression of proteins characteristic of differentiated lineages, whereas the cystic structures exhibit gene expression patterns consistent with high levels of Wnt signaling and cell turnover, but low levels of differentiation. Taken together these data suggest that the reduced-factor conditions promote a more morphologically relevant colonoid with a phenotype more similar to a crypt compared to the conventional culture conditions.

A critical attribute of any culture system is the efficiency of passage or the length of time that the culture system can be maintained *in vitro*. To assess the ability to grow colonoids under

the reduced growth factor concentrations on long time scales, cells from freshly isolated crypts were plated at identical densities and cultured. After 5 days, the total number of colonoids arising from the plated cells was counted and then harvested, fragmented and 10^4 cells from this harvest re-plated in culture. This process was repeated every 5 days, for a total of 3 passages. Colonoid outgrowth was similar for both the reduced factor and conventional culture systems, with no statistical difference in the number of colonoids generated after each passage step (Figure 4E). These data suggest that the identified, minimal concentrations of Wnt-3a and R-spondin1 did not affect bulk size or longevity of colonoid culture, but did produce a more morphologically appropriate mini-gut compared to standard culture conditions. Additionally, the reduction in factor concentrations needed to maintain the colonoids in culture is expected to lower the reagent cost of colonoid culture by 66% (Table 12, 14).

3.4 Conclusions

We describe the implementation of a microengineered technology to create tightly controlled linear gradients of morphogenic factors along a defined culture region housing a population of primary colonic organoids to enable efficient and rapid screening of cell proliferation and differentiation within the colonoids. The microdevice enabled a substantial reduction in the quantity of Matrigel and expensive growth factors needed to assay a wide range of factor concentrations for colonoid growth since the volume of the microchannel (~10 μL) was small compared that on a 96-well plate. For example, 10 microwells of a standard 96-well plate would consume 25 mL of these reagents, 5 × greater volumes. The reduction in the assay volume needed to survey a wide range of factor concentrations would similarly greatly decrease the numbers of mice needing to be sacrificed to optimize factor concentrations. The decreased need for tissue would in turn translate to smaller breeding numbers and transgenic mouse colony

size.

The technology made possible the efficient elucidation of optimum protein factor concentrations for stem-cell renewal (proliferation) and colonoid growth. Colonoids were exposed to four experimental conditions: no gradient in a high Wnt-3a and high R-spondin1 environment, a Wnt-3a gradient in a high R-spondin1 environment, an R-spondin1 gradient in a high Wnt-3a environment, and a combined Wnt-3a and R-spondin1 gradient. Thresholds of 60 ng/mL of Wnt-3a and 88 ng/mL of R-spondin1 were the minimal concentrations of these factors required to stimulate stem cell proliferation and overall colonoid growth. Prior research utilizing cultured colonoids has in general used substantially greater concentrations with Wnt-3a concentrations up to 100 ng/mL and R-spondin1 concentrations up to 1,000 ng/mL. The overstimulation of Wnt signaling pathways in these colonoid culture systems may account for their paucity of absorptive enterocytes and excessive numbers of stem cells relative to that in normal colon. By utilizing the threshold concentrations of Wnt-3a and R-spondin1 identified in this work, a colonoid phenotype was generated displaying crypt-like budding and columnar morphology with greater expression of enteroendocrine lineages. Use of these reduced factor concentrations will permit more physiologically relevant colonoid culture conditions at significant cost savings by virtue of the reduced concentrations of expensive growth factors. The microfluidic device and protocols described in this series of experiments will enable intestinal biologists to pursue further in-depth combinatorial screens of factors and pharmacologic compounds for controlling colon stem-cell renewal and differentiation.

3.5 Figures

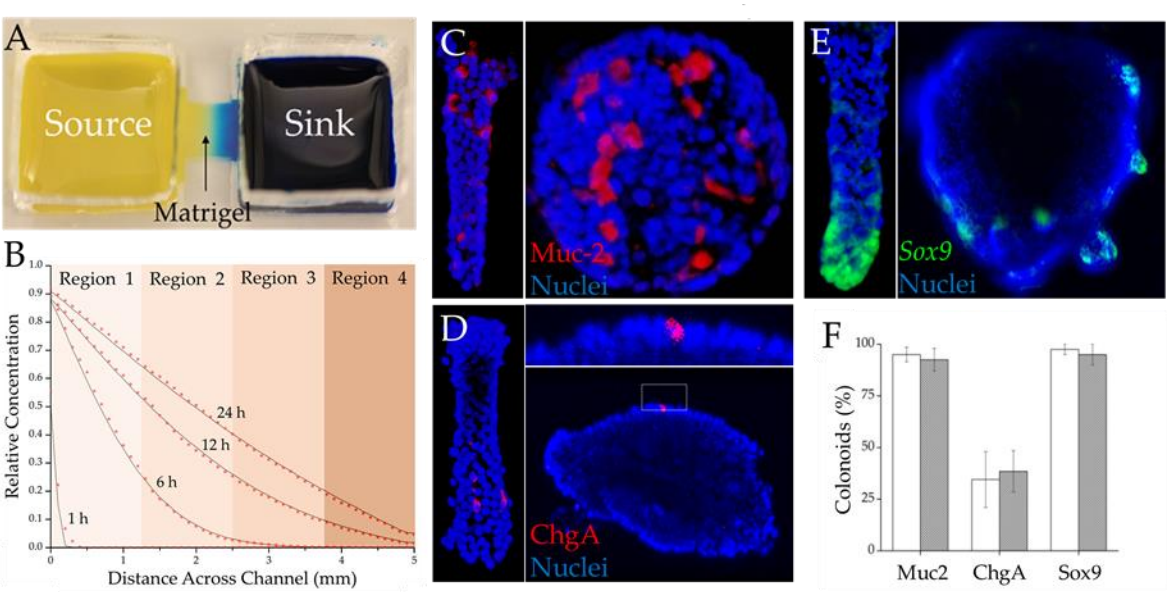

Figure 3.1 Characterization of the gradient-generating microdevice. (A) Photograph of the device. The Matrigel-filled gradient region resides between the source (left with yellow dye) and sink (right with blue dye) reservoirs. (B) Gradient characterization on the microdevice. Movement of a 40 kDa FITC-dextran through the channel was monitored using time-lapse fluorescence imaging. The experimentally measured data is marked as red stars. The solid black line is the fit to the data using Fick's Law. (C, D) Freshly isolated crypts and colonoids (Sox9EGFP-only mice) cultured for 5 days on the microdevice were stained for goblet cells (Muc2) (C), and enteroendocrine cells (ChgA) (D) and imaged by confocal microscopy. Nuclei were stained with Hoechst 33342 (blue). (E) Crypts/colonoids treated as in panels C and D but imaged for EGFP (EGFP-Sox9) which marks stem/transit amplifying cells (E). (F) Histogram showing percentages of colonoids possessing goblet cells (Muc2+), enteroendocrine cells (ChgA+), and stem/transit-amplifying cells (EGFP-Sox9+) in colonoids cultured on the microdevice (white bars) or conventional Matrigel-patty culture (grey bars).

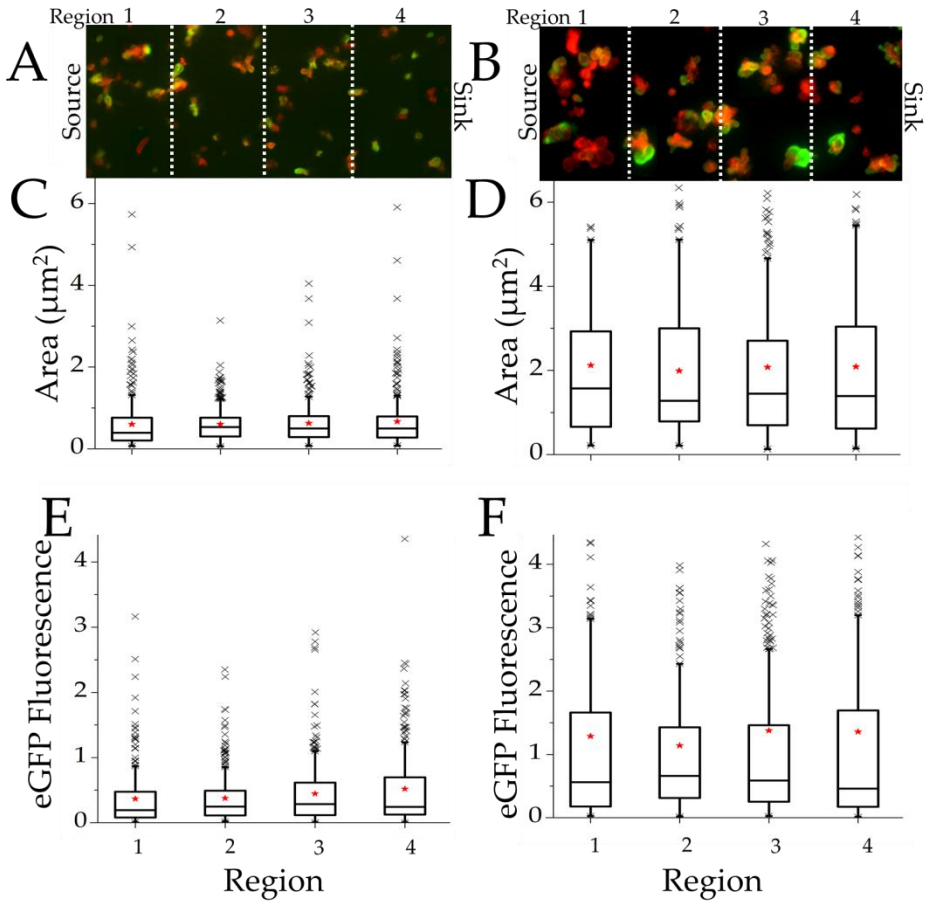

Figure 3.2 Culture of colonoids in the absence of a gradient. Colonoid data is shown at days 1 (A, C, E) and 5 (B, D, F) of culture. Overlaid DsRed-EGFP fluorescence images of the colonoids are shown (A, B). The scale bar represents 500 μm. Boxplots were used to represent the non-normal distribution of the area (C, D) or EGFP-Sox9 fluorescence (E, F) per colonoid. Colonoid area is represented as μm^2 (× 104) and integrated EGFP fluorescent intensity is represented as RFUs (× 105). For the boxplots, the red stars indicate the mean of the data, the bar shows the median, and the upper and lower boxes represent the 75% and 25% of the data, respectively. The whiskers extend to the 5% and 95% with the individual points showing outliers.

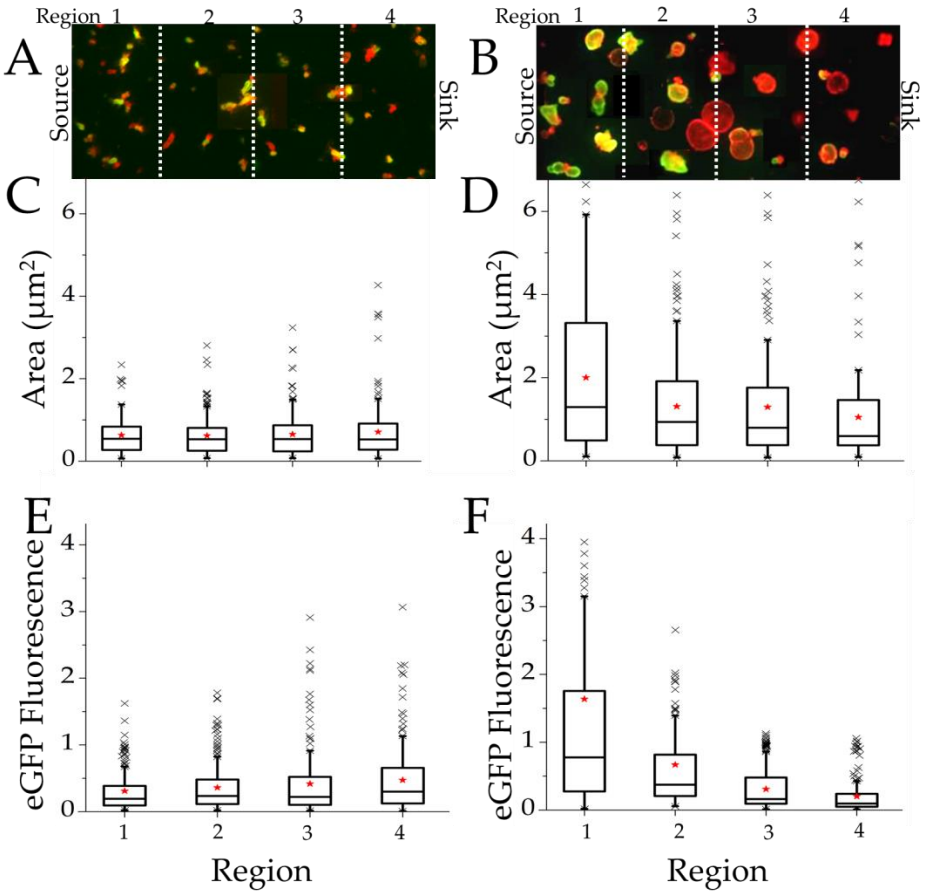

Figure 3.3 Culture of colonoids in the presence of a combined R-spondin1 and Wnt-3a gradient. Colonoid data is shown at days 1 (A, C, E) and 5 (B, D, F) of culture. Overlaid DsRed-EGFP fluorescence images of the colonoids are shown (A, B). The scale bar represents 500 μm. Boxplots as described in the legend of Fig 2 were used to represent the non-normal distribution of the area (C,D) or EGFP-Sox9 fluorescence (E, F) per colonoid. Colonoid area is represented as μm^2 ($\times 10^4$) and integrated EGFP fluorescent intensity is represented as RFUs ($\times$ 105). The Wnt-3a and R-spondin1 concentrations in the sink were 0 ng/mL while that in the source was and 120 and 175 ng/mL, respectively. The threshold concentration of each factor occurred at the interface between regions 2 and 3 and is marked by the yellow arrow.

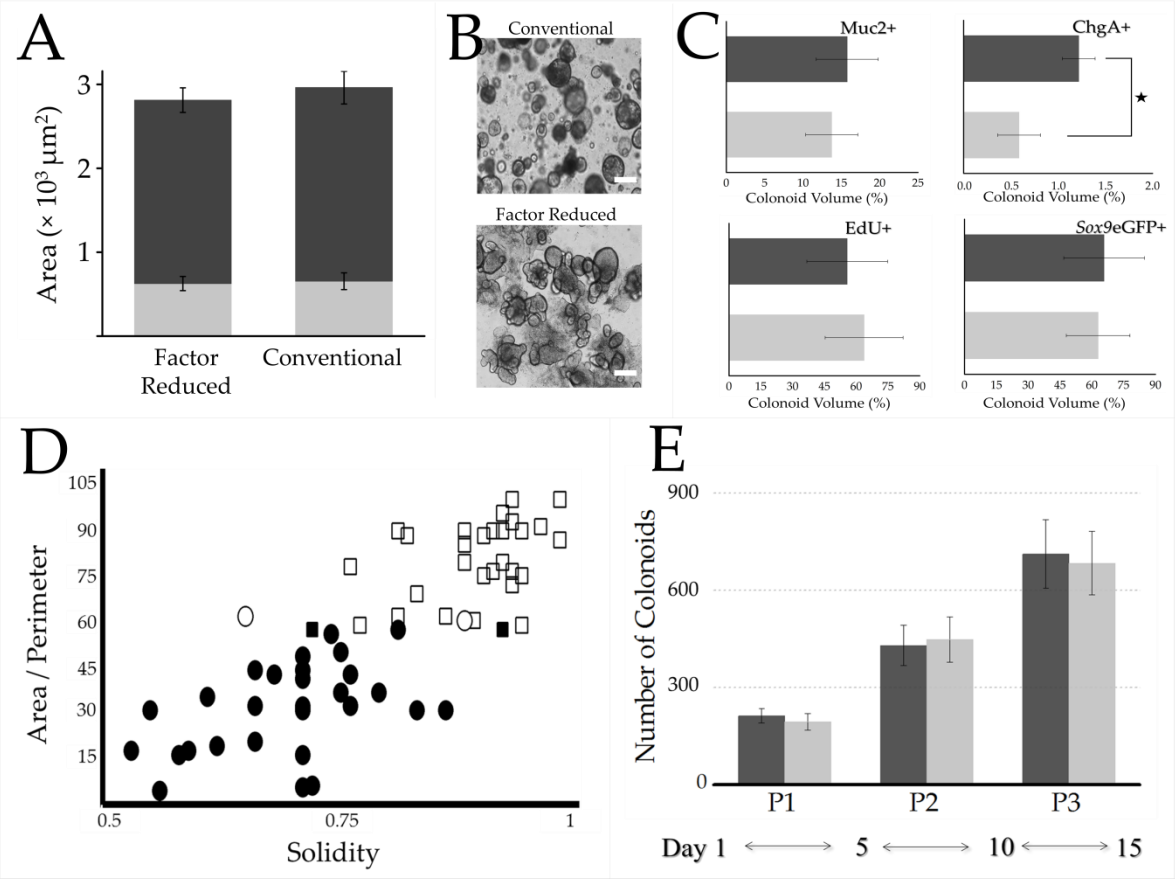

Figure 3.4 Properties of colonoids cultured under both conditions. Properties of colonies cultured under growth factor reduced (Wnt-3a: 60 ng/mL, R-spondin1: 88 ng/mL) vs. conventional (Wnt-3a: 100 ng/mL, R-spondin1: 1,000 ng/mL) conditions. (A) Colonoid size at day 1 (light gray) and 5 (dark gray) of culture. (B) Representative image of colonoids cultured under the conventional conditions and the reduced growth factor conditions. Scale bar is 200 µm. (C) Upper two panels: Immunofluorescence staining of mucin 2 (Muc2) and chromogranin A (ChgA) for colonoids grown under conventional (light grey) and growth reduced growth factor (dark grey) conditions. Lower left panel: EdU-based assay for proliferation. Lower right panel: eGFP expressed under a Sox9 promoter. Each data set represents n=5 colonoids. (D) Colonoid solidity plotted against colonoid area divided by colonoid perimeter. Each symbol represents a single colonoid cultured under either the conventional (square) or reduced growth factor (circle)

conditions. Solid symbols (square or circle) represent the colonoids that were classified as budding and open symbols (square or circle) represent the colonoids that are classified as non-budding. (E) Quantification of the number of colonoids formed after 3 passages (P1, P2, P3) in conventional (light grey) growth reduced growth factor (dark grey) conditions.

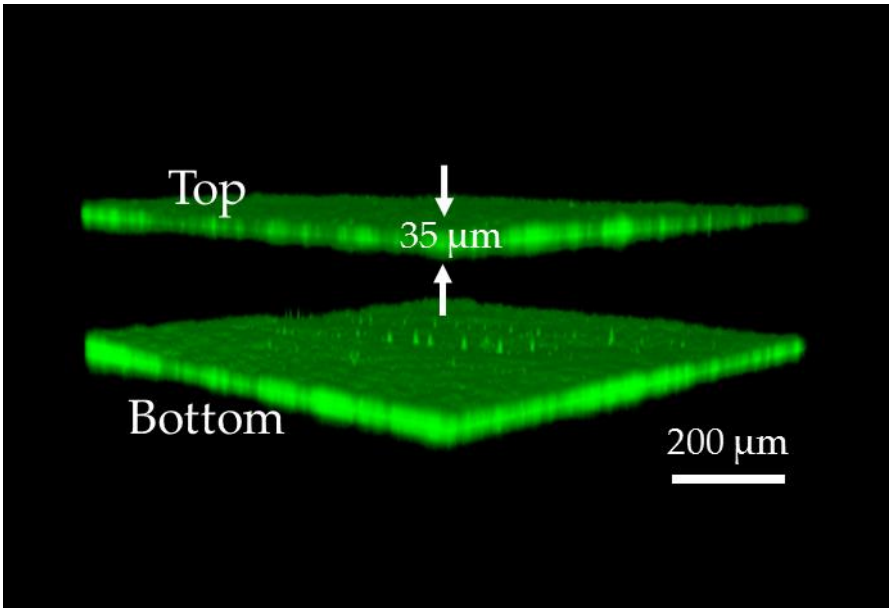

Figure 3.5 Matrigel pre-coat characterization. Shown is a reconstructed confocal image through a device pre-coated with Matrigel mixed with fluorescein-dextran. The coating on the top and bottom surfaces of the channel are visible as green sheets (top panel) or green lines (bottom panel), but the side walls are out of the field-of-view. The top panel is a tilted 3-D reconstruction while the lower panel is a single reconstructed Z-slice. The coatings were highly reproducible with the average coating thickness of 35 ± 5 µm, surveyed across 3 independent devices.

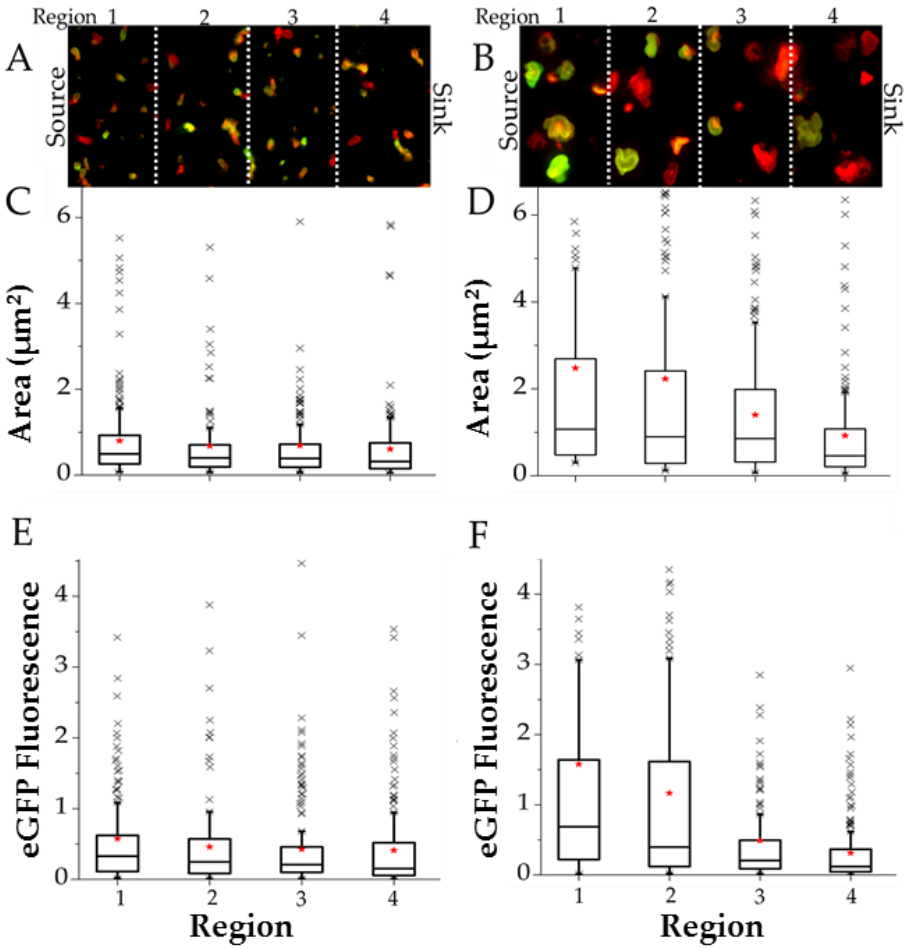

Figure 3.6 Culture of colonoids in the presence of a Wnt-3a gradient.

Colonoid data is shown at days 1 (A, C, E) and 5 (B, D, F). Overlaid red-green images of the colonoids are shown (A,B). The scale bar represents 500 µm. Boxplots were used to represent the non-normal distribution of the area (C, D) or EGFP fluorescence (E, F) per colonoid. Colonoid area is represented as μm^2 ($\times 10^4$) and integrated EGFP fluorescent intensity is represented as RFUs (× 105). The R-spondin1 concentration in the source and sink was 175 ng/mL while the Wnt-3a concentration was 0 ng/mL (sink) and 120 ng/mL (source). The threshold concentration (60 ng/mL) coincided at the interface between region 2 and region 3 and is marked by the arrow.

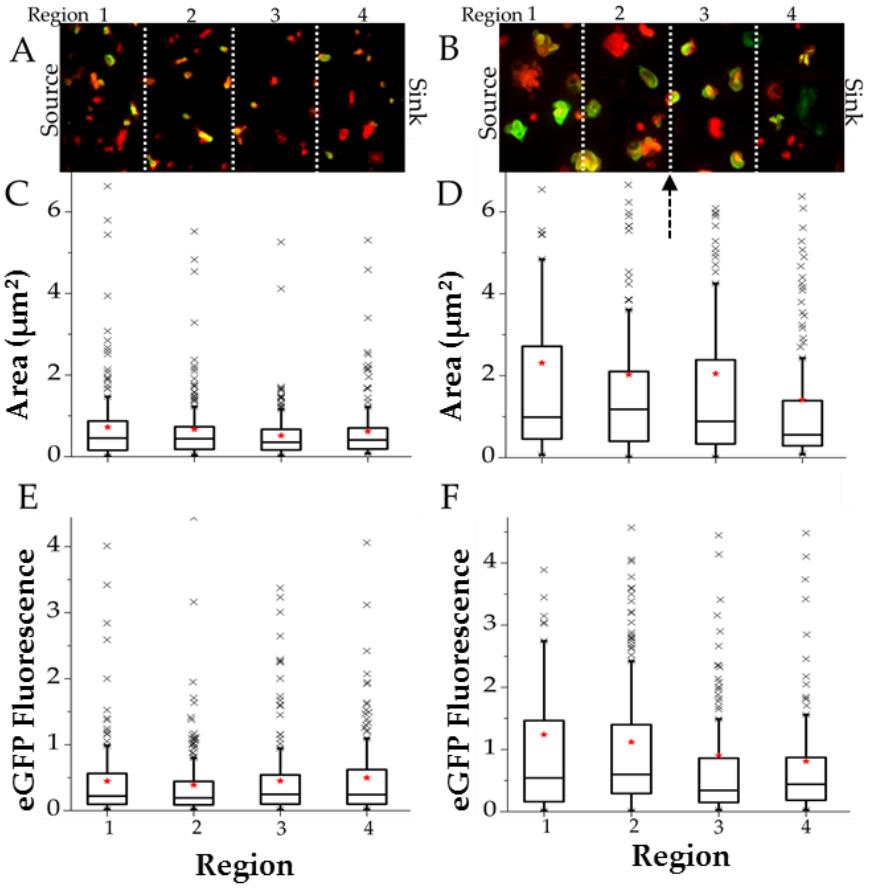

Figure 3.7 Culture of colonoids in the presence of an R-spondin1 gradient. Colonoid data is shown at days 1 (A, C, E) and 5 (B, D, F). Overlaid red-green images of the colonoids are shown (A, B). The scale bar represents 500 μm. Boxplots as described in the legend of Fig. 2 were used to represent the non-normal distribution of the area (C,D) or EGFP fluorescence (E, F) per colonoid. Area is represented as μm^2 ($\times 10^4$) and integrated EGFP fluorescence intensity is represented as RFUs ($\times 10^5$).The Wnt-3a concentration in the source and sink was 120 ng/mL while the R-spondin1 concentration was 0 ng/mL (sink) and 175 ng/mL (source). The threshold concentration (90 ng/mL) coincided at the interface between region 2 and region 3 and is marked by the arrow.

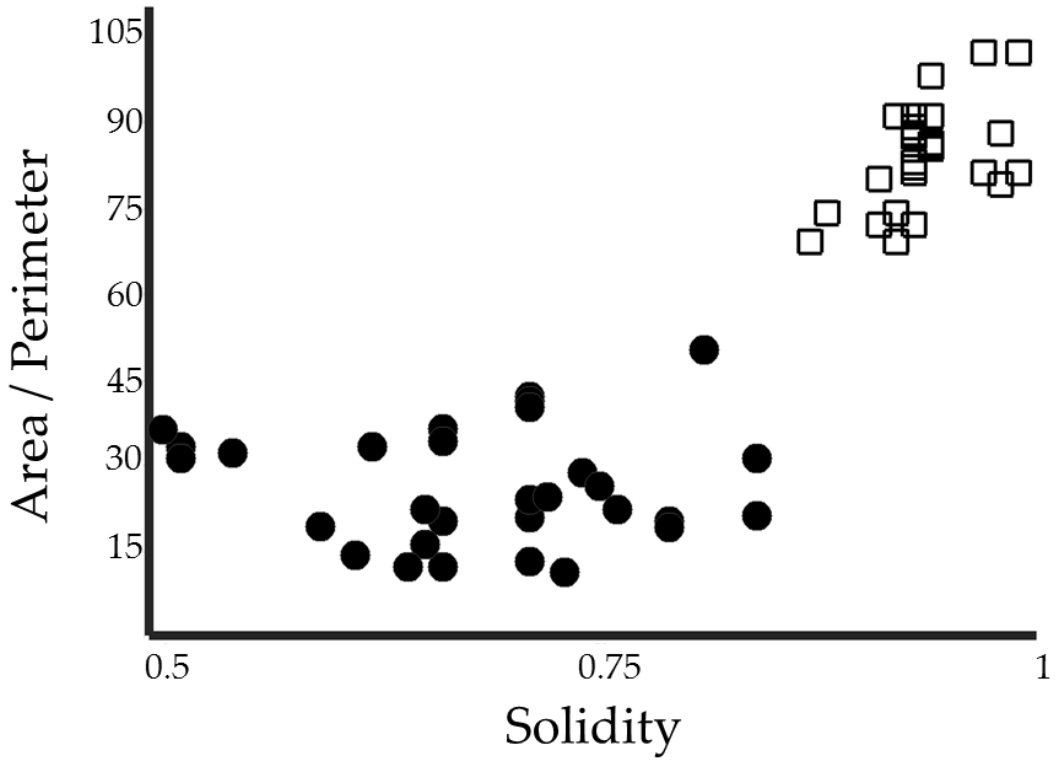

Figure 3.8 Training set used to classify budding. Training colonoid set to used to classify budding *vs* nonbudding colonoids based on area/perimeter and solidity with a learned Support Vector Machine model. Colonoid solidity was plotted against colonoid area divided by colonoid perimeter for colonoids manually identified as budding (n = 30, solid circles) or nonbudding (n = 30, open squares).

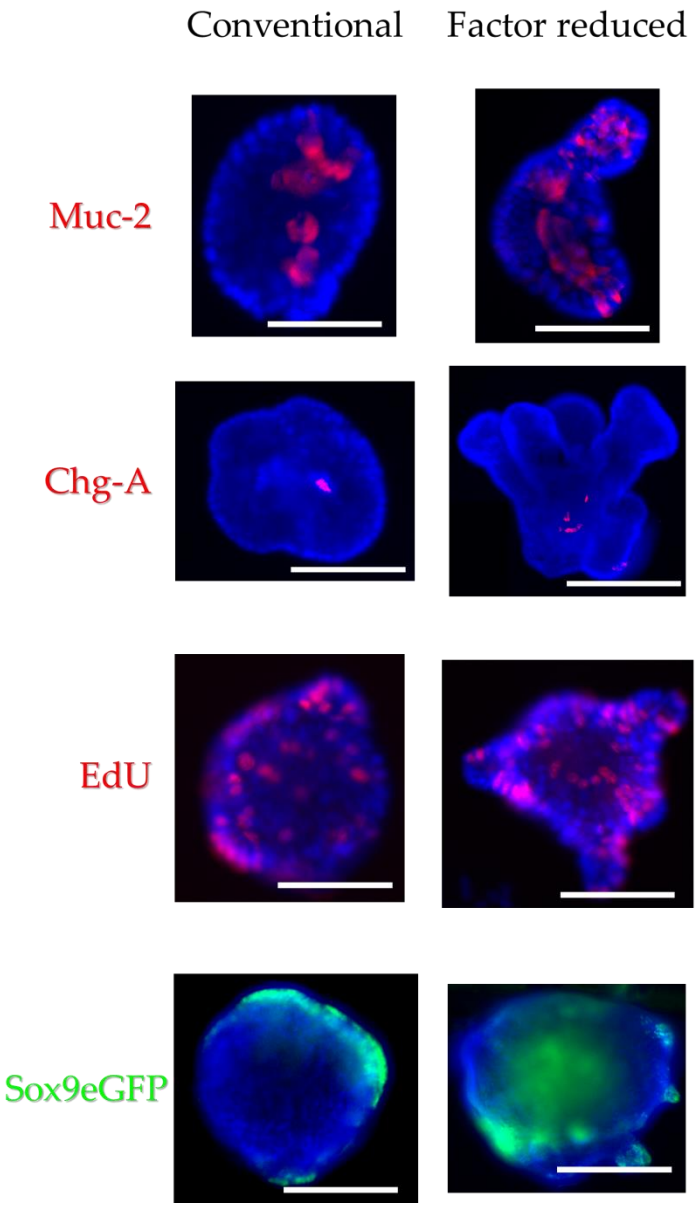

Figure 3.9 Fluorescence images of colonoids on day 5.

Shown are immunofluorescence images for mucin 2 (Muc-2, top row) and chromogranin A (Chg-A, 2nd row). The 3rd row shows a fluorescent EdU-based stain while the final row is EGFP expression (under a Sox9 promoter). The columns are colonoids grown under conventional (left) or reduced factor (right) culture conditions. The scale bars are 150 µm.

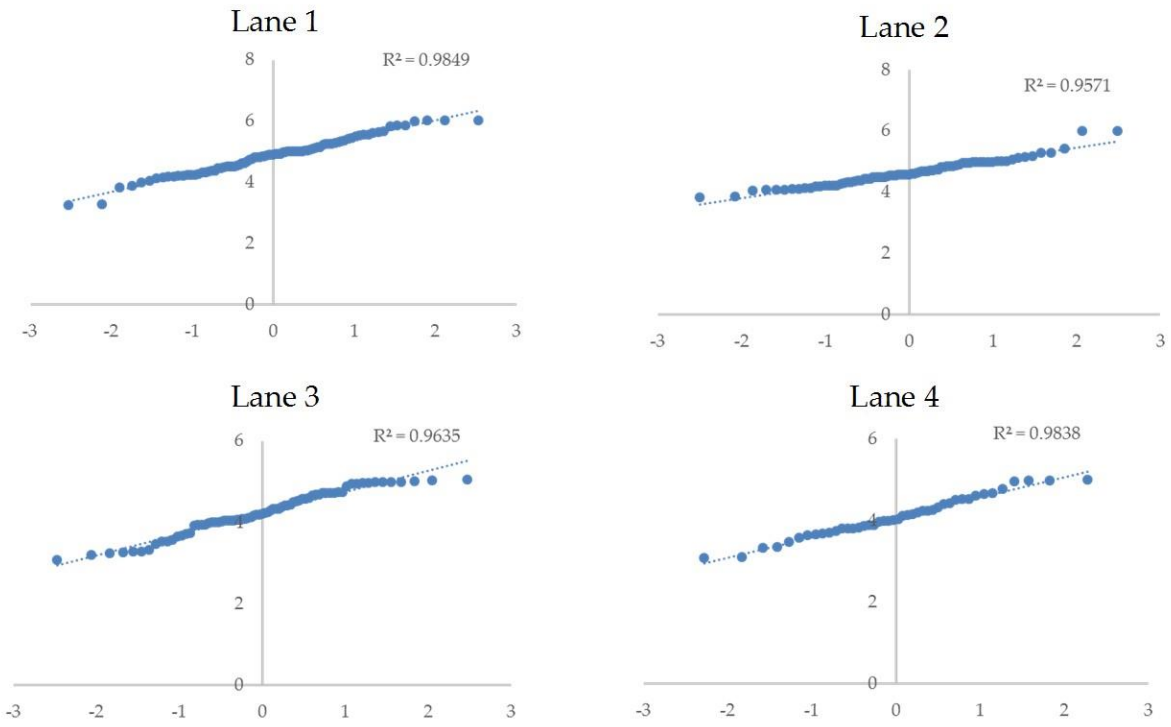

Figure 3.10 Q-Q Plot for the normalized data.

Quantile-quantile plots for the log transformed eGFP fluorescence intensity for the Wnt-3a + R-spondin gradient (Fig. 3E,F) on day 5. A quantile-quantile plot allows for the comparison of a sample of data on the vertical axis to a statistical population on the horizontal. The vertical axis of each plot represents the log-transformed experimental data (eGFP fluorescence intensity) while the horizontal axis displays the normal theoretical quantiles. The theoretical quantiles plotted on the x-axis are the predicted values if the data followed a purely Gaussian distribution. To calculate these theoretical quantiles, a percentile for each value of the data is computed followed by a rank based z-score analysis of the percentile values. The rank based z-score

determines how many standard deviations away from the mean you need to go to reach that percentile on a Gaussian distribution. For example, for the 18.78^{th} percentile, the rank based z-score is -0.886 (computed by the excel formula =*normsinv*(0.1878). This means that 18.78 percent of a standard normal distributed data set (mean =0, SD=1.0) is less than -0.886. The dashed line is the best-fit straight line through the data. R^2 is the adjusted coefficient of determination for the fit to the straight line.

3.6 Tables

Region	Wnt-3a ng/mL range (Average)	R-spondin1 ng/mL range (Average)
1	91-120 (105)	131-175 (153)
2	61-90 (75)	89-130 (109)
3	31-60 (45)	44-88 (66)
4	0-30 (15)	0-43 (22)

Table 3.1 Growth factor concentrations in the 4 regions of the microdevice.

Conditions	Day	Number of Crypts/Colonoids	Quartile 1	Median	Quartile 3
Microdevice	1	30	3,655	4,326	5,748
Standard	1	30	3,912	4,760	6,950
Microdevice	5	30	11,550	15,010	28,434
Standard	5	30	10,044	16,425	25,140

Table 3.2 Area occupied by each colonoid in a 2-D image slice in the absence of a gradient after 1 and 5 days of culture on the microdevice.

Conditions	Day	Number of Crypts/Colonoids	Quartile 1	Median	Quartile 3
Microdevice	1	30	9,458	23,250	61,280
Standard	1	30	10,760	26,810	55,434
Microdevice	5	30	35,966	60,830	147,415
Standard	5	30	37,840	66,610	163,320

Table 3.3 Area occupied by each colonoid cultured in a 2-D image slice in the absence of a gradient after 1 and 5 days of culture on the microdevice.

Region*	Day	Number of Crypts/Colonoids	Quartile 1 (μm^2)	Median (μm^2)	Quartile 3 (μm^2)
1	1	338	2,054	3,936	7,616
2	1	356	3,018	5,337	7,631
3	1	335	2,856	4,998	8,000
4	1	327	2,750	4,988	7,929
1	5	253	6,587	15,731	29,290
2	5	277	7,878	12,767	29,994
3	5	266	6,981	13,930	26,953
4	5	254	6,175	13,320	30,475

*Wnt-3a was at 120 ng/mL in the sink and source while R-spondin1 was at 175 ng/mL in the sink and source.

** Number of colonoids decreased from day 1 to day 5 as a result of merging colonoids and growth attrition.

Table 3.4 Area occupied by each colonoid in a 2-D image slice in the absence of a gradient after 1 and 5 days of culture on the microdevice.

Region*	Day	Number of Crypts/Colonoids	Quartile 1	Median	Quartile 3
1	1	338	7,858	19,360	47,520
2	1	356	11,210	24,688	49,017
3	1	335	11,602	28,408	61,585
4	1	327	12,519	24,277	69,591
1	5	253	17,769	56,157	166,056
2	5	277	31,138	66,039	142,704
3	5	266	25,782	58,758	143,274
4	5	254	21,561	58,766	156,359

Table 3.5 eGFP intensity per colonoid in the absence of a gradient after 1 and 5 days of culture on the microdevice.

*Wnt-3a was at 120 ng/mL in the sink and source while R-spondin1 was at 175 ng/mL in the sink and source.

Region*	Day	Number of Crypts/Colonoids	Quartile 1 (μm^2)	Median (μm^2)	Quartile 3 (μm^2)
1	1	257	2,615	4,939	9,264
2	1	244	1,925	4,000	7,058
3	1	268	1,869	3,881	7,204
4	1	250	1,501	3,178	7,496
1	5	181	4,790	10,721	26,912
2	5	173	2,879	8,960	24,129
3	5	194	3,182	8,566	19,859
4	5	179	2,095	4,610	10,797

Table 3.6 Area occupied by each colonoid in a 2-D image slice in the presence of a Wnt-3a gradient after 1 and 5 days of culture on the microdevice.

Region*	Day	Number of Crypts/Colonoids	Quartile 1	Median	Quartile 3
1	1	257	11,013	32,826	62,141
2	1	244	8,386	24,665	57,161
3	1	268	9,977	20,941	45,992
4	1	250	5,547	15,183	51,707
1	5	181	21,910	68,773	164,134
2	5	173	12,109	39,738	161,655
3	5	194	8,912	20,605	48,852
4	5	179	4,711	12,082	36,403

Table 3.7 eGFP intensity per colonoid in the presence of a Wnt-3a gradient after 1 and 5 days of culture on the microdevice.

*Wnt-3a was at 0 and 120 ng/mL in the sink and source, respectively, while R-spondin1 was at 175 ng/mL in the sink and source.

Region*	Day	Number of Crypts/Colonoids	Quartile 1 (μm^2)	Median (μm^2)	Quartile 3 (μm^2)
1	1	234	1,576	4,538	8,713
2	1	237	1,805	4,388	7,339
3	1	258	1,634	3,547	6,700
4	1	229	1,876	4,112	7,038
1	5	162	4,564	9,870	27,165
2	5	152	4,022	11,798	21,048
3	5	181	3,357	8,857	23,865
4	5	164	2,916	5,569	13,916

Table 3.8 Area occupied by each colonoid in a 2-D image slice in the presence of an R-spondin1 gradient after 1 and 5 days of culture on the microdevice.

Region*	Day	Number of Crypts/Colonoids	Quartile 1	Median	Quartile 3
1	1	234	9,761	22,194	56,434
2	1	237	8,694	19,452	44,429
3	1	258	9,833	24,665	54,164
4	1	229	9,890	24,401	62,144
1	5	162	15,966	54,298	146,460
2	5	152	19,220	59,967	140,036
3	5	181	14,931	34,149	85,976
4	5	164	18,332	43,982	87,193

Table 3.9 eGFP intensity per colonoid in the presence of an R-spondin1 gradient after 5 days of culture on the microdevice.

*R-spondin1 was at 0 and 175 ng/mL in the sink and source, respectively, while Wnt-3a was at 120 ng/mL in the sink and source.

Region*	Day	Number of Crypts/Colonoids	Quartile 1 (μm^2)	Median (μm^2)	Quartile 3 (μm^2)
1	1	221	2,737	5,448	8,364
2	1	233	2,515	5,314	8,057
3	1	220	2,397	5,374	8,696
4	1	225	2,799	5,297	9,114
1	5	147	4,973	13,923	32,335
2	5	163	3,775	9,343	19,165
3	5	152	3,762	7,975	17,616
4	5	148	3,751	5,963	14,630

Table 3.10 Area occupied by each colonoid in a 2-D image slice in the presence of a Wnt-3a and an R-spondin1 gradient after 1 and 5 days of culture on the microdevice.

Region*	Day	Number of Crypts/Colonoids	Quartile 1	Median	Quartile 3
1	1	221	9,458	19,460	38,596
2	1	233	11,514	23,572	48,315
3	1	220	10,366	22,168	52,063
4	1	225	12,469	30,102	65,651
1	5	147	27,395	77,744	175,614
2	5	163	20,739	37,311	81,546
3	5	152	9,314	16,232	47,912
4	5	148	4,823	9,660	23,978

Table 3.11 eGFP intensity per colonoid in the presence of a Wnt-3a and an R-spondin1 gradient after 1 and 5 days of culture on the microdevice.

*R-spondin1 was at 0 and 175 ng/mL in the sink and source, respectively, while Wnt-3a was at 0 and 120 ng/mL in the sink and source, respectively.

	Conventional		Factor Reduced	
Growth-Factor	Wnt-3a*	R-spondin 1*	Wnt-3a	R-spondin 1
Price/Amount	$230/2 µg	$315/25 µg	$230/2 µg	$315/25 µg
Stock Concentration	40 µg/mL	250 µg/mL	40 µg/mL	250 µg/mL
Working Concentration	100 ng/mL (400×)	1,000 ng/mL (250×)	60 ng/mL (667×)	88 ng/mL (2,841×)
Volume per Well**	10 µL / week	16 µL / week	6 µL / week	1.4 µL / week
Price per 12-Well Plate	$552.00 / week	$604.80 / week	$324.00 / week	$53.28 / week
Price per Year***	$16,560	$18,144	$9,720	$1,599
	$34,704 per year		**$11,319** per year	

Table 3.12 The cost-savings benefit of the reduced factor conditions identified in this research vs. conventional culture concentrations.

* Wnt-3a and R-spondin1purchased from the vendors listed in table S13.

**Calculations were made for cultures consisting of a total of 1 mL of media. Cultures were maintained for one week with media and growth factor exchanges occurring every other day. Each well therefore each required 3 mL of total media for the entirety of the week.

***Calculations were made for a total of 30-independent cultures that were maintained throughout the duration of a year.

Reagent	Vendor	Catalog Number	Stock Concentration	Working Concentration	Resuspended in:
Matrigel (GFR)	BD Bioscience	354230	100%	50%	Media
Murine Noggin	eBioscience	34-8004	100 µg/mL	100 ng/mL	PBS + 0.1% BSA
Murine Wnt-3a	R&D	1324-WN-002	40 µg/mL	60-100 ng/mL	PBS + 0.1% BSA
Human R-spondin1	R&D	4645-RS	250 µg/mL	88-1,000 ng/mL	PBS + 0.1% BSA
Murine EGFP	Invitrogen	PMG8-041	1 mg/mL	50 ng/mL	PBS + 0.1% BSA
Y27632 Inhibitor	Sigma-Aldrich	Y0503	10 mM	10 µM	PBS
Adv DMEMD/F12	Invitrogen	12634-010	-	-	-
NAC	Sigma-Aldrich	A9165	500 mM	1 mM	H_2O
N2	Invitrogen	17502-048	100×	1×	-
B27	Invitrogen	12587-010	50×	1×	-
GlutaMAX	Invitrogen	35050-061	100×	1×	-
Pen/Strep	Invitrogen	15070-063	5,000 µg/mL	1 µg/mL	H_2O
HEPES	Invitrogen	15630-080	1 M	10 mM	H_2O

Table 3.13 Media preparation for the off-chip colonoid characterization experiments.

There were two main components of this culture technique: Matrigel preparation and media preparation. The components of the Matrigel preparation can be seen in the light orange shading. All of the above growth factors and small molecules were added to the Matrigel (100 µL of Matrigel was used to plate ~10,000 crypts). The components of the media preparation can be seen with the light blue shade regions. Additives were added to the base media to create the culture media. After Matrigel polymerization, the culture media was overlaid (1 mL per 12-well plate). Before plating of the crypts, the Matrigel (containing all of the growth factors) was diluted in media at a 1:1 ratio.

	P1	P2	P3
Conventional	10.0 ± 1.7	10.0 ± 1.9	10.0 ± 2.4
Factor Reduced	10.0 ± 0.9	10.0 ± 2.5	10.0 ± 2.1

Number of Cells (× 10^3)

Table 3.14 Number of cells reseeded at each passage step.

DsRed Fluorescent Areas (Column 1 lists the gradients)

	Lane 4	Lane 3	Lane 2	Lane 1
W + R	.953	.982	.987	.977
Wnt	.932	.963	.982	.986
Rspo	.952	.971	.980	.988

Integrated eGFP Fluorescent Intensities (Column 1 lists the gradients)

	Lane 4	Lane 3	Lane 2	Lane 1
W + R	.985	.957	.964	.984
Wnt	.984	.968	.983	.970
Rspo	.982	.971	.975	.988

Table 3.15 Adjusted R-squared values indicating the log-transformed data approaches normality.

3.7 REFERENCES

1. Sato T, Vries RG, Snippert HJ, van de Wetering M, Barker N, Stange DE, van Es JH, Abo A, Kujala P, Peters PJ, Clevers H: Single Lgr5 stem cells build crypt-villus structures in vitro without a mesenchymal niche. *Nature* 2009, 459:262-U147.

2. van der Flier LG, Clevers H: Stem Cells, Self-Renewal, and Differentiation in the Intestinal Epithelium. *Annual Review of Physiology* 2009, 71:241-260.

3. He XC, Zhang JW, Tong WG, Tawfik O, Ross J, Scoville DH, Tian Q, Zeng X, He X, Wiedemann LM, et al: BMP signaling inhibits intestinal stem cell self-renewal through suppression of Wnt-beta-catenin signaling. *Nature Genetics* 2004, 36:1117-1121.

4. Humphries A, Wright NA: Colonic crypt organization and tumorigenesis. *Nature Reviews Cancer* 2008, 8:415-424.

5. Takayama T, Miyanishi K, Hayashi T, Kukitsu T, Takanashi K, Ishiwatari H, Kogawa T, Abe T, Niitsu Y: Aberrant crypt foci: detection, gene abnormalities, and clinical usefulness. *Clinical gastroenterology and hepatology : the official clinical practice journal of the American Gastroenterological Association* 2005, 3:S42-45.

6. Ramalingam S, Daughtridge GW, Johnston MJ, Gracz AD, Magness ST: Distinct levels of Sox9 expression mark colon epithelial stem cells that form colonoids in culture. *American Journal of Physiology-Gastrointestinal and Liver Physiology* 2012, 302:G10-G20.

7. Sato T, Stange DE, Ferrante M, Vries RGJ, van Es JH, van den Brink S, van Houdt WJ, Pronk A, van Gorp J, Siersema PD, Clevers H: Long-term Expansion of Epithelial Organoids From Human Colon, Adenoma, Adenocarcinoma, and Barrett's Epithelium. *Gastroenterology* 2011, 141:1762-1772.

8. Stelzner M, Helmrath M, Dunn JCY, Henning SJ, Houchen CW, Kuo C, Lynch J, Li LH, Magness ST, Martin MG, et al: A nomenclature for intestinal in vitro cultures. *American Journal of Physiology-Gastrointestinal and Liver Physiology* 2012, 302:G1359-G1363.

9. Clevers H: Stem Cells: A unifying theory for the crypt. *Nature* 2013, 495:53-54.

10. Ootani A, Li XN, Sangiorgi E, Ho QT, Ueno H, Toda S, Sugihara H, Fujimoto K, Weissman IL, Capecchi MR, Kuo CJ: Sustained in vitro intestinal epithelial culture within a Wnt-dependent stem cell niche. *Nature Medicine* 2009, 15:1-U140.

11. Sato T, Clevers H: Growing Self-Organizing Mini-Guts from a Single Intestinal Stem Cell: Mechanism and Applications. *Science* 2013, 340:1190-1194.

12. Yui S, Nakamura T, Sato T, Nemoto Y, Mizutani T, Zheng X, Ichinose S, Nagaishi T, Okamoto R, Tsuchiya K, et al: Functional engraftment of colon epithelium expanded in vitro from a single adult Lgr5(+) stem cell. *Nature Medicine* 2012, 18:618-623.

13. Yin X, Farin HF, van Es JH, Clevers H, Langer R, Karp JM: Niche-independent high-purity cultures of Lgr5(+) intestinal stem cells and their progeny. *Nature Methods* 2014, 11:106-+.

14. Chung BG, Choo J: Microfluidic gradient platforms for controlling cellular behavior. *Electrophoresis* 2010, 31:3014-3027.

15. Tehranirokh M, Kouzani AZ, Francis PS, Kanwar JR: Microfluidic devices for cell cultivation and proliferation. *Biomicrofluidics* 2013, 7.

16. Zhang YS, Sevilla A, Wan LQ, Lemischka IR, Vunjak-Novakovic G: Patterning Pluripotency in Embryonic Stem Cells. *Stem Cells* 2013, 31:1806-1815.

17. Mahadik BP, Wheeler TD, Skertich LJ, Kenis PJA, Harley BAC: Microfluidic Generation of Gradient Hydrogels to Modulate Hematopoietic Stem Cell Culture Environment. *Advanced Healthcare Materials* 2014, 3:449-458.

18. Kwon GH, Choi YY, Park JY, Woo DH, Lee KB, Kim JH, Lee S-H: Electrically-driven hydrogel actuators in microfluidic channels: fabrication, characterization, and biological application. *Lab on a Chip* 2010, 10:1604-1610.

19. Kim C, Chung S, Kim YE, Lee KS, Lee SH, Oh KW, Kang JY: Generation of core-shell microcapsules with three-dimensional focusing device for efficient formation of cell spheroid. *Lab on a Chip* 2011, 11:246-252.

20. Allazetta S, Hausherr TC, Lutolf MP: Microfluidic Synthesis of Cell-Type-Specific Artificial Extracellular Matrix Hydrogels. *Biomacromolecules* 2013, 14:1122-1131.

21. Alcendor DJ, Block FE, Cliffel DE, Daniels JS, Ellacott KLJ, Goodwin CR, Hofmeister LH, Li D, Markov DA, May JC, et al: Neurovascular unit on a chip: implications for translational applications. *Stem Cell Research & Therapy* 2013, 4.

22. Evensen L, Micklem DR, Link W, Lorens JB: A Novel Imaging-based High-throughput Screening Approach to Anti-angiogenic Drug Discovery. *Cytometry Part A* 2010, 77A:41-51.

23. Liu Y, Markov DA, Wikswo JP, McCawley LJ: Microfabricated scaffold-guided endothelial morphogenesis in three-dimensional culture. *Biomedical Microdevices* 2011, 13:837-846.

24. Wu LY, Di Carlo D, Lee LP: Microfluidic self-assembly of tumor spheroids for anticancer drug discovery. *Biomedical Microdevices* 2008, 10:197-202.

25. Yu L, Chen MCW, Cheung KC: Droplet-based microfluidic system for multicellular tumor spheroid formation and anticancer drug testing. *Lab on a Chip* 2010, 10:2424-2432.

26. Sung JH, Shuler ML: A micro cell culture analog (mu CCA) with 3-D hydrogel culture of multiple cell lines to assess metabolism-dependent cytotoxicity of anti-cancer drugs. *Lab on a Chip* 2009, 9:1385-1394.

27. Kimura H, Yamamoto T, Sakai H, Sakai Y, Fujii T: An integrated microfluidic system for long-term perfusion culture and on-line monitoring of intestinal tissue models. *Lab on a Chip* 2008, 8:741-746.

28. Yeon JH, Park J-K: Drug Permeability Assay Using Microhole-Trapped Cells in a Microfluidic Device. *Analytical Chemistry* 2009, 81:1944-1951.

29. Imura Y, Asano Y, Sato K, Yoshimura E: A Microfluidic System to Evaluate Intestinal Absorption. *Analytical Sciences* 2009, 25:1403-1407.

30. van Midwoud PM, Merema MT, Verpoorte E, Groothuis GMM: A microfluidic approach for in vitro assessment of interorgan interactions in drug metabolism using intestinal and liver slices. *Lab on a Chip* 2010, 10:2778-2786.

31. Gracz AD, Ramalingam S, Magness ST: Sox9 expression marks a subset of CD24-expressing small intestine epithelial stem cells that form organoids in vitro. *American Journal of Physiology-Gastrointestinal and Liver Physiology* 2010, 298:G590-G600.

32. Ahmad AA, Wang Y, Gracz AD, Sims CE, Magness ST, Allbritton NL: Optimization of 3-D organotypic primary colonic cultures for organ-on-chip applications. *Journal of Biological Engineering* 2014, 8:9 1754-1611.

33. Crank J: *The mathematics of diffusion.* Oxford university press; 1979.

34. Bai XZ: Image analysis through feature extraction by using top-hat transform-based morphological contrast operator. *Applied Optics* 2013, 52:3777-3789.

35. Ng H-F: Automatic thresholding for defect detection. *Pattern Recognition Letters* 2006, 27:1644-1649.

36. Frigge M, Hoaglin DC, Iglewicz B: SOME IMPLEMENTATIONS OF THE BOXPLOT. *American Statistician* 1989, 43:50-54.

37. Glantz SA: Primer of biostatistics. 2005.

38. Wang Y, Ahmad AA, Shah PK, Sims CE, Magness ST, Allbritton NL: Capture and 3D culture of colonic crypts and colonoids in a microarray platform. *Lab on a Chip* 2013, 13:4625-4634.
39. Abhyankar VV, Toepke MW, Cortesio CL, Lokuta MA, Huttenlocher A, Beebe DJ: A platform for assessing chemotactic migration within a spatiotemporally defined 3D microenvironment. *Lab on a Chip* 2008, 8:1507-1515.

40. Abhyankar VV, Lokuta MA, Huttenlocher A, Beebe DJ: Characterization of a membrane-based gradient generator for use in cell-signaling studies. *Lab on a Chip* 2006, 6:389-393.

41. Roskoski Jr R: Vascular endothelial growth factor (VEGF) signaling in tumor progression. *Critical reviews in oncology/hematology* 2007, 62:179-213.
42. Chen RR, Silva EA, Yuen WW, Mooney DJ: Spatio-temporal VEGF and PDGF delivery patterns blood vessel formation and maturation. *Pharmaceutical Research* 2007, 24:258-264.

43. Barker N, Tan S, Clevers H: Lgr proteins in epithelial stem cell biology. *Development* 2013, 140:2484-2494.

44. Gracz AD, Williamson IA, Roche KC, Johnston MJ, Wang F, Wang Y, Attayek PJ, Balowski J, Liu XF, Laurenza RJ, et al: A high-throughput platform for stem cell niche co-cultures and downstream gene expression analysis. *Nature cell biology* 2015, 17:340-349.

CHAPTER 4: GENERATION OF A COLONIC STEM-CELL NICHE UTILIZING WNT-SIGNALING FACTOR GRADIENTS

4.1 Introduction

The health of the colon is largely dependent on the chemical milieu surrounding the colonic stem-cell niche. This niche resides at the base of colonic crypts, local invaginations that harbor the intestinal stem cells and their immediate progeny and supporting cells.[1, 2] The stem cells give rise to transit-amplifying cells that proliferate and terminally-differentiate into one of the three cellular lineages of the colon: absorptive colonocytes, mucus-producing goblet cells, and hormone-producing enteroendocrine cells.[3] The lifetime of these fully-differentiated cells is only 4-7 days, during which time these cells migrate to the luminal surface where they undergo apoptosis. A new generation of differentiated, non-dividing cells is rapidly produced through division of the transit-amplifying cells. This series of events drives complete replacement of the colonic epithelium making this tissue the most actively self-renewing tissue in the body.[4] It is believed that the orderly movement of cells along the crypt axis from the stem cell compartment to the lumenal epithelial layer is orchestrated by both intrinsic and extrinsic signaling mechanisms, for example, gradients of mitogens, morphogens, and differentiation factors.[5] The complicated architecture and cell composition of the intestinal crypts is critically dependent upon the spatial organization of these signals with perturbations of the pathways and gradients resulting in disrupted cell positioning and disordered epithelial renewal.[6-8] Much remains to be understood regarding how these various chemical factors regulate stem-cell self-renewal and differentiation.

Recent advances in culture technologies now enable long-term culture of organoids derived from colonic epithelial tissue, termed colonoids. These colonoids possess stem cells and all appropriate differentiated lineages. [1, 9, 10] Colonoid culture requires explicit growth conditions in which the cells are suspended in Matrigel, a 3D laminin and collagen-rich matrix similar to the colonic basal lamina propria. This system is further supplemented with a mixture of growth factors including Wnt-3a, R-spondin1/2, epidermal growth factor (EGF), Noggin, and Jagged which maintain stem-cell multipotency and enable culture of the colonoids for greater than 1 year while maintaining a normal karyotype.[11, 12] When placed into culture, isolated crypts or individual stem cells grow into colonoids with multiple crypt-like buds projecting outward from a central lumen.[13] Although these culture systems display a great deal of potential, the colonoids grow into large circular structures with arbitrary distribution of the various cell types with little resemblance *to* crypt architecture *in vivo*. It is hypothesized that the random cellular distribution and disorganized epithelium is likely due to the absence of the chemical gradients necessary to define appropriate cell-type locations. The current *ex vivo*, colonoid culture systems have been limited to standard tissue culture dishes in which spatial variations in factor concentrations are not possible. These limitations significantly hinder the ability to test the influence of fundamental, morphogenetic cues in crypt homeostasis and cellular organization in healthy and diseased states.

Microengineered systems can provide novel tools for studying intestinal crypt development and function. With the advent of *in vitro* expansion of intestinal stem cells, what is now needed is an improved microengineered technology that can more accurately recreate the complex chemical cues along the crypt axis on an *in vitro* platform. Since microengineered systems possess the ability to chemically pattern the microenvironment of cells and tissues, a microdevice

with gradient-forming capabilities should be competent to recreate such a physiologically-relevant environment enabling testing of mechanistic hypotheses in intestinal homeostasis.[1, 10, 14, 15] Microfluidic devices, permitting tight spatial and temporal control on a cell's microenvironment[16-18], have been described for a number of assays on gut-derived, tumor cell physiology; however, none have been utilized to replicate the complex 3-D crypt environment.[19-24] These assays resorted to the use of tumor cell lines grown on the devices to mimic a partial function of the gut but the devices were not compatible with the culture of primary gut tissue. Efforts have also been made to produce culture substrates with comparable architectures to that of the intestinal crypt.[21, 25, 26] These studies, though, all employed the use of the tumor cell line, Caco-2, as a surrogate for the intestinal epithelium. This human colon carcinoma cell line has been adapted for tissue culture and has little resemblance to normal intestine in terms of growth factor response, gene expression and susceptibility to apoptosis.[27] Additionally, the microdevices were made out of impermeable polymers preventing the possibility of gradient formation.[21, 25] A single exception to the usage of tumor cells in the microengineered platforms was the culture of short-lived jejunum tissue explants.[28] To date, no effort has been made to produce a viable, fully polarized colonic epithelium utilizing primary cells with recapitulation of key features of the crypt architecture such as the stem-cell microenvironment.

Previous studies have provided indirect evidence that key signaling pathways are activated across the crypt in spatially distinct patterns likely due to the presence of gradients in pathway activators and inhibitors. The exact mechanism as to how gradients in pathway activation might interact coordinating cell movement and positioning along the crypt long axis remains unknown since the spatial patterning of the chemical gradients cannot be recreated *ex vivo*.[29] What is now needed is a microdevice that can introduce tightly controlled gradients of relevant signaling

factors across primary intestinal cells to recapitulate the polarized signaling thought to be present *in vivo*.[2, 15, 30, 31] There is consensus amongst intestinal biologists that the Wnt-signaling growth factors, specifically Wnt-3a and R-spondin1, play critical roles in maintenance of the stem cell niche with high and low concentrations near the crypt base and lumen, respectively.[6, 18, 32, 33] In the present work we developed a microengineered, gradient-forming microdevice to expose colonoids along their length to gradients of Wnt-3a and/or R-spondin1. The goal was to determine whether simple, linear gradients of 1 or 2 factors might produce a polarized colonoid by recreating microenvironments of high and low Wnt-pathway signaling within a single colonoid. Such gradients might effectively generate a stem and differentiated compartment within a colonoid much as exists *in vitro* within a crypt.

4.2 Materials and Methods

4.2.1 Transgenic mouse models and isolation of colonic crypts

Crypts were isolated from either Sox9EGFP mice or Sox9EGFP-CAGDsRed mice (6-9 weeks old) using previously described methods.[34] The CAGDsRed mouse line ubiquitously expresses the red fluorescent protein DsRed under the control of a chicken beta-actin promoter (CAG). The Sox9EGFP mice possessed the *Sox9* promoter controlling EGFP (enhanced green fluorescent protein) expression on a modified bacterial artificial chromosome.[22, 41] Mice genetically engineered with this construct express EGFP in intestinal stem cells and transit-amplifying cells. Single cells were obtained from crypts harvested from heterozygous Sox9EGFP: CAGDsRED mice between 6 and 10 weeks of age by fluorescence-activated cell sorting (FACS). Colons were harvested from mice that were bred, handled and sacrificed under protocols approved by the UNC Institutional Animal Care and Use Committee.

4.2.2 Off-chip colonoid culture

Colonoid culture media (CCM) consisted of a mixture of advanced DMEM/F12 medium (Invitrogen), Wnt-3A (120 ng/mL) and R-spondin1 (175 ng/mL) unless otherwise specified (Table S13). CCM also contained Noggin (100 ng/mL), EGF (50 ng/mL), Y27632 ROCK inhibitor (10 µM), NAC (1 mM), GlutaMAX (1×), HEPES (10 mM), penicillin (100 unit/mL), and streptomycin (100 µg/mL). Wnt-3A and R-spondin1 were prepared from conditioned medium as described previously or purchased purified from a supplier.[47] The CCM was prepared in a bulk volume of 500 mL, split into 6-mL aliquots, and stored at -80 °C until use. For crypt culture, 100% Matrigel was used. A 1 mL suspension of freshly isolated crypts (5000 crypts/mL) was added to standard 12-well plates at 4 °C. The Matrigel was then polymerized for 15 min at 37 °C. After polymerization, 1.5 mL of CCM was overlaid onto the Matrigel.

4.2.3 Diffusion-based gradient generation and characterization

Gradient formation through the Matrigel layer on the device was characterized by imaging the movement of a 40 kDa FITC-dextran (Sigma-Aldrich, St. Louis, MO) in 50% Matrigel by time-lapse imaging using an Olympus MVX10 Macroview microscope. Fluorescence images were acquired every 15 min over 24 h to measure gradient formation. The volume of the source and sink was 500 µL and that of the channel was 5 µL. Gradient formation over time was modeled using Fick's Law:[48]

$$C(x,t) = A + \frac{1}{2} C_O \, erfc\left(\frac{x}{2\sqrt{(Dt)}}\right)$$

where A is an integration constant, x ranges from 0 to 5 mm corresponding to the positions along the length of the channel, *t* is time, *D* is the diffusion coefficient, *erfc* is the complementary error function, and C_O is the concentration of the species of interest loaded into the source. COMSOL

Multiphysics with finite-element analysis (FEA) was used to model the data and calculate *D*. For experiments applying gradients to colonoids, the media in both the source and sink were replaced every 24 h.

4.2.4 Placement and culture of crypts and matrigel on the gradient device

Before use, the device was sterilized with 70% ethanol and rinsed with phosphate buffered saline (PBS) ×5. The gradient-generating region of the device was coated by incubation with 2% Matrigel in PBS for 6 h at 4 °C, and then rinsed with PBS ×3 prior to loading crypts or colonoids. This step resulted in deposition of a thin coat (15 ± 5 μm, n=4) of Matrigel (Dow Corning, Midland, MI) on the channel walls that improved adhesion of the subsequently loaded Matrigel plug, improved loading of the crypt/Matrigel suspension (see below) and centered subsequently loaded crypts/colonoids along the z axis of the device. Crypts were isolated from the distal colon of a mouse as previously described. The crypts were pelleted by centrifugation at 300 × G for 90 s. The supernatant was aspirated and the crypts were mixed with cold liquid Matrigel (100% in CCM, 4 °C). A 7 μL aliquot of this suspension containing 7 ± 3 crypts was pipetted into the device's gradient-generating region. The Matrigel pre-coat layer enabled the crypt/Matrigel solution to quickly enter the central channel by surface tension. Excess gel entering the reservoirs was removed and the gel was polymerized by incubation at 37 °C for 15 min. Once the Matrigel solidified, CCM (400 μl) was immediately added to each reservoir. For experiments in which a gradient was formed, Wnt-3A and/or R-spondin1 were omitted from the CCM added to the sink as appropriate for the specific experiment.

4.2.5 Microscopy

Colonoid formation and growth was monitored over time using a Nikon Eclipse TE2000-U microscope fitted with a Photometrics CoolSNAP HQ2 digital camera. Objective lenses used

were 10× and 20× with numerical apertures of 0.30 and 0.55 respectively. Fluorescein-dextran movement in the microchannel was tracked by wide-field imaging of the entire device using an Olympus MVX-10 research macro zoom fluorescence microscope with a 1.0×, 0.25 N.A. objective and 0.63× demagnification. Confocal images of gradient formation were obtained using a Zeiss CLSM 710 Spectral Laser Scanning Microscope equipped with a 488 nm laser to excite fluorescein.

4.2.6 Preliminary on-chip quantification of colonoid area and proliferative cell presence

To validate that colonoids size and proliferative capabilities were similar on the device as within a petri-dish culture, colonoids size and proliferative cell presence were compared (see: Fig. 1D). Crypts isolated from a *Sox9*EGFP-CAGDsRed mice mouse and were cultured in 12-well plates and compared to the growth on the microdevice. A custom script was written in MATLAB (MathWorks; Natick, MA) to quantify the number of DsRed-positive pixels and the EGFP fluorescence intensity of pixels in each colonoid in the 2D image, correlating the presence of these fluorescent signatures to cross-sectional area and proliferative cell presence, respectively. Prior to quantitation, images from the DsRed channel were pre-processed to reduce background noise using top-hat filtering. The images were then thresholded using Otsu's method and "holes" were closed to identify the number of pixels occupied by each colonoid in the device. The number of pixels was then converted to the area occupied by the colonoid in the 2-D image. In addition to identifying the colonoids, the number of DsRed-positive pixels or colonoid area was also used as a proxy for colonoid size or total cell number. The images from the EGFP channel were pre-processed to reduce background noise (top-hat filtering) and the fluorescence intensity of each pixel previously identified as being within the boundaries of colonoid (using the DsRed mask) was summed. For quantitation purposes, colonoids were only considered to be

healthy if they possessed a DsRed fluorescent area greater than 10,000 μm, had integrated eGFP fluorescent intensities were greater than 25,000 RFUs. Additionally, an EdU-based assay was also used to measure proliferating cells (Life Technologies, product #10640). A nuclear stain was always coupled with an EdU-based stain (Hoechst 33342 (10 μg/mL in PBS) using a 30 min incubation). For quantitation purposes, colonoids were considered to have proper amounts of proliferative behavior if the EdU+ regions occupied greater than 25% of the colonoids total volume (EdU+ regions / Hoescht + regions). (Fig. 7-9).

4.2.7 On-chip fluorescence staining

Crypts isolated from a *Sox9*EGFP-only mouse were used for immunofluorescence staining to avoid interference from the DsRed fluorescence of the CAG-DsRed/*Sox9*EGFP mouse. For immunofluorescence staining, freshly isolated crypts, and colonoids on the device and on tissue-culture plates were fixed with 4% paraformaldehyde for 20 min, followed by permeabilization with 0.5% Triton X-100 (Thermo-Fisher, Waltham, MA) for 20 min. Following rinsing ×3 with PBS containing 100 mM glycine, the colonoids were incubated in immunofluorescence wash (0.2% Triton X-100, 0.1% BSA, 0.05% Tween-20, 7.7 mM NaN3 in PBS and 5% normal goat serum) for 90 min to block nonspecific binding. The polyclonal rabbit α-Muc2 primary antibody (1:200) was applied in immunofluorescence wash for 12 h at 4ºC (Invitrogen, Carlsbad, CA). Secondary antibodies (α-rabbit-Cy3) were applied in immunofluorescence wash (1:500) for 45 min (Invitrogen, Carlsbad, CA). All nuclei were stained with Hoechst 33342 (10 μg/mL in PBS) using a 30 min incubation. Microdevices were imaged by brightfield and fluorescence microscopy. An EdU-based assay was also used to measure proliferating cells (Life Technologies, product #10640). A nuclear stain was always coupled with an EdU-based assay as well. For the compass plots generated for the EdU analysis,

a similar image analysis pipeline was used with the Hoescht 33342 fluorescent signal replacing the DsRed and the EdU fluorescent signal replacing the Sox9eGFP.

4.2.8 Quantification of colonoids possessing different fluorescent signatures

Crypts isolated from wild-type, *Sox9*EGFP mice were cultured in 12-well plates and compared to the growth on the microdevice. Three endpoint lineages were assessed: Sox9 (under an eGFP promoter), EdU and Mucin-2. After 5 days in culture, colonoids were fixed, and stained with a fluorescent marker as described above. Hoechst 33442 staining was used to identify nuclei. Imaging was performed at low resolution (91 μm depth of field) so that the entire colonoid was captured in a single image plane. Blue Hoechst fluorescence was used to identify and segment colonoids. All other image processing was as described above. Based on percentages obtained when freshly isolated crypts were stained and assayed, a colonoid was judged to possess goblet cells if the number of pixels positive for Muc-2 was greater than 10% of the total colonoid pixel number. Similarly, a colonoids was considered to be colonoid was judged to possess proliferative cells if the number of pixels positive for EdU was greater than 25% of the total colonoid pixel number. Finally, colonoid was judged to possess stem cells if the number of pixels positive for Sox9 was greater than 25% of the total colonoid pixel number.

4.2.9 Colonoid Segmentation using DsRed or Hoechst 33342

A custom script written in MATLAB (MathWorks; Natick, MA) was used to segment the colonoids by identifying DsRed-or Hoechst 33342 positive pixels. Fluorescence images were filtered using a top hat filter to remove background autofluorescence and any uneven illumination using a disk-shaped structuring element.[49-52] The images were then thresholded using minimum cross entropy thresholding.[50, 51] In the resultant binary image, all objects with a total area less than 2800 μm^2 were removed and all interior holes within objects were filled to

generate a mask of the segmented colonoids (Fig. 7-9). Bright field images were then used to remove large cellular debris by applying a Chan-Vese active contour to the bright field image using the previously generated mask as an initialization.[52] Cellular debris was defined as objects that possessed bright field segmentation boundaries that were 20% larger than the segmentation boundary obtained from the DsRed or Hoechst fluorescence suggesting an object consisting of noncellular or degrading cellular material. The number of pixels was then converted to the area occupied by the colonoid in the 2-D image. In addition to identifying the colonoids, the number of DsRed or Hoechst -positive pixels or colonoid area was also used as a proxy for colonoid size or total cell number.

4.2.10 Sox9eGFP polarization characterization

After the images were sufficiently pre-processed as described above, the green channel image was used to characterize the direction and magnitude of EGFP polarization within each colonoid. The mask of segmented colonoids was applied to both the red channel image (DsRed fluorescence) and green channel image (EGFP fluorescence) to remove all background information. The subsequent green channel image was divided by the red channel image to normalize EGFP intensity to DsRed intensity. Each colonoid was then cropped from the resultant image. Within each cropped image, the mean pixel intensity of the non-zero pixels in each column was calculated, generating an intensity profile along the horizontal axis of the image. The cropped image was rotated by 1 degree about the colonoid centroid and the intensity profile was re-computed every degree for 180 degrees of rotation. Each of the 180 profiles were integrated and the angle of rotation having the largest integration value was determined to be the axis parallel to the polarization direction. The direction of the EGFP polarization was determined by examining the slope of the intensity profile. The magnitude of the polarization was

determined by splitting the colonoid in half along a line orthogonal to the polarization direction and through the centroid of the colonoid, calculating the total intensity on each half, and dividing the lower intensity half by the higher intensity half (Fig. 8-9).

4.2.11 Measurement of EdU Polarization in a Colonoid

Colonoids were segmented based on Hoechst 33342 fluorescence to identify individual colonoids, and the resultant mask was applied to both the Hoechst 33342 and EdU images. Subsequently, the EdU fluorescence was normalized to the Hoechst 33342 fluorescence as described above for EGFP and DsRed. Each colonoid was then cropped from the resultant image. Since a minority of cells were EdU-positive, the EdU fluorescence exhibited a punctate distribution in images (unlike EGFP fluorescence). For this reason the polarization measurements were customized for the EdU-based measurements. For each segmented colonoid, the geographic centroid and the normalized EdU intensity-weighted centroid were identified. The angle of the vector from the geographic centroid to the intensity-weighted centroid was used as the angle of polarization. The magnitude of this vector was normalized to the total length of the colonoid along the axis of polarization to generate the magnitude of polarization (Fig. 10).

4.2.12 Statistics

Boxplots were used to represent the non-normal distribution of colonoid area and EGFP fluorescence intensity of the developing colonoids.[53] Within the boxplots, stars represented the mean, a bar represented the median, and the upper and lower boxes showed the 75% and 25% percentile of the data, respectively. The whiskers extended to the 5^{th} and 95^{th} percentile with outlying data shown as individual points. The data are presented in the text as medians, first- and third-quartile values for colonoid DsRed area and colonoid EGFP fluorescence intensity within the regions. For statistical comparison, the data were converted to a normal distribution using a logarithmic transform and then assessed using Q-Q plots for their fit to a Normal distribution.

The adjusted coefficient of determination (R^2) values for the Q-Q plots was always ≥ 0.91. Statistical differences between data were identified using a Holm-Sidak t test in the analysis of variance.[54] Data are also presented as average ± standard deviation where appropriate, with the compass plot data being represented as the standard error. Propagation of uncertainty using the standard error was used to calculate the variation in the EGFP/EdU polarization angle and magnitude. Once this was found, statistical differences in the compass plot data (Fig. 2-6) were assessed using a standard t-test to statistically determine the differences between polarization directions of colonoids grown in the presence of specific gradients.[55] Finally, a standard t-test was used to examine the statistical differences between the percentages of colonoids possessing stem/transit-amplifying cells (Sox9EGFP), goblet cells (Muc2+) and actively proliferating cells (EdU+) in colonoids cultured on- and off-chip. For all of the statistical tests, a p-value less than 0.05 were considered to be significant.

4.3 Results and Discussion

4.3.1 Gradient-Microdevice Device Design and Characterization

Poly(dimethyl siloxane) (PDMS) was selected as the material of choice for the device as PDMS is gas permeable and compatible with colonic stem cell culture.[34, 35] Devices formed from PDMS are also readily fabricated using soft lithography.[36] The device incorporated a central microchannel (1 mm wide, 5 mm long, 300 μm deep with a volume of 1.5 μL) across which a gradient was formed. Two fluid reservoirs (16 mm wide, 5 mm long, and 15 mm deep with a volume of 0.5 mL) placed to either side of the microchannel served as a source and sink (Fig. 1). Matrigel was loaded into the central channel via a small inlet and outlet port (500 μm diameter) at the ends of the microchannel. An array of hexagonal posts (250 μm height, 6 μm side and 50 μm inter-post spacing) bounded the sides of the gradient-generating region and acted to localize

Matrigel to the central microchannel via surface-tension forces. Every third post was labelled with a number permitting the channel location to be reproducibly identified over time during microscopy.

Fluorescein-labeled dextran (40 kDa) was used to characterize the time evolution and stability of a gradient formed across the 1-mm width of the microchannel. Fluorescein-dextran was loaded into the source reservoir and the microchannel was imaged over time by fluorescence microscopy. By 1 h, a gradient of fluorescence formed across the microchannel decreasing linearly from the concentration in the source to that in the sink. When the temporal evolution of the fluorescence intensity was fit to Fick's Second Law of diffusion, a diffusion coefficient of $7.2 \pm 0.6 \times 10^{-11}$ m^2/sec (n = 3 devices) was calculated for the fluorescein-dextran which was similar to that measured for a 42-kDa protein, vascular epithelial growth factor, in Matrigel (7.0×10^{-11} m^2/sec).[37, 38] To maintain the linear gradient over long time scales (5 days), the source and sink solutions were replaced every 24 h. Modeling the device and solution changes suggested that once a gradient was established, the concentration of a 40 kDa analyte across the microchannel varied by no more than 0.9% over a 5 day period. The daily reservoir refreshment combined with the 100× volume of the source and sink reservoirs relative to that of the gradient-forming microchannel enabled the source and sink reservoirs to behave as infinite compartments and permit formation of a time-invariant molecular gradient.[39] Similar gradient strategies have been employed successfully by others.[39, 40] These data also suggest that stable, linear Wnt-3a (39.7 kDa) and R-spondin1 (40.0 kDa) gradients could be formed across the Matrigel-filled microchannel.

4.3.2 Comparison of Colonoids Cultured in the Microdevice and a Multiwell Plate

Colonoid growth in a standard format (12-well plate) was compared to that on the microdevice in the absence of factor gradients. Crypts from Sox9EGFP-CAGDsRed or Sox9EGFP mice were used in these assays since EGFP expression marks the stem/transit-amplifying cells (EGFP+ cells).[41] For mice with ubiquitous expression of DsRed (Sox9EGFP-CAGDsRed mice), the DsRed+ colonoid area recorded using non-confocal fluorescence imaging was used to estimate colonoid size. Freshly isolated crypts were mixed with Matrigel and loaded into the microchannel and 60 ng/mL of Wnt-3a and 90 ng/mL of R-spondin1 were placed into both the source and sink reservoirs and replenished every 24 h during culture. In parallel, crypts were cultured in a conventional Matrigel patty placed in a multi-well plate and overlaid with media containing 60 ng/mL of Wnt-3a and 90 ng/mL of R-spondin1. The media was replenished every 24 h for both formats.

Of the crypts plated in the microdevice, 55.0 ± 14.0% (avg. ± s.d.) developed into colonoids with a median DsRed area/colonoid of 20,387 μm^2 and first and third quartile values of 11,148 and 33,520 μm^2 after 5 days in culture, respectively (n = 25 colonoids from 6 microchannels). In comparison, 60.0 ± 8.5% of crypts plated and cultured for 5 days in the Matrigel patties developed into colonoids with a median DsRed area/colonoid of 17,392 μm^2 and first and third quartile values of 9,359 and 36,637 μm^2 after 5 days in culture, respectively (n = 29 organoids from 3 wells) (Fig. 1D, Table 1).The DsRed area/colonoid in the microchannel and multiwell plate was not statistically different suggesting that colonoids grew in the same manner in these two formats.

The percentage of colonoids demonstrating EGFP expression in $\geq$25% of the colonoid area, was similar for the microchannel and multi-well environment with 83 ± 8.0% and 85 ± 9.0% of colonoids positive for EGFP, respectively. After 5 days of culture, the median integrated EGFP

fluorescence/colonoid in the microchannel was 74,352 RFUs, with first and third quartile values of 46,611 and 199,382 RFUs, respectively (n = 25 colonoids in 6 microchannels) (Table 2,3). In comparison, the median integrated EGFP fluorescence/colonoid in the multi-well plate was 85,468 RFUs, with first and third quartile values of 27,759 and 171,836 RFUs, respectively (n = 29 organoids in 3 wells) (Fig. 1D). The EGFP fluorescence/colonoid of the microchannel and well-plate colonoids was not statistically different again suggesting that the two formats yielded identical colonoid properties.

A second assay based on an EdU pulse[34] was used to assess actively proliferating cells in both culture formats. The percentage of colonoids in the microchannel with EdU+ cells (occupying >25% of the colonoid area) was 96.0 ± 3.0%, compared to 92.0 ± 7.0% in the standard Matrigel patty on the multiwell plate (Fig, 1C & Table 4). The presence of Goblet cells, a differentiated cell type producing mucous was assayed by immunofluorescence staining of mucin 2.[22] The percentage of colonoids in the microchannel with Goblet cells (Muc-2+ staining in $\geq$10% of the colonoid area) was 90.0 ± 5.0% (n = 20 colonoids in 5 microchannels), compared to 92.0 ± 6.5% (n = 20 colonoids in 3 wells) in the multiwell plate (Fig. 1C & Table 5). These data were not statistically different demonstrating that colonoids cultured in the microchannel and in the standard Matrigel-patty format developed similarly in terms of size, presence of stem/transit amplifying cells, and differentiated cells such as Goblet cells.

4.3.3 Spatial Location of Stem/Transit Amplifying Cells in Colonoids in the Absence of a Chemical Gradient

While the distinct progression of cells from stem to differentiated phenotype along the crypt axis is thought to be due to chemical gradients, it is not clear whether the epithelial cells themselves may play a role in creating the gradient. For this reason the spatial localization of EGFP within

colonoids in the absence of an external chemical gradient was measured. Colonoids derived from a *Sox9*EGFP-CAGDsRed mouse were loaded into microchannels or a multiwell plate and cultured in the presence of Wnt-3a (60 ng/mL) and R-spondin1 (90 ng/mL). The developing colonoids (n= 49 colonoids in 10 microchannels and n = 30 colonoids in 5 wells) were imaged every 24 h and the location of EGFP within each colonoid measured (Fig. 7-9). For the microchannel device, a line perpendicular to the long axis of the microchannel was defined as the line through 0 to 180 degrees. Zero and 180 degrees were arbitrarily defined for each multiwell plate but consistent across all wells. An EGFP polarization vector was calculated by searching for the steepest gradient in EGFP intensity as the colonoid was rotated through 180 degrees. Using this strategy, unpolarized colonoids possess an EGFP vector magnitude approaching zero while the vector magnitude for highly polarized colonoids was near 0.04. For the multiwell plate, the average EGFP polarization vector possessed a length of 0.0006 ± 0.0006 and an angle of 150 ± 110 degrees. The colonoids in the microchannel displayed an average EGFP polarization vector with a length of 0.0009 ± 0.0007 and an angle of 152 ± 107 degrees. When the EGFP polarization angle was examined for each colonoid in both the multiwell plate and microchannel, the angle appeared to be randomly distributed through all quadrants. Thus colonoids cultured under these gradient-free conditions displayed little ability to polarize or to align themselves any in a single direction. Multiple different cell types (stem, transit-amplifying and progenitors) with cell division times of 12-24 h express the Sox9 protein (and hence EGFP) at varying levels[42] Additionally EGFP is a long lived protein with a half-life of >24 hours.[43, 44] Thus, it was possible that the colonoids might be polarized with respect to the stem/transit-amplifying cells but the long half-life of EGFP coupled with cell movement from their birth location led to loss of polarization with respect to EGFP fluorescence (Fig. 2).

To determine whether the stem/transit-amplifying cells were localized within colonoids, a snap shot of actively dividing cells was acquired by applying an EdU-pulse to the cells. EdU and its analogs are incorporated into cells during DNA replication marking only cells in S phase during the pulse time window. Colonoids were cultured for 5 days after which EdU was added to the culture for 2 h followed by cell fixation (n= 18 colonoids in 5 microchannels and n = 16 colonoids in 3 wells). Colonoids were then stained with Hoechst 33442, a DNA-binding dye, to mark all cells and permit facile colonoid segmentation. For EdU polarization measurements, the axes were defined as described previously. Since only a small subset of cells were marked by EdU, the algorithm used for EGFP could not be employed. Instead the geographic centroid and the intensity weighted centroid were identified and the vector of the between these two locations used to assess EdU polarization. Using this algorithm, unpolarized colonoids possess an EGFP vector magnitude approaching zero while the largest possible vector magnitude for highly polarized colonoids was 0.5. For the multiwell plate, the average EdU polarization vector possessed a length of 0.009 ± 0.064 and an angle of 61 ± 26 degrees. The colonoids in the microchannel displayed an average EdU polarization vector with a length of 0.011 ± 0.053 and an angle of 38 ± 41 degrees (Fig. 3). As with the EGFP vectors, the EdU vectors appeared to have random angles appearing in all angular quadrants. These data suggested that the rapidly proliferating cells within a colonoid were spatially distributed throughout that colonoid *i.e.* the colonoids were not polarized with respect to cells in S phase.

4.3.4 Effect of Wnt-3a Concentration on Colonoid Growth and Polarization

The Wnt-3a signaling pathway is known to promote stem cell maintenance and to support cell proliferation. Thus, formation of a gradient of Wnt-3a across a single colonoid might act to support stem cells and transit amplifying cells in only the small spatial region of the colonoid

exposed to a high Wnt-3a concentration. To test this hypothesis, colonoids were loaded into the microchannel and media containing or 0 or 75 ng/mL of Wnt-3a was loaded into the source or sink reservoirs respectively. After 5 d of culture under the linear Wnt-3a gradient, the colonoid area, EGFP expression, and EdU incorporation were measured. In total, 28 colonoids were surveyed over five independent devices/experiments. The median DsRed area/colonoid for in the microchannel device was 24,373 μm^2 per colonoid, with first and third quartile values of 7,998 and 48,326 μm^2, respectively. After 5 days in culture, the colonoid area under the Wnt-3a gradient was not statistically different relative to that without a gradient (microchannel or multi-well plate). The median integrated EGFP fluorescence/colonoid was 73,591 RFUs with first and third quartile values of 25,445 and 143,216 RFUs, respectively (Table 6). As with the DsRed fluorescence, the integrated EGFP fluorescence/colonoid was not statistically different from that of colonoids in the absence of a gradient. These data suggested that the colonoids under the Wnt-3a gradient possessed similar numbers of stem, transit-amplifying and other cell types as the colonoids in the absence of a gradient. In these experiments R-spondin1, an activator of the Wnt signaling pathway, was at uniformly high concentrations throughout the microchannel. It is possible that the R-spondin1 alone provided sufficient Wnt pathway activation to support the EGFP-expressing cells throughout the colonoids.

Although the total size and EGFP fluorescence per colonoid in the gradient and no-gradient conditions were similar, it is conceivable that the distribution under these two conditions may be distinct. To assess this possibility, the average EGFP polarization vector of the Wnt3-a gradient-exposed colonoids was measured. The averaged vector possessed a magnitude of 0.0044 ± 0.0019 and an angle of 58 ± 21 degrees. The average EGFP polarization magnitude and angle were statistically different from that in the microchannel in the absence of a gradient ($p<0.05$).

Of the 28 colonoids surveyed under the Wnt-3a gradient, 22 colonoids possessed EGFP polarization vectors facing the Wnt-3a source (Fig. 4). After 5 days in culture, the average colonoid within the microchannel possessed a length along the 0-to-180 degree axis of 212 ± 41 μm. Thus the Wnt-3a concentration drop across the average colonoid was 16 ng/mL. That 79% of the colonoids grew with their stem/transit amplifying cells oriented towards the source reservoir suggests that most colonoids were exquisitely sensitive to the Wnt-3a concentration. It is possible that even a very modest increase in Wnt-3a can confer a growth advantage to stem/transit amplifying cells enabling those cells to out compete others in the colonoid. An intriguing and alternative hypothesis is that stem/transit amplifying cells undergo chemotaxis within the colonoid boundaries migrating to an optimal location nearest the source-side of the colonoid. 21% of the colonoids did not respond to the Wnt-3a gradient. It is possible that for these colonoids, the relatively shallow Wnt-3a gradient combined with their location in the microchannel did not act to overcome the sustained high R-spondin1 concentration across the microchannel. Taken together, these results suggest that many but not all of the colonoids were able to sense and respond to the Wnt-3a gradient. The high concentration of R-spondin1, a Wnt signaling activator, across the microchannel may have acted to mitigate the impact of the Wnt-3a gradient.

4.3.5 Effect of Wnt-3a and R-Spondin1 Gradient on the Creation of a Stem-Cell Compartment within Passage Colonoids

In vivo Wnt-3a and R-spondin1 are thought to work synergistically to orient crypts with the stem/transit amplifying cells at the crypt base in the high Wnt-signaling environment provided by Wnt-3a and R-spondin1. To determine whether a gradient of Wnt-signaling across the microchannel might provide a similarly polarizing environment, R-spondin1 and Wnt-3a were

removed from the sink reservoir but maintained at high concentrations in the source reservoir (75 ng/mL Wnt-3a, 110 ng/mL R-spondin1). Colonoids were cultured for a total of 5 days. In total, 33 colonoids were surveyed from six devices. The median DsRed fluorescent area/colonoid after 5 d of culture was 16,576 μm^2 with first and third quartiles of 10,074 and 27,281 μm^2, respectively. The median EGFP fluorescence intensity/colonoid in the presence of the dual gradient was 105,823 RFUs per colonoid with first and third quartiles of 53,542 and 189,949 RFUs, respectively. The area/colonoid and the EGFP intensity/colonoid in the presence of the Wnt-3a + R-spondin1 gradient were not statistically different from that in the absence of a gradient or in the presence of a Wnt-3a gradient (Fig.11-12 & Table 7).

Colonoid polarization with respect to stem/transit-amplifying and proliferating cells was assessed by measuring EGFP and EdU spatial localization under the impact of the Wnt-3a + R-spondin1 gradient. The average EGFP polarization vector of these gradient-exposed colonoids exhibited a magnitude of 0.0049 ± 0.0019 and an angle of 35 ± 31 degrees. The average EGFP polarization vector was statistically different than the colonoids in no-gradient condition ($p<0.05$); however, they was not statistically different from that of the Wnt-gradient colonoids. Of the 24 colonoids assessed in the double gradient, 22 (92%) possessed EGFP vectors orientated toward the source reservoir *i.e.* the region of high Wnt-3a/R-spondin1. A 2-h EdU pulse was also applied to 11 colonoids (4 microchannels) after 5 d of culture under the influence of the Wnt-3a + R-spondin1 gradient. The average EdU polarization vector possessed a length of 0.09 ± 0.07 and an angle of 15 ± 19 degrees. The EdU polarization vector was statistically different from that of colonoids in the microchannel without a factor gradient ($p<0.05$). All but one of the colonoids demonstrated an EdU vector facing toward the Wnt-3a/R-spondin1 source (Fig. 5). These data suggest that nearly all of the colonoids were able to sense the growth-factor

gradient and respond by spatially localizing their stem/transit amplifying cells to colonoid regions with sufficient Wnt-pathway activation. These data demonstrate the ability to create a stem cell niche within a colonoid by applying external growth factors in a graded fashion across the colonoid. The cellular response to perturbants such as drugs, nutrient limitation, and chemical toxins can be tracked to develop a greater understanding of stem-cell niche dynamics.

4.3.6 Effect of Wnt-3a and R-Spondin1 Gradient on the Creation of a Stem-Cell Compartment within Colonoids Developed from Single Stem Cells

Prior experiments utilized colonoid fragments as the cell-source material in the microchannel. While the fragments were small (~30 μm diameter with ~25 cells), they did contain many cell types (differentiated, stem, and transit amplifying cells) and thus may have pre-established cellular interactions which might hinder spatial relocalization of cells under a growth-factor gradient. The colonoid fragments were also obtained from continuously cultured colonoids (>1 month). While all evidence to-date indicates that these cells are identical to those *in vivo* and maintain a normal karyotype, it is conceivable that the cultured colonoids differ in an as yet unknown manner from their *in vivo* counterparts.[45, 46] For this reason, single stem cells were isolated from freshly obtained crypts from colons of a Sox9EGFP-CAGDsRed mouse. The stem cells were isolated by fluorescence-activated cell sorting based on their characteristic $Sox9^{EGFP}low{:}CAG^{DsRED}$ signature.[41] The stem cells intermixed with Matrigel were loaded into a microchannel and cultured for 5 d in the presence of a Wnt-3a/R-spondin1 gradient. The median DsRed fluorescent area per colonoid was 22,146 μm^2 with first and third quartiles of 7,799 and 44,504 μm^2, respectively. After 5 days in culture the area of the colonoids developed from single stem cells in the double gradient was not statistically different from that obtained in all of the prior experiments. Similarly, the EGFP fluorescence/colonoid of the single-stem cell derived

colonoids (median of 94,501 RFUs with first and third quartiles of 49,645 and 151,374 RFUs, respectively at 5 d) was not statistically different from that of prior experiments. These data suggested that colonoids originating from the single stem cells grew robustly, catching up in size and stem/transit amplifying cell numbers to that formed from the colonoid fragments (Table 8).

The EGFP polarization vector for the single-cell-derived colonoids was measured to test the hypothesis that these colonoids might readily polarize under the Wnt-3a/R-spondin1 gradient since the single cells were free of other outside influence. The average EGFP polarization vector of the single-cell-derived colonoids possessed a magnitude of 0.012 ± 0.002 and an angle of 17 ± 16 degrees (Fig. 6). The EGFP vector was statistically different from that of the Wnt-3a/R-spondin1 gradient-exposed colonoids ($p<0.05$ for both). Of the 23 colonoids surveyed in the dual gradient condition, 20 colonoids or 87% possessed EGFP vectors pointing in the direction of the growth factor source. A similar percentage of colonoids arising from the single cells and colonoid fragments successfully polarized to align with the growth factor gradient. Colonoids developed from the single stem cells, however, were more highly polarized than those arising from the colonoid fragments. Thus it is likely that the cells within the colonoid fragments interact with each other exerting an influence on and modifying the behaviors of the stem and/or transit-amplifying cells.

4.4 Conclusions

In this work, we describe the implementation of a microengineered technology to introduce tightly controlled linear gradients of morphogenic factors along the length of an individual colonic organoid. The use of a transgenic mouse model enabled fluorescence measurements to be utilized as readouts of biological activity. The technology enabled the introduction of threshold concentrations of the two key Wnt-signaling factors across an individual colonoids: resulting in

the recreation of the colonic stem cell niche. Leveraging previous research from our group which identified threshold concentrations needed for suitable stem, progenitor and differentiated cell survival (60 ng/mL of Wnt-3a and 88 ng/mL of R-spondin1), colonoids were exposed to three experimental conditions: no gradient in a high Wnt-3a and high R-spondin1 environment, a Wnt-3a gradient in a high R-spondin1 environment, a combined Wnt-3a and R- spondin1 gradient. Prior research utilizing cultured colonoids has developed them within homogenous, substantially elevated levels of Wnt-3a and R-spondin. The overstimulation of Wnt signaling pathways in these colonoid culture systems may account for the randomly distributed stem cells within the colonoids, which is likely due to the absence of protein gradients present in vivo.[35, 48] After 5 days in culture within a Wnt-3a and R-spondin gradient, a stem-cell niche was recreated in colonoids developed from both passaged colonoids and single stem cells. In fact, the sub-population of colonoids developed within these gradients had polarization magnitude more than ten times that of colonoids developed under homogenous growth conditions. The microfluidic device and novel results described in this series of experiments not only lay the ground work for future development of in vitro models of the colon, but will also enable intestinal biologists to pursue further in-depth combinatorial screens of factors and pharmacologic compounds for controlling colon stem-cell renewal and differentiation.

4.5 Figures

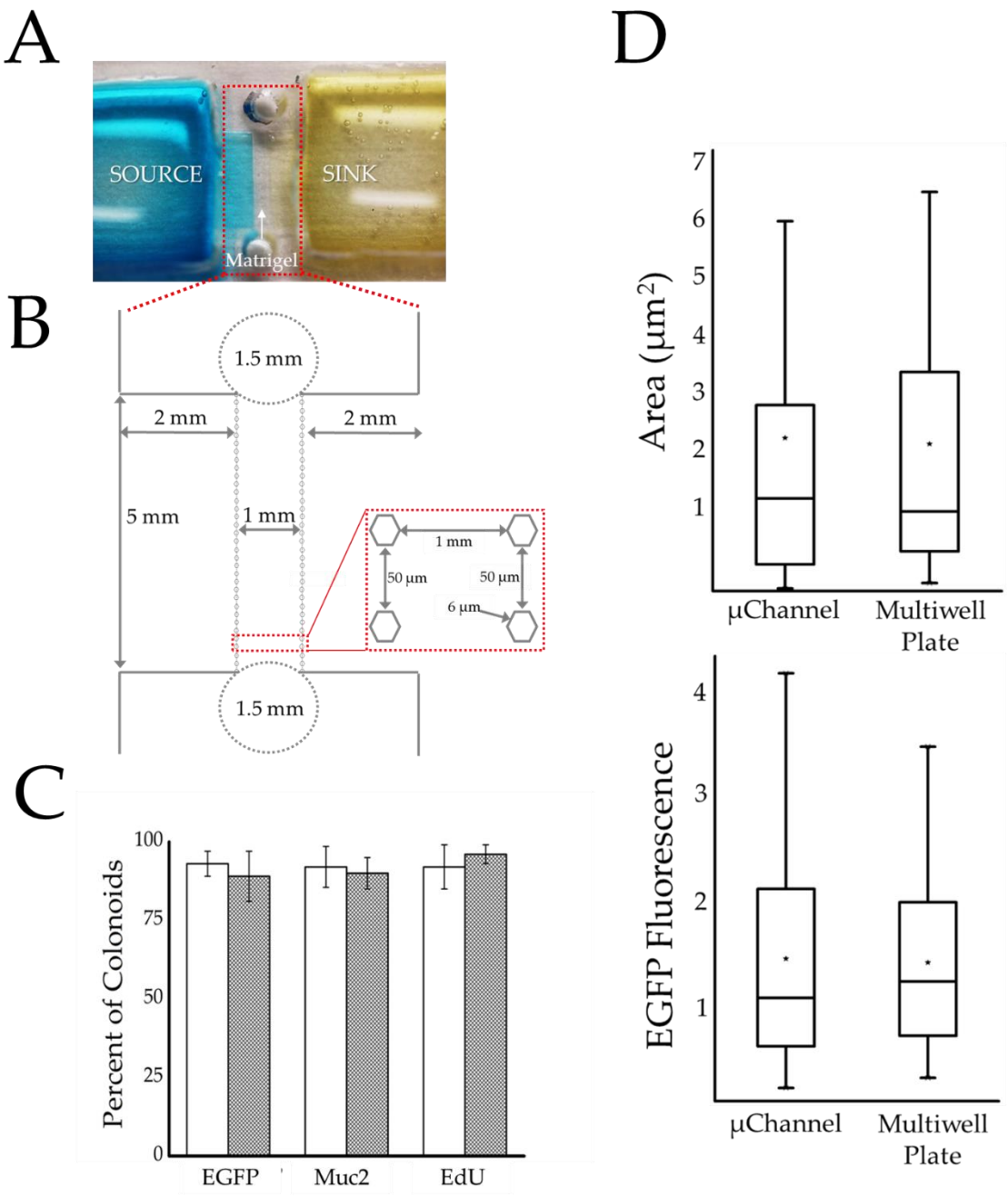

Figure 4.1 Characterization of the gradient-generating microdevice.

(A) Photograph of the device. The Matrigel-filled gradient region resides between the source (left with yellow dye) and sink (right with blue dye) reservoirs. (B) Schematic of the gradient generating microchannel of the device. (C) Histogram showing percentages of colonoids

possessing expressing EGFP (stem/transit-amplifying cell), exhibiting Muc2 (goblet cells) and labeling with EdU (actively proliferating cells) in colonoids cultured on the microchannel (white bars) or conventional multi-well plate (grey bars). (D) Colonoid data is shown at 5 days of culture on either the microchannel or a microwell. Boxplots were used to represent the non-normal distribution of the area (left column) or EGFP fluorescence (right column) per colonoid. Colonoid area is represented as μm^2 ($\times 10^4$) and EGFP fluorescent intensity is represented as RFUs ($\times 10^5$). For the boxplots, the black star indicates the mean of the data, the bar shows the median, and the upper and lower boxes represent the 75% and 25% of the data, respectively. The whiskers extend to the 5% and 95% of the data.

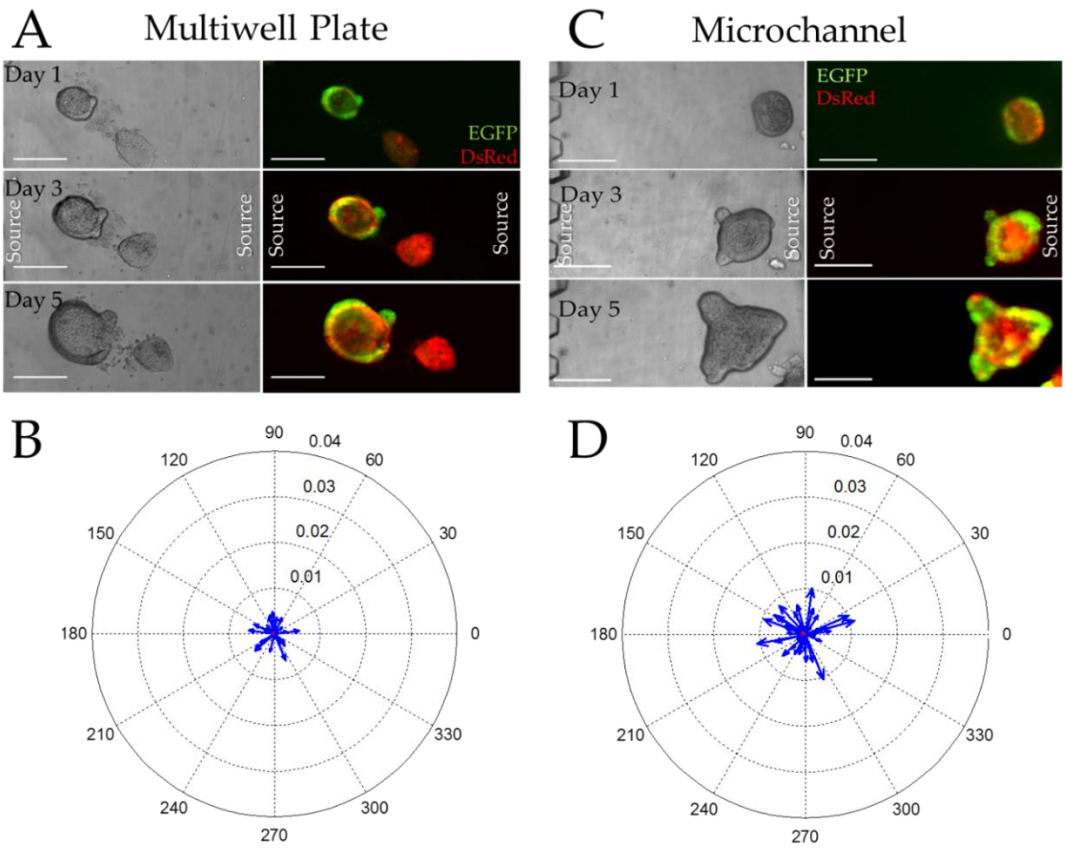

Figure 4.2 Colonoid properties in the absence of an extrinsic gradient.

(A, C) Brightfield (left) and overlaid red/green fluorescence (right) images of colonoids cultured within a standard multi-well plate (A) or microchannel (C) for 1, 3, and 5 d. Scale bars are 250 μm. (B, D) Compass plots displaying the EGFP polarization magnitude and angle for individual colonoids cultured in the multi-well plate (B) or microchannel (C) for 5 d. The average magnitude and angle vector can be seen in red.

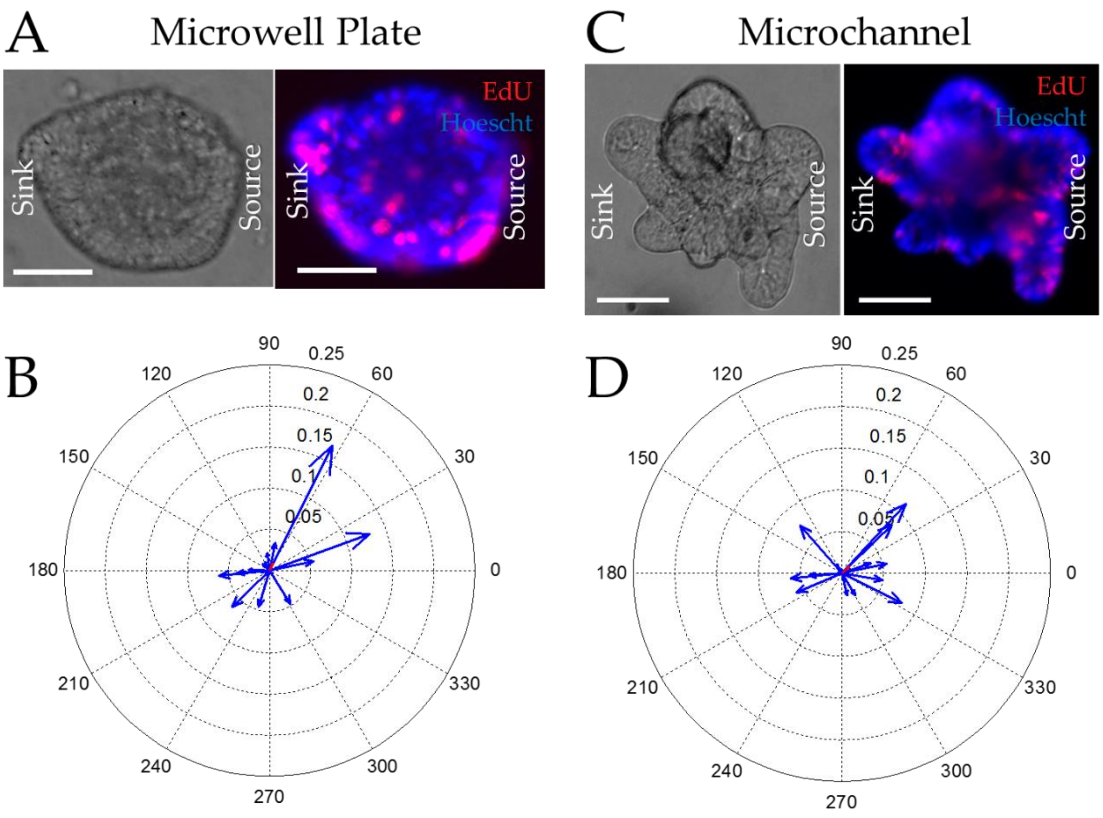

Figure 4.3 Incorporation of EdU into colonoids after a 2 h pulse in the absence of an extrinsic gradient. (A,C) Brightfield (left) and overlaid red/blue fluorescence (right) images of colonoids cultured within a standard multi-well plate (A) or microchannel (C) for 5 d then labeled with EdU (red) and the Hoechst 33342 (blue). Scale bars equal 50 µm. (B, D) Compass plots displaying the EDU polarization magnitude and angle for individual colonoids cultured in the multi-well plate (B) or microchannel (C) for 5 d and pulsed with EdU. The average magnitude and angle vector can be seen in red.

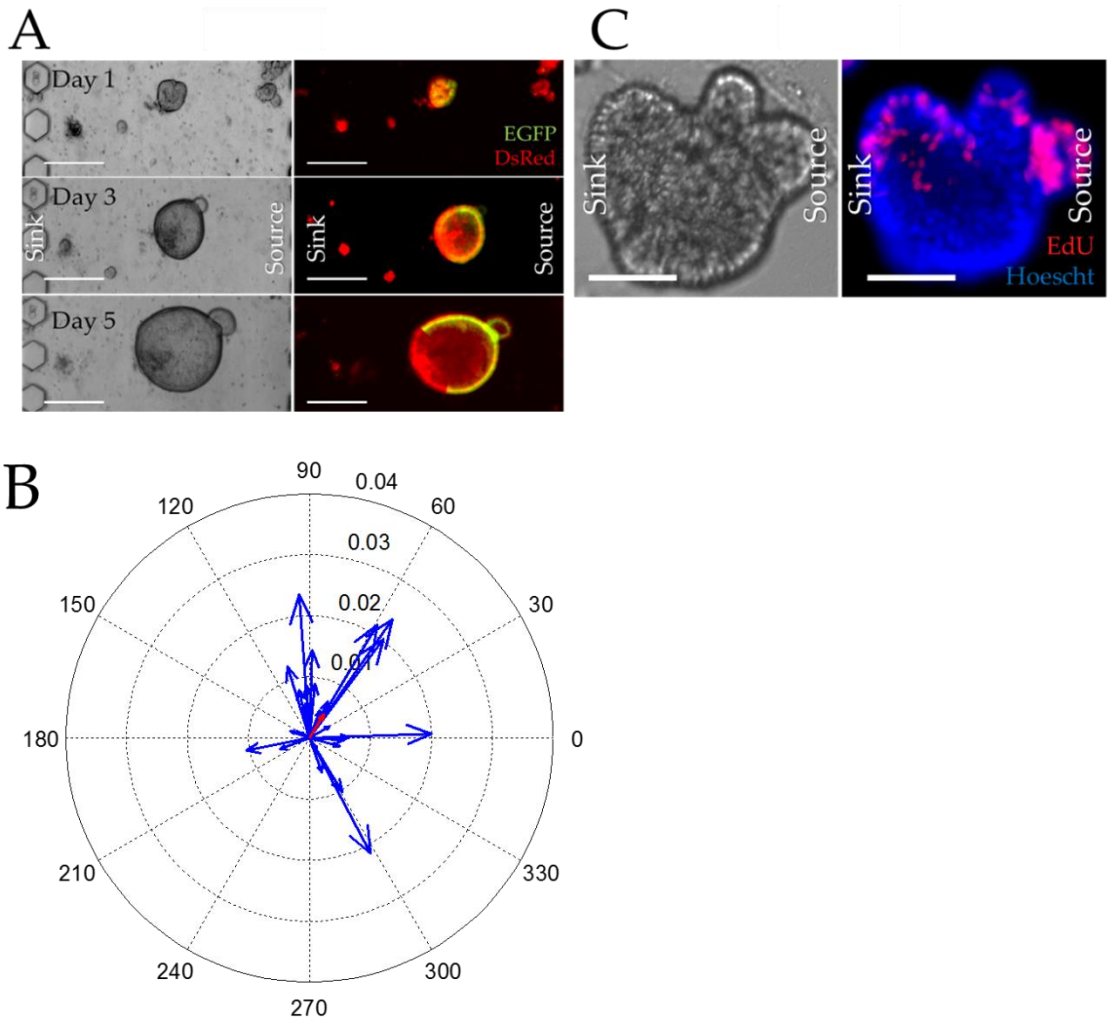

Figure 4.4 Colonoid Growth in the presence of a Wnt-3a gradient across the microchannel. A) Brightfield (left) and overlaid red/green fluorescence (right) images of colonoids cultured under a Wnt-3a gradient for 1, 3, and 5 d. The scale bars is 250 µm. B) Compass plot displaying the EGFP polarization magnitude and angle for individual colonoids cultured under the Wnt-3a gradient for 5 d. The average magnitude and angle vector can be seen in red. C) Brightfield (left) and overlaid red/blue fluorescence (right) images of colonoids cultured under a Wnt-3a gradient for 5 d then pulse-labeled with EdU (red) for 2 h. Hoechst 33342 fluorescence is shown in blue. The scale bar represents 50 µm.

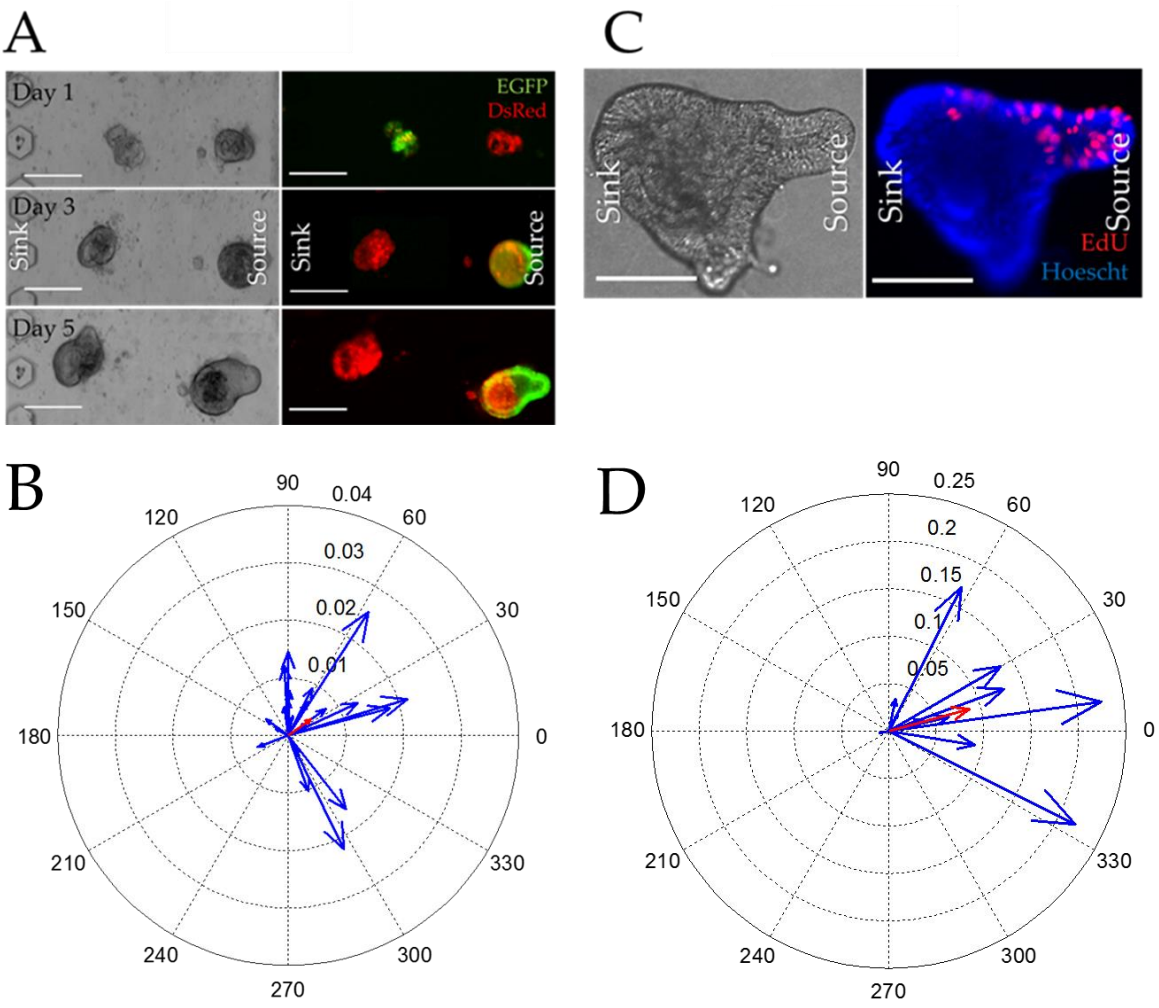

Figure 4.5 Colonoid Growth in the presence of a Wnt-3a/R-spondin gradient. (A) Brightfield (left) and overlaid red/green fluorescence (right) images of colonoids cultured under a Wnt-3a/R-spondin gradient for 1, 3, and 5 d in the microchannel. The scale bar is 250 µm. (B) Compass plot displaying the EGFP polarization magnitude and angle for individual colonoids cultured under the Wnt-3a/R-spondin gradient for 5 d. The average magnitude and angle vector can be seen in red. (C) Brightfield (left) and overlaid red/blue fluorescence (right) images of colonoids cultured the gradient for 5 d then pulse-labeled with EdU (red) for 2 h. Hoechst 33342 fluorescence is shown in blue. The scale bar represents 50 µm. (D) Compass plot displaying the

EDU polarization magnitude and angle for individual colonoids cultured as described in (C). The average magnitude and angle vector can be seen in red.

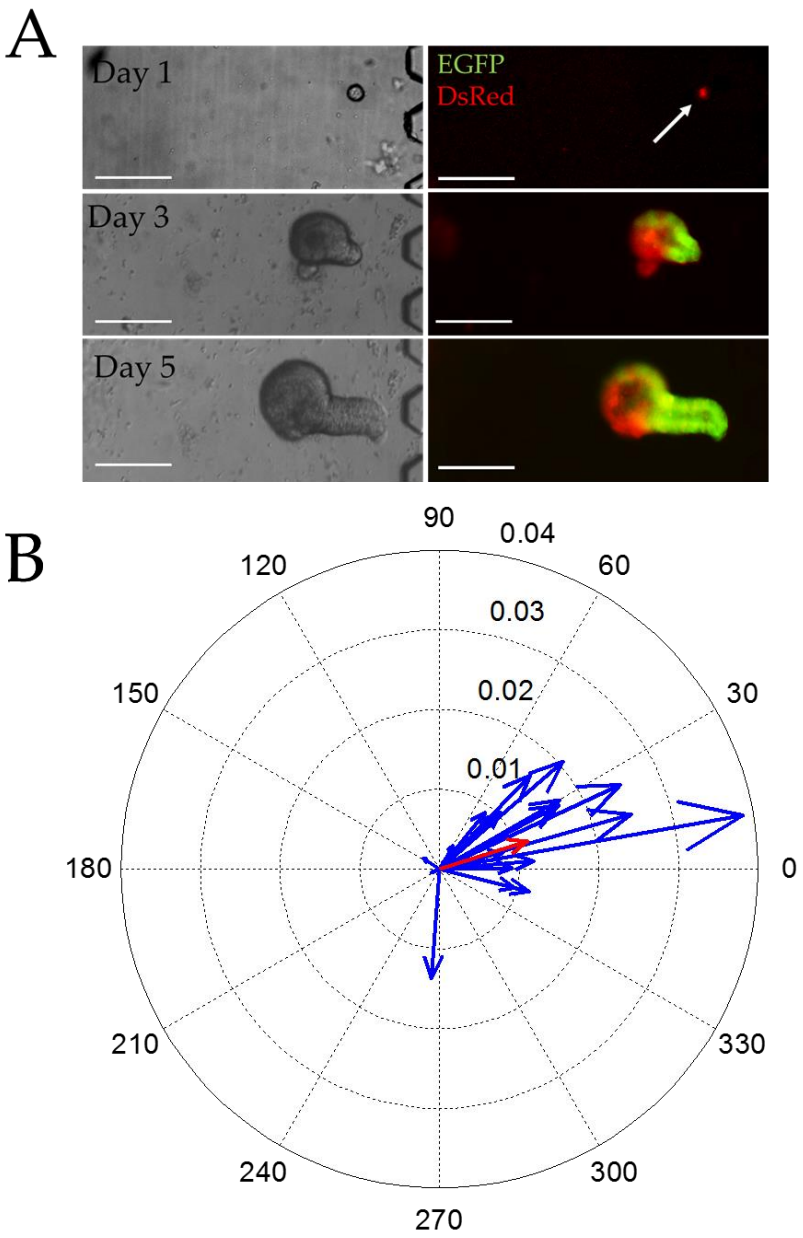

Figure 4.6 Growth of Single Stem Cells in the presence of a Wnt-3a/R-spondin1 gradient. A) Brightfield (left) and overlaid red/green fluorescence (right) images of single stem cells cultured under a Wnt-3a/R-spondin1 gradient for 1, 3, and 5 d in the microchannel. The scale bar is 250 μm. B) Compass plot displaying the EGFP polarization magnitude and angle for the colonoids under the Wnt-3a/R-spondin1 gradient for 5 d. The average magnitude and angle vector can be seen in red.

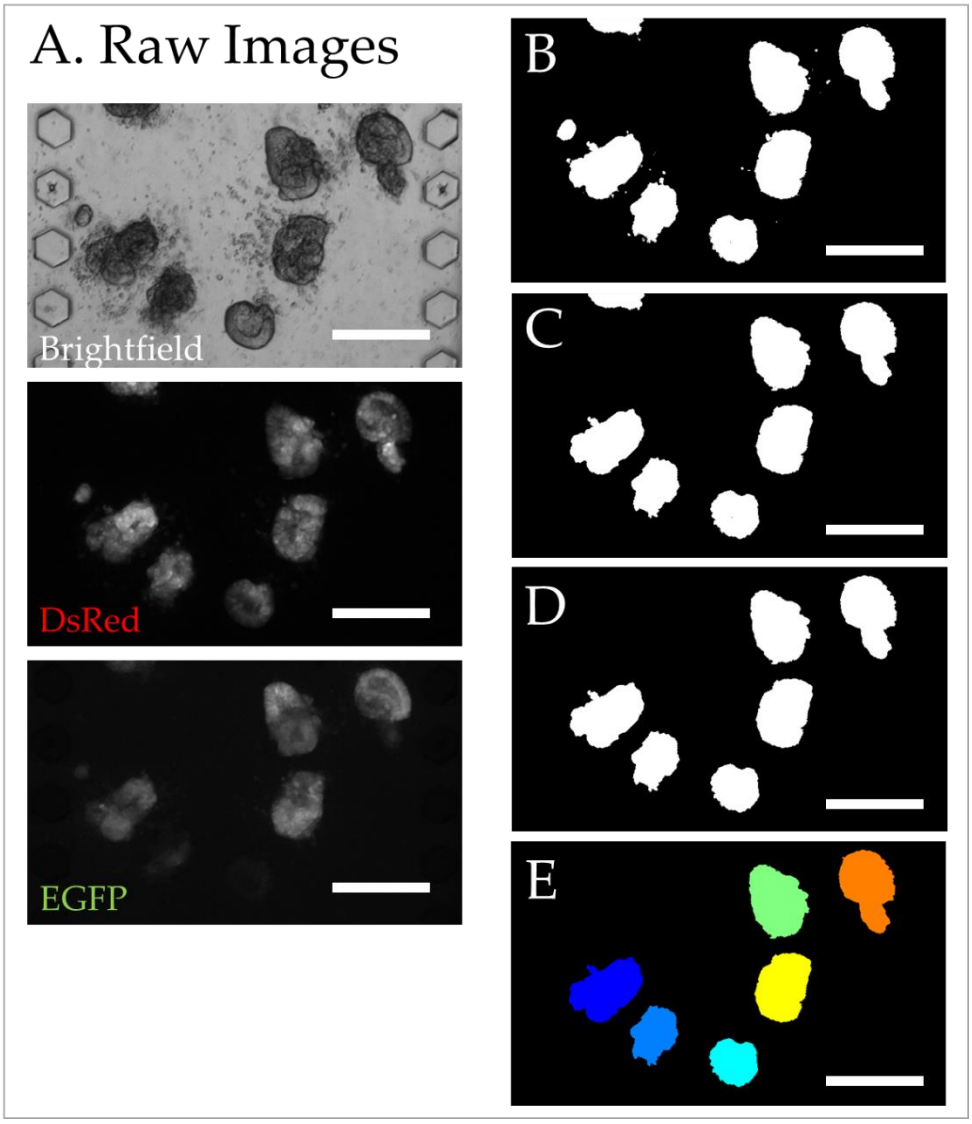

Figure 4.7 Example of colonoid segmentation using DsRed. (A) Raw images from brightfield microscopy and fluorescence microscopy of EGFP and DsRed of the sample field of colonoids. (B) A threshold for the processed image was automatically determined by minimum cross entropy thresholding [3]. (C) In the resultant binary image, all objects with a total area less than 1000 μm^2 were removed and all interior holes within objects were filled to generate a mask of the segmented colonoids. (D) Large cellular debris was then removed from the images. Cellular debris was defined objects with bright field segmentation boundaries that were 20% larger than

the segmentation boundary obtained from the red fluorescence channel. Colonoids touching the edges of the image were also removed. (E) Finally, each of the colonoids were labelled with a color code for subsequent measurements on that colonoid. Scale bars are 250 μm.

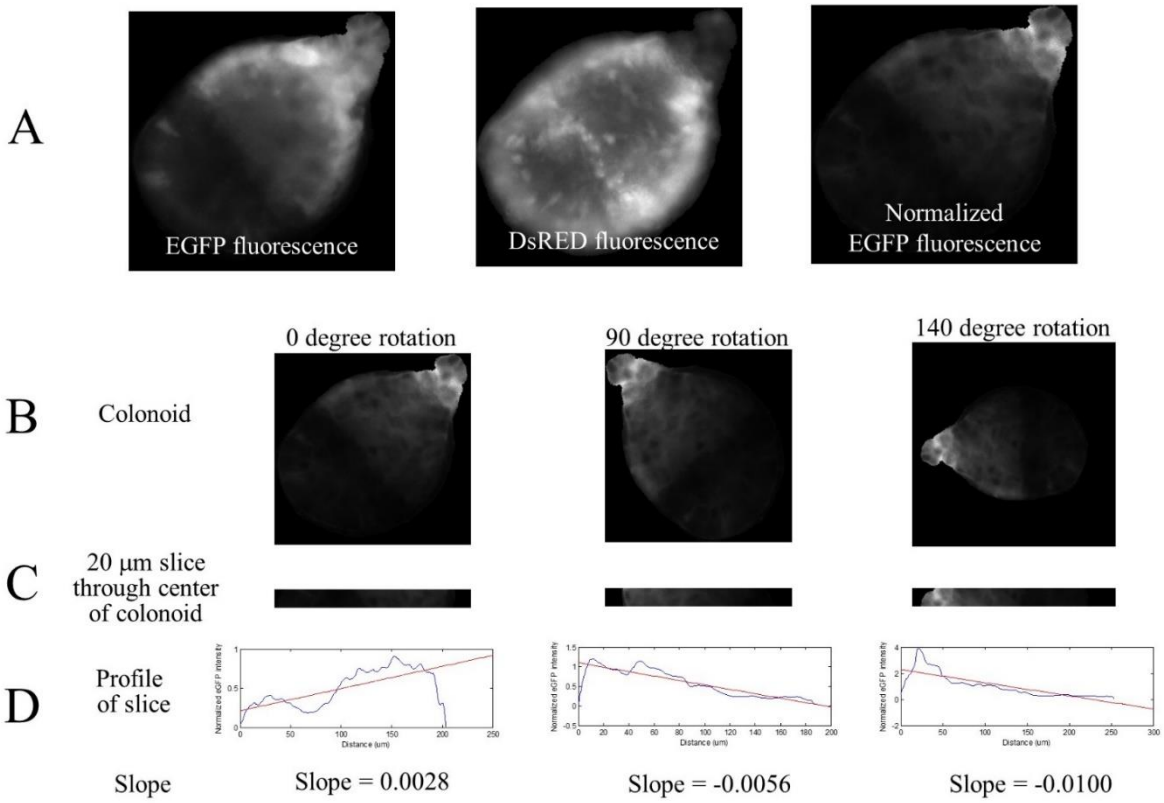

Figure 4.8 Identification of the EGFP polarization angle and magnitude.

A) Images of the DsRED fluorescence, EGFP fluorescence, and EGFP divided by DsRED fluorescence. B) The EGFP divided by DsRED image was rotated every one degree over 180 degrees. C) A 20 µm horizontal slice through the center of the colonoid was identified. D) The intensity profile along the 20 µm slice was calculated and a linear fit was performed on the intensity profile to obtain the slope of the best-fit line.

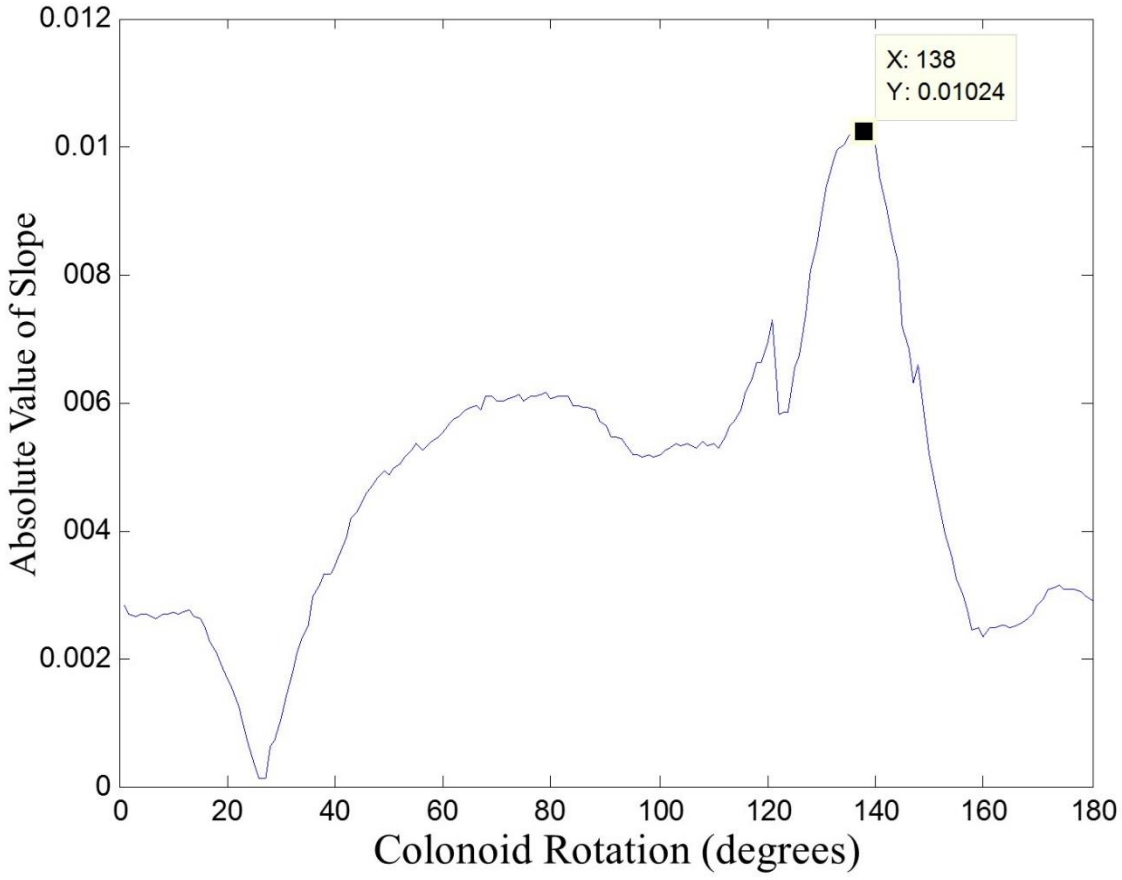

Figure 4.9 Identification of the EGFP polarization angle.

The colonoid rotation angle was plotted against the absolute value of the slope. The rotated image that produced the largest absolute value of the slope was identified. This angle of the rotated image and sign of the slope determined the direction of colonoid polarization. The absolute value of the slope was used as the magnitude of the polarization. In this example the angle of polarization was 138 degrees with a magnitude of 0.01.

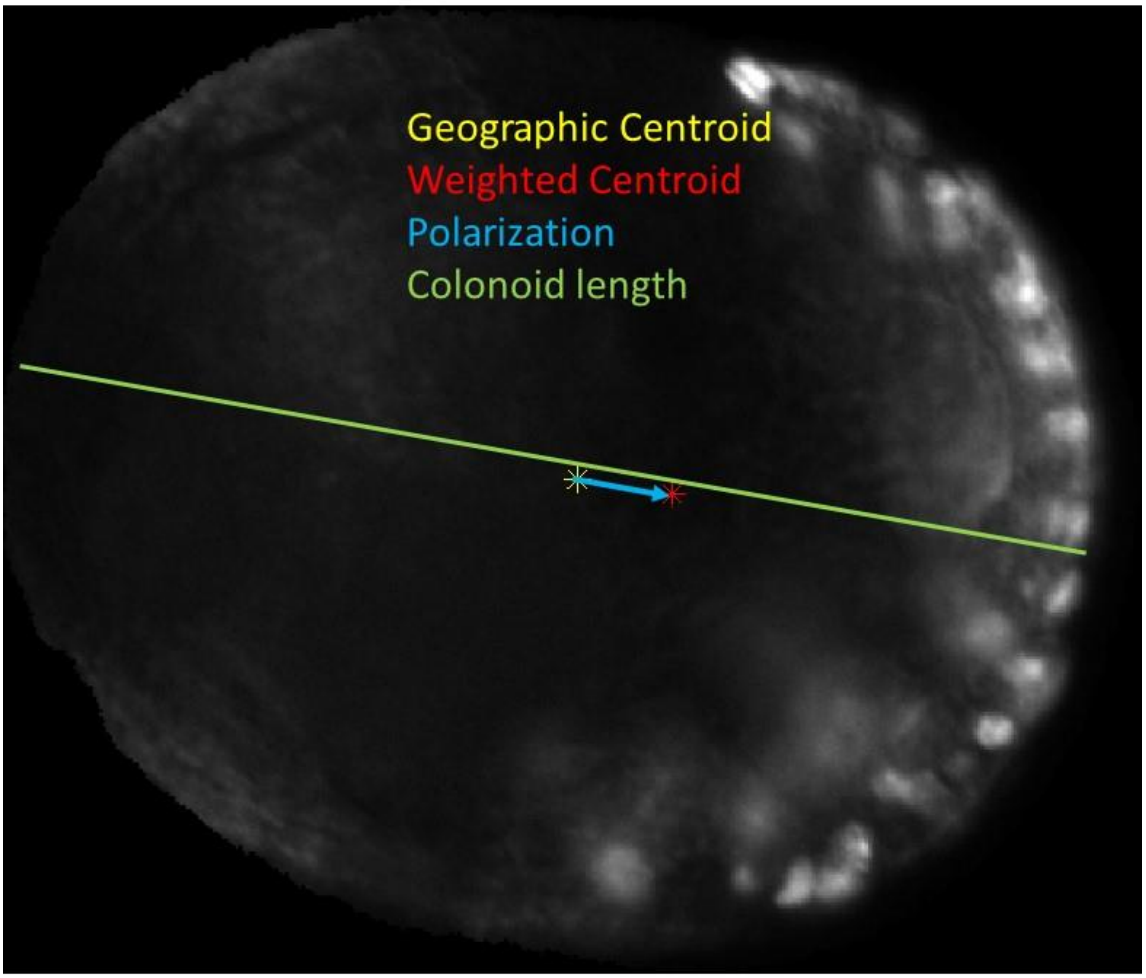

Figure 4.9 Example calculation of colonoid EdU polarization.

Shown is the EdU fluorescence image of a colonoid. The geographic centroid (yellow asterisk) was obtained from the Hoechst 33342 image (not shown). The EdU-intensity weighted centroid (red asterisk) was also calculated. The angle of polarization was the angle of the vector (blue arrow) that pointed from the geographic centroid to the intensity weighted centroid. The magnitude of the vector was normalized to the colonoid length (346 μm in this example).

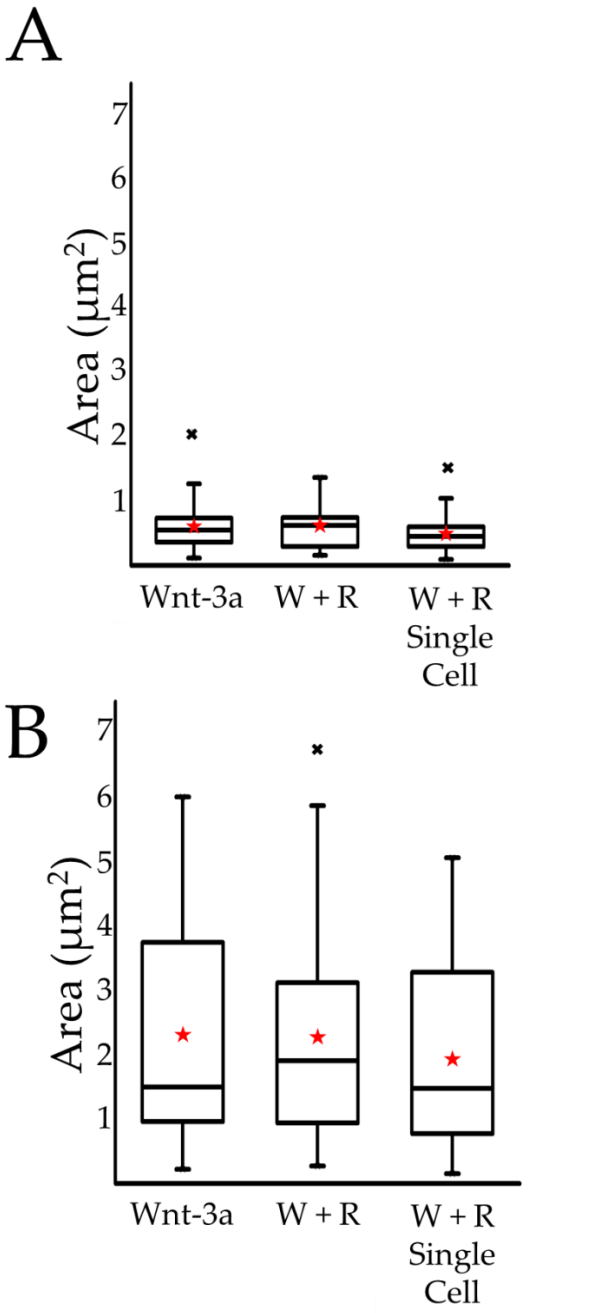

Figure 4.10 Boxplots were used to represent the DsRed fluorescent area of the colonoids for the three gradient conditions.

The non-normal distribution of the colonoid area is represented as μm^2 ($\times 10^4$). For the boxplots, the gray star indicates the mean of the data, the horizontal line shows the median, and the upper

and lower boxes represent the 75% and 25% of the data, respectively. The whiskers extend to the 5% and 95% with the individual points showing outliers. (A) Day 1 and (B) Day 5.

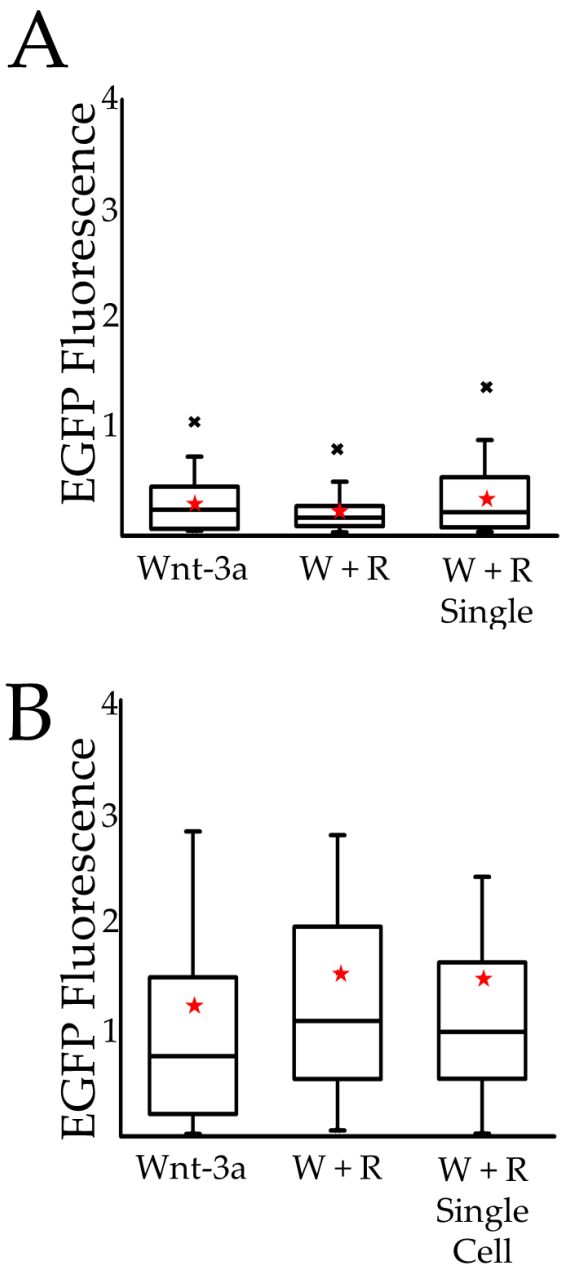

Figure 4.11 Boxplots were used to represent the integrated EGFP intensity of the colonoids for the three gradient conditions.

The non-normal distribution of the colonoid integrated EGFP fluorescent intensity is represented as RFUs ($\times 10^5$). For the boxplots, the black star indicates the mean of the data, the bar shows the median, and the upper and lower boxes represent the 75% and 25% of the data, respectively. The

whiskers extend to the 5% and 95% with the individual points showing outliers. (A) Day 1 and (B) Day 5.

4.6 Tables

Conditions	Day	Number of Crypts/Colonoids	Quartile 1 (μm^2)	Median (μm^2)	Quartile 3 (μm^2)
Microchannel	1	25	2,950	4,225	6,040
Multi-well Plate	1	25	3,185	4,660	6,445
Microchannel	5	25	11,148	20,387	33,520
Multi-well Plate	5	25	9,359	17,392	36,637

Table 4.1 Area occupied by each colonoid in a 2-D image slice in the absence of a gradient after 1 and 5 days of culture in the microchannel or multi-well plate.

Conditions	Day	Number of Crypts/Colonoids	Quartile 1	Median	Quartile 3
Microchannel	1	25	10,255	22,100	59,860
Multi-well Plate	1	25	9,970	25,800	57,580
Microchannel	5	25	46,611	74,352	199,382
Multi-well Plate	5	25	27,759	85,468	171,836

Table 4.2 EGFP fluorescent intensity of colonoids in a 2-D image slice in the absence of a gradient after 1 and 5 days of culture in the microchannel or multi-well plate.

Conditions	Day	Number of Colonoids	Average % of pixels with EGFP fluorescence	% of colonoids with >25% of the pixels positive for EGFP fluorescence
Microchannel	5	15	66 ± 17%	89 ± 8
Multi-well Plate	5	15	69 ± 14%	93 ± 4

Table 4.3 Percentage of each colonoid with EGFP fluorescence in a 2-D image slice in the absence of a gradient after 5 days of culture on the microchannel and multi-well plate.

Conditions	Day	Number of Colonoids	Average % of pixels with EdU fluorescence	% of colonoids with >25% of the pixels positive for EdU fluorescence
Microchannel	5	15	57 ± 10%	96 ± 3
Multi-well Plate	5	15	64 ± 14%	92 ± 7

Table 4.4 Percentage of each colonoid with EdU fluorescence in a 2-D image slice in the absence of a gradient after 5 days of culture on the microchannel and multi-well plate.

Conditions	Day	Number of Colonoids	Average % of pixels with Muc-2 immunofluorescence	% of colonoids with >10% of the pixels positive for Muc-2 immunofluorescence
Microchannel	5	15	32 ± 7%	90 ± 5
Multi-well Plate	5	15	28 ± 9%	92 ± 6.5

Table 4.5 Percentage of each colonoid with Muc-2 immunofluorescence in a 2-D image slice in the absence of a gradient after 5 days of culture on the microchannel and multi-well plate.

Conditions	Day	Number of Colonoids	Quartile 1	Median	Quartile 3
Wnt-3a	1	35	6,769	23,916	43,490
Wnt-3a	5	28	25,445	73,591	143,216

Table 4.6 Integrated EGFP intensity of a 2-D image slice of colonoids developed within a Wnt-3a gradient after 1 and 5 days of culture on the microdevice.

Conditions	Day	Number of Colonoids	Quartile 1	Median	Quartile 3
W + R	1	40	10,074	16,576	27,275
W + R	5	35	53,542	105,823	189,950

Table 4.7 Integrated EGFP intensity of a 2-D image slice of colonoids developed within a Wnt-3a + Rspondin1 gradient after 1 and 5 days of culture on the microdevice.

Conditions	Day	Number of Cells/Colonoids	Quartile 1	Median	Quartile 3
W + R	1	37	7,751	20,816	44,503
W + R	5	30	52,901	95,734	159,551

Table 4.8 Integrated EGFP intensity of a 2-D image slice of colonoids developed from single cells within a Wnt-3a + Rspondin1 gradient after 1 and 5 days of culture on the microdevice.

4.7 REFERENCES

1. Sato T, Vries RG, Snippert HJ, van de Wetering M, Barker N, Stange DE, van Es JH, Abo A, Kujala P, Peters PJ, Clevers H: Single Lgr5 stem cells build crypt-villus structures in vitro without a mesenchymal niche. *Nature* 2009, 459:262-U147.

2. Huh D, Torisawa Y-s, Hamilton GA, Kim HJ, Ingber DE: Microengineered physiological biomimicry: Organs-on-Chips. *Lab on a Chip* 2012, 12:2156-2164.

3. Barker N, van de Wetering M, Clevers H: The intestinal stem cell. *Genes & Development* 2008, 22:1856-1864.

4. van der Flier LG, Clevers H: Stem Cells, Self-Renewal, and Differentiation in the Intestinal Epithelium. *Annual Review of Physiology* 2009, 71:241-260.

5. He XC, Zhang JW, Tong WG, Tawfik O, Ross J, Scoville DH, Tian Q, Zeng X, He X, Wiedemann LM, et al: BMP signaling inhibits intestinal stem cell self-renewal through suppression of Wnt-beta-catenin signaling. *Nature Genetics* 2004, 36:1117-1121.

6. Mariadason JM, Nicholas C, L'Italien KE, Zhuang M, Smartt HJM, Heerdt BG, Yang WC, Corner GA, Wilson AJ, Klampfer L, et al: Gene expression profiling of intestinal epithelial cell maturation along the crypt-villus axis. *Gastroenterology* 2005, 128:1081-1088.

7. Gregorieff A, Pinto D, Begthel H, Destree O, Kielman M, Clevers H: Expression pattern of Wnt signaling components in the adult intestine. *Gastroenterology* 2005, 129:626-638.

8. van Es JH, Clevers H: Notch and Wnt inhibitors as potential new drugs for intestinal neoplastic disease. *Trends in Molecular Medicine* 2005, 11:496-502.

9. Takayama T, Miyanishi K, Hayashi T, Kukitsu T, Takanashi K, Ishiwatari H, Kogawa T, Abe T: Aberrant Crypt Foci: Detection, Gene Abnormalities, and Clinical Usefulness. *Clinical Gastroenterology and Hepatology* 2005, 3:S42-S45.

10. Sato T, Stange DE, Ferrante M, Vries RGJ, van Es JH, van den Brink S, van Houdt WJ, Pronk A, van Gorp J, Siersema PD, Clevers H: Long-term Expansion of Epithelial Organoids From Human Colon, Adenoma, Adenocarcinoma, and Barrett's Epithelium. *Gastroenterology* 2011, 141:1762-1772.

11. Sato T, Vries RG, Snippert HJ, van de Wetering M, Barker N, Stange DE, van Es JH, Abo A, Kujala P, Peters PJ, Clevers H: Single Lgr5 stem cells build crypt-villus structures in vitro without a mesenchymal niche. *Nature* 2009, 459:262-265.

12. Clevers H: The intestinal crypt, a prototype stem cell compartment. *Cell* 2013, 154:274-284.

13. Ootani A, Li XN, Sangiorgi E, Ho QT, Ueno H, Toda S, Sugihara H, Fujimoto K, Weissman IL, Capecchi MR, Kuo CJ: Sustained in vitro intestinal epithelial culture within a Wnt-dependent stem cell niche. *Nat Med* 2009, 15:701-706.

14. Sato T, Clevers H: Growing self-organizing mini-guts from a single intestinal stem cell: mechanism and applications. *Science* 2013, 340:1190-1194.

15. Clevers H: The Intestinal Crypt, A Prototype Stem Cell Compartment. *Cell* 2013, 154:274-284.

16. Rosenberg DW, Giardina C, Tanaka T: Mouse models for the study of colon carcinogenesis. *Carcinogenesis* 2009, 30:183-196.

17. Barker N, Ridgway RA, van Es JH, van de Wetering M, Begthel H, van den Born M, Danenberg E, Clarke AR, Sansom OJ, Clevers H: Crypt stem cells as the cells-of-origin of intestinal cancer. *Nature* 2009, 457:608-U119.

18. Takayama T, Miyanishi K, Hayashi T, Kukitsu T, Takanashi K, Ishiwatari H, Kogawa T, Abe T, Niitsu Y: Aberrant crypt foci: detection, gene abnormalities, and clinical usefulness. *Clinical gastroenterology and hepatology : the official clinical practice journal of the American Gastroenterological Association* 2005, 3:S42-45.

19. Ootani A, Li XN, Sangiorgi E, Ho QT, Ueno H, Toda S, Sugihara H, Fujimoto K, Weissman IL, Capecchi MR, Kuo CJ: Sustained in vitro intestinal epithelial culture within a Wnt-dependent stem cell niche. *Nature Medicine* 2009, 15:1-U140.

20. Kim HJ, Ingber DE: Gut-on-a-Chip microenvironment induces human intestinal cells to undergo villus differentiation. *Integrative Biology* 2013, 5:1130-1140.

21. Koo B-K, Stange DE, Sato T, Karthaus W, Farin HF, Huch M, van Es JH, Clevers H: Controlled gene expression in primary Lgr5 organoid cultures. *Nature Methods* 2012, 9:81-U197.

22. Gracz AD, Ramalingam S, Magness ST: Sox9 expression marks a subset of CD24-expressing small intestine epithelial stem cells that form organoids in vitro. *American Journal of Physiology-Gastrointestinal and Liver Physiology* 2010, 298:G590-G600.

23. Miyoshi H, Stappenbeck TS: Counteracting stem cell expansion during wound repair Distinct roles of non-canonical Wnt and TGF-beta. *Cell Cycle* 2013, 12:387-388.

24. de Lau W, Barker N, Low TY, Koo B-K, Li VSW, Teunissen H, Kujala P, Haegebarth A, Peters PJ, van de Wetering M, et al: Lgr5 homologues associate with Wnt receptors and mediate R-spondin signalling. *Nature* 2011, 476:293-U257.

25. Yui S, Nakamura T, Sato T, Nemoto Y, Mizutani T, Zheng X, Ichinose S, Nagaishi T, Okamoto R, Tsuchiya K, et al: Functional engraftment of colon epithelium expanded in vitro from a single adult Lgr5(+) stem cell. *Nature Medicine* 2012, 18:618-623.

26. Schwitalla S, Fingerle AA, Cammareri P, Nebelsiek T, Goektuna SI, Ziegler PK, Canli O, Heijmans J, Huels DJ, Moreaux G, et al: Intestinal Tumorigenesis Initiated by Dedifferentiation and Acquisition of Stem-Cell-like Properties. *Cell* 2013, 152:25-38.

27. van der Meer AD, van den Berg A: Organs-on-chips: breaking the in vitro impasse. *Integrative Biology* 2012, 4:461-470.

28. Mizutani T, Nakamura T, Morikawa R, Fukuda M, Mochizuki W, Yamauchi Y, Nozaki K, Yui S, Nemoto Y, Nagaishi T, et al: Real-time analysis of P-glycoprotein-mediated drug transport across primary intestinal epithelium three-dimensionally cultured in vitro. *Biochemical and Biophysical Research Communications* 2012, 419:238-243.

29. Kosinski C, Li VSW, Chan ASY, Zhang J, Ho C, Tsui WY, Chan TL, Mifflin RC, Powell DW, Yuen ST, et al: Gene expression patterns of human colon tops and basal crypts and BMP antagonists as intestinal stem cell niche factors. *Proceedings of the National Academy of Sciences of the United States of America* 2007, 104:15418-15423.

30. Huh D, Matthews BD, Mammoto A, Montoya-Zavala M, Hsin HY, Ingber DE: Reconstituting Organ-Level Lung Functions on a Chip. *Science* 2010, 328:1662-1668.

31. Huh D, Hamilton GA, Ingber DE: From 3D cell culture to organs-on-chips. *Trends in Cell Biology* 2011, 21:745-754.

32. Medema JP, Vermeulen L: Microenvironmental regulation of stem cells in intestinal homeostasis and cancer. *Nature* 2011, 474:318-326.

33. Stelzner M, Helmrath M, Dunn JCY, Henning SJ, Houchen CW, Kuo C, Lynch J, Li LH, Magness ST, Martin MG, et al: A nomenclature for intestinal in vitro cultures. *American Journal of Physiology-Gastrointestinal and Liver Physiology* 2012, 302:G1359-G1363.

34. Ahmad AA, Wang Y, Gracz AD, Sims CE, Magness ST, Allbritton NL: Optimization of 3-D organotypic primary colonic cultures for organ-on-chip applications. *Journal of Biological Engineering* 2014, 8:9 1754-1611.

35. Wang Y, Ahmad AA, Shah PK, Sims CE, Magness ST, Allbritton NL: Capture and 3D culture of colonic crypts and colonoids in a microarray platform. *Lab on a Chip* 2013, 13:4625-4634.

36. Xia YN, Whitesides GM: Soft lithography. *Annual Review of Materials Science* 1998, 28:153-184.

37. Roskoski Jr R: Vascular endothelial growth factor (VEGF) signaling in tumor progression. *Critical reviews in oncology/hematology* 2007, 62:179-213.

38. Chen RR, Silva EA, Yuen WW, Mooney DJ: Spatio-temporal VEGF and PDGF delivery patterns blood vessel formation and maturation. *Pharmaceutical Research* 2007, 24:258-264.

39. Abhyankar VV, Toepke MW, Cortesio CL, Lokuta MA, Huttenlocher A, Beebe DJ: A platform for assessing chemotactic migration within a spatiotemporally defined 3D microenvironment. *Lab on a Chip* 2008, 8:1507-1515.

40. Abhyankar VV, Lokuta MA, Huttenlocher A, Beebe DJ: Characterization of a membrane-based gradient generator for use in cell-signaling studies. *Lab on a Chip* 2006, 6:389-393.

41. Ramalingam S, Daughtridge GW, Johnston MJ, Gracz AD, Magness ST: Distinct levels of Sox9 expression mark colon epithelial stem cells that form colonoids in culture. *American Journal of Physiology-Gastrointestinal and Liver Physiology* 2012, 302:G10-G20.

42. Marshman E, Booth C, Potten CS: The intestinal epithelial stem cell. *Bioessays* 2002, 24:91-98.

43. Li XQ, Zhao XN, Fang Y, Jiang X, Duong T, Fan C, Huang CC, Kain SR: Generation of destabilized green fluorescent protein transcription reporter. *Journal of Biological Chemistry* 1998, 273:34970-34975.

44. Yen H-CS, Xu Q, Chou DM, Zhao Z, Elledge SJ: Global Protein Stability Profiling in Mammalian Cells. *Science* 2008, 322:918-923.

45. Gracz AD, Williamson IA, Roche KC, Johnston MJ, Wang F, Wang Y, Attayek PJ, Balowski J, Liu XF, Laurenza RJ, et al: A high-throughput platform for stem cell niche co-cultures and downstream gene expression analysis. *Nature cell biology* 2015, 17:340-349.

46. Sato T, Clevers H: Growing Self-Organizing Mini-Guts from a Single Intestinal Stem Cell: Mechanism and Applications. *Science* 2013, 340:1190-1194.

47. Ahmad AA, Wang Y, Gracz AD, Sims CE, Magness ST, Allbritton NL: Optimization of 3-D organotypic primary colonic cultures for organ-on-chip applications. *J Biol Eng* 2014, 8:1754-1611.

48. Crank J: *The mathematics of diffusion.* Oxford university press; 1979.

49. Bright DS, Steel EB: TWO-DIMENSIONAL TOP HAT FILTER FOR EXTRACTING SPOTS AND SPHERES FROM DIGITAL IMAGES. *Journal of Microscopy-Oxford* 1987, 146:191-200.

50. Li CH, Lee CK: MINIMUM CROSS ENTROPY THRESHOLDING. *Pattern Recognition* 1993, 26:617-625.

51. Li CH, Tam PKS: An iterative algorithm for minimum cross entropy thresholding. *Pattern Recognition Letters* 1998, 19:771-776.

52. Chan TF, Vese L: Active contours without edges. *Image processing, IEEE transactions on* 2001, 10:266-277.

53. Frigge M, Hoaglin DC, Iglewicz B: SOME IMPLEMENTATIONS OF THE BOXPLOT. *American Statistician* 1989, 43:50-54.

54. Glantz SA: Primer of biostatistics. 2005.

55. Scott M: CIRCULAR STATISTICS IN BIOLOGY - BATSCHELET,E. *Journal of the American Statistical Association* 1983, 78:736-736.